IVW - Schriftenreihe Band 74
Institut für Verbundwerkstoffe GmbH - Kaiserslautern

Péter Molnár

Stitching Technique Supported Preform Technology for Manufactoring Fiber Reinforced Polymer Composites

Bibliografische Information Der Deutschen Bibliothek

Die Deutsche Bibliothek verzeichnet diese Publikation in der Deutschen Nationalbibliografie; detaillierte bibliografische Daten sind im Internet über <http://dnb.ddb.de> abrufbar.

Bibliographic information published by Die Deutsche Bibliothek

Die Deutsche Bibliothek lists this publication in the Deutsche Nationalbibliografie; detailed bibliographic data is available in the Internet at <http://dnb.ddb.de>.

Herausgeber: Institut für Verbundwerkstoffe GmbH
Prof. Dr.-Ing. Alois K. Schlarb
Erwin-Schrödinger-Straße
TU Kaiserslautern, Gebäude 58
67663 Kaiserslautern
http://www.ivw.uni-kl.de

Verlag: Institut für Verbundwerkstoffe GmbH

Druck: Technische Universität Kaiserslautern
ZBT – Abteilung Foto-Repro-Druck

D 386

Als Manuskript gedruckt. Printed in Germany.
ISSN 1615-021X
ISBN 978-3-934930-70-0
ISBN 3-934930-70-4

Stitching Technique Supported Preform Technology for Manufacturing Fiber Reinforced Polymer Composites

Beim Fachbereich für Maschinenbau und Verfahrenstechnik
der Universität Kaiserslautern
genehmigte Dissertation
zur Erlangung des akademischen Grades

Doktor-Ingenieur (Dr.-Ing.)

vorgelegt von

MSc. Péter Molnár

aus Szeged, UNGARN

Tag der mündlichen Prüfung:	12.07.2007
Prüfungsvorsitzender:	Prof. Dr.-Ing. Rainer Renz
1. Berichterstatter:	Prof. Dr.-Ing. Peter Mitschang
2. Berichterstatter:	Prof. Dr.-Ing. Tibor Czigány

D 386

Vorwort

Die vorliegende Dissertation entstand während meiner Tätigkeit als wissenschaftlicher Mitarbeiter bei der Institut für Verbundwerkstoffe GmbH in der Zeit von 2002 bis 2007 in Kaiserslautern.

Meinem Doktorvater Herrn Prof. Dr.-Ing. Peter Mitschang danke ich für das mir entgegenbrachte Vertrauen, die produktiven fachlichen Gespräche und für die umfassende Unterstützung während meiner Zeit am IVW.
Ebenso danke ich Herrn Prof. Dr.-Ing. Rainer Renz für die Übernahme des Prüfungsvorsitzes und Herrn Prof. Dr.-Ing. Tibor Czigány für die Übernahme des Korreferats, für die Unterstützung während meines Studiums an der Technischen und Wirtschaftswissenschaftlichen Universität Budapest und für seine konstruktive Kritik an dieser Arbeit.

Den Mitarbeitern der IVW GmbH, insbesondere den Kollegen der Abteilung Verarbeitungstechnik, danke ich herzlich für die gute Zusammenarbeit, die viele Hilfe und Unterstützung während der wertvollen fünf Jahre.

Besonderes möchte ich mich auch bei A. Hodács, A. Ogale, B. Fodor, B. Zsigmond, C. Reizer, D. Felhös, F. Weyrauch, H. Stadtfeld J. Langmack, J. Schlimbach, K-H. Hammer, V. Disandt und V. Nagy für die schöne Zeit und kreative Zusammenarbeit am Institut und an der Dissertation bedanken.

Für die vielen interessanten Forschungsarbeiten bedanke ich mich bei der BMBF, der German Honda Initiation Grant und der Europäischen Kommission für die gewährte finanzielle Unterstützung der Projekte, innerhalb derer Teile diese Arbeit entstanden.

Ganz besonderer Dank gilt meiner Familie für die kontinuierliche Unterstützung sowie den Rückhalt während meiner Ausbildung und meines bisherigen beruflichen Werdegangs.

Kaiserslautern, August 2007 Péter Molnár

Für meine Familie

Kurzfassung

Im Zuge der steigenden Anzahl von Einsatzmöglichkeiten der Faserverbundwerkstoffe in den verschiedensten Industriebereichen spielt die Entwicklung bzw. Weiterentwicklung neuer und effektiverer Verarbeitungstechniken eine bedeutende Rolle.

Dabei findet derzeit das Harzinjektionsverfahren (LCM) ausschließlich für kleinere bis mittlere Stückzahlen seinen Einsatz. Aufgrund der sehr großen Stückzahlen im Automobilbereich, ist dieses Verfahren hier zurzeit weniger interessant. Daher werden große Anstrengungen unternommen, das Harzinjektionsverfahren besonders für solche Bauteile attraktiver zu machen, die gegenwärtig mit Hilfe des Prepreg-Verfahrens hergestellt werden. Dabei spielt die Reduktion der hier vergleichsweise hohen Zykluszeit eine tragende Rolle. Die Dauer eines Zyklus wird hierbei hauptsächlich durch die Vorbereitung und Herstellung der Verstärkungsstruktur (Preform) sowie durch die Bestückung des Werkzeuges bestimmt. Diese so genannte Preform-Technik weist daher ein sehr großes Entwicklungspotential auf, mit dem Ziel, solche Verstärkungsstrukturen herzustellen, die nach der Injektion keine Nacharbeit erfordern. Solche Strukturen werden auch als „net shape, ready-to-impregnate“- Preform bezeichnet. Die hierfür notwendigen Techniken stammen vornehmend aus der Textilindustrie, wie z.B. die direkte Preformtechnik, das Nähen oder Kleben (Binder-Technik).

Ziel der vorliegenden Dissertation ist es, die Möglichkeiten der Nähtechnik bezogen auf die Herstellung der Preforms zu untersuchen. Hierfür werden die verschiedenen Naht- und Verbindungsarten hinsichtlich ihres Einsatzes in der Preformtechnik, wie die *Fixier- und Positionier-*, die *Füge- oder Verbindungs*naht und die *Montage*naht, untersucht.

Im Rahmen dieser Arbeit wurde zunächst innerhalb einer Studie zur „net shape“-Preformtechnik eine Versteifungsstruktur entwickelt und hergestellt. Diese Struktur soll dabei der Veranschaulichung der Möglichkeiten und Einsatzbereiche der Nähtechnik bei der Preformtechnologie dienen. Zudem kann so ein mehrstufiger Preformherstellungsprozess demonstriert werden. Ferner zeigt diese Studie, dass ein hochgradiger, automatisierter Prozess, welcher zudem eine durchgängige Qualitätskontrolle ermöglicht, realisiert werden konnte.

Als ein weiterer Schritt wurde ein Prozess zur Herstellung eine dreidimensionalen Preform, der die Anwendung verschiedener thermoplastischer, niedrigtemperaturschmelzender Nähgarne zulässt, ausgearbeitet. Hierbei wurden die Vorteile der Näh- und der Binder-Technologie miteinander verbunden. Außerdem konnte durch die bereits formstabile und imprägnierungsfertige Preformstruktur, die Bestückung des Werkzeuges wesentlich vereinfacht werden. Um die mechanischen Eigenschaften der Preforms bestimmen zu können, wurden quantitative Messmethoden erarbeitet. Hierdurch konnten anschließend die Einflüsse der Orientierung sowie der Stichdichte ermittelt werden. Zudem wurden die folgenden drei grundlegenden Eigenschaften untersucht: die spezifische Biegesteifigkeit, der so genannte Rückspringwinkel sowie die Rückstellkraft nach dem Thermoformen hinsichtlich der verschiedenen Nähtypen.

Um dies zu ergänzen, wurden weiterführende Untersuchungen zu den Materialeigenschaften der Nähfäden, die bei der dreidimensionalen Preformtechnik eingesetzt werden können, durchgeführt. Dabei ist neben der niedrigen Schmelztemperatur die vollständige Auflösbarkeit der Nähgarne in den ungesättigten Polyester- und Epoxidharzen besonders wichtig. Auf Grund dieser vollständigen Auflösung der Fäden in der Matrix können die Stichlöcher wieder vollkommen verschlossen werden. Dadurch kann eine Reduktion des Einflusses solcher Stichlöcher auf die mechanischen Eigenschaften des Faserverbundwerkstoffes erreicht werden. Mit Hilfe dieser Untersuchungen wurden schließlich zwei polymere Nähgarne als vielversprechend beurteilt. Diese weisen eine Schmelztemperatur von weniger als 100 °C sowie eine gute Lösbarkeit, besonders im Harzsystem *RTM 6*, auf.

In der Preformtechnik werden die Nähte nicht nur als *Positionier*- oder *Montage*naht eingesetzt, sondern können in einer Struktur als auch als Verstärkungselement, eine so genannte *Verstärkungsnaht*, verwendet werden. Der Zweck einer solchen Naht ist die interlaminare Verstärkung von monolitischen oder Sandwichstrukturen. Zudem besteht die Möglichkeit, diese zur Fixierung von metallischen Funktionselementen (Inserts) in den Faserverbundwerkstoff zu benutzen. Hinsichtlich diese Möglichkeiten wurden im Rahmen dieser Arbeit erfolgreich Untersuchung durchgeführt. Dabei wiesen die eingenähten Krafteinleitungselemente in durchgeführten statischen Zugversuchen eine annähernd 200 % höhere maximale Zugkraft verglichen mit entsprechenden Elementen (BigHead®), die nicht durch eine Naht fixiert wurden.

Weitere Untersuchungen zeigten auch, dass eine doppelte Naht nicht eine proportionale Verdoppelung der maximal erreichbaren Zugkraft bewirkt. Der Grund hierfür liegt an einer partiellen Zerstörung des vorhandenen Nähgarns der ersten Naht begründet durch den doppelten Einstich in die bereits bestehenden Löcher beim mehrmaligen Durchlaufen der Nadel. Der größte Verstärkungseffekt konnte schließlich bei der interlaminaren Einbettung und der Vernähung des Insert erreicht werden. In diesem Fall kann eine Delamination, wie sie bei lediglich interlaminar eingebetteten Inserts auftritt, verhindert werden.

Zusätzlich wurden statische Scherversuche durchgeführt, um auch in diesem Belastungsfall die Versagensart zu untersuchen. Dabei stellte sich heraus, dass nicht die Nähte sondern der Insert versagte. Auf Grund des Materialbruchs des Inserts, sowohl in Zug- als auch in Scherversuchen, wurde in einem weiteren Schritt ein optimiertes Insert entwickelt. Bei diesem wurde der Sockel in soweit modifiziert, dass die maximale Versagenslast des Nähgarns ermittelt werden konnte. Dabei stellte sich heraus, dass Glas-, Kohlenstoff- und Aramidfasern sich nur bedingt als Verstärkungsgarn zur Fixierung von Inserts eignen. Im Gegensatz dazu sind die Polyestergarne als ausreichende Verstärkung gut geeignet. Weitere Vorteile des Polyestergarns sind die niedrigeren Kosten sowie die gute Vernähbarkeit. Anschließend wurde eine solche Verbindung des Inserts mit einem Faserverbundwerkstoff mit Hilfe der Finite-Elemente-Methode (FEM) simuliert. Dabei zeigte sich eine gute Übereinstimmung der simulierten Ergebnisse mit denen aus dem statischen Zugversuch mit dem weiterentwickelten Insert.

Auf Grund der elektrischen Leitfähigkeit von Kohlenstofffasern, können Fäden aus diesem Material auch als Sensoren zur Überwachung einer Struktur oder Verbindung eingesetzt werden. Hierfür wurden ebenfalls Untersuchungen durchgeführt. Dabei konnte mit Hilfe der Änderung des elektrischen Widerstandes auf Schädigungen der Fasern geschlossen werden. Somit können nicht nur das Bestehen einer Schädigung, sondern auch der annähernde Ort ermittelt werden. Die Untersuchungen zeigten somit, dass die Kohlenstofffasern nicht lediglich als Verstärkung sondern auch als Überwachungssensor bei einem eingebetteten Insert dienen können.

Im Rahmen aller Untersuchungen konnte das große und vielversprechende Potential der Nähtechnik bei der Herstellung von Preform-Bauteilen aufgezeigt sowie ein Einblick in einige von vielen Anwendungsmöglichkeiten gegeben werden.

Content

Symbols

Symbol	Unit	Significance
a	[mm]	Notch length (SEN-T specimen)
a	[m/s^2]	Acceleration
A_5	[%]	Maximum elongation
$A_{preform}$	[m^2]	Base area of preform
A_s	[mm^2]	Critical cross section area
α	[°]	Enlacement angle
b	[mm]	Width of specimen
B	[-]	Number of stitches
B	[mm]	Thickness (SEN-T specimen)
$\underline{\underline{B}}$	[-]	Node displacement connection of deformation
$\underline{\underline{B}}_{L0}$	[-]	Linear term that - in case of small displacements
$\underline{\underline{B}}_{L1}$	[-]	Nonlinear term that depends on the displacement
C	[mm]	Length (SEN-T specimen)
$\underline{\underline{C}}'$	[GPA]	Stiffness matrix in the primed coordinate system
d_3	[mm]	core diameter of the screwed botl
δ	[(J/cm^3)$^{1/2}$]	Solubility parameter
δ_{ec}	[mm]	Electrical effective length
E_x, E_y	[GPa]	Young´s-modulus in x and y direction of the laminates
$\underline{\varepsilon}'$	[%]	Strain matrix in the primed coordinate system
$\underline{\underline{\varepsilon}}^L$	[-]	Lagrange type deformation tensor
$\underline{f}$	[-]	Typical right side vector and the external loading is presented in nodes
F	[mm]	Clamping length (SEN-T specimen)
F	[N]	Force

F_c	[N]	Compaction force
F_{BT}	[N]	Tensile force of the bobbin thread
F_{max}	[N]	Maximum force
F_{NT}	[N]	Tensile force of the needle thread
g	[m/s^2]	Gravitational constant
G	[mN cm]	Specific bending stiffness
G	[J]	Gibbs potential
H	[J]	Enthalpy (in chapter 2.5)
H	[mm]	Notch width (SEN-T specimen)
I	[A]	Electric current
$\underline{\underline{K}}$	[-]	Sum of the stiffness matrix of the elements
$\underline{\underline{K}}_G$	[-]	Tangential stiffness matrix
$\underline{\underline{K}}_M$	[-]	Tangential stiffness matrix
L	[mm]	Fiber length
l	[mm]	Length of specimen
$l_ü$	[mm]	Free length of specimen
m	[g]	Mass of specimen
μ	[-]	Friction coefficient
n	[-]	Number of reinforcing layers
N_{CP}	[-]	Number of the carbon fiber contact points
ή	[mPa s]	Viscosity
P	[bar, mbar]	Pressure / vacuum
$\underline{p}$	[-]	Force vector
R	[Ohm]	Electric resistance
R_{eH}	[MPa]	Minimum yield strength
R_{cf}	[Ohm]	Electrical resistance of carbon fiber
R_m	[MPa]	Tensile strength

S	[JK^{-1}]	Entropy
SA	[-]	Stitch number
S_{item}/a	[-]	Production volume in units per year
σ	[MPa]	Tensile stress
s	[mm]	Clamping distance
SD	[-]	Standard deviation
$\underline{\sigma'}$	[MPa]	Stress matrix in the primed coordinate system
σ_{ReH}	[Mpa]	Stress that belongs to the yield point
t	[s]	Time
T	[K]	Absolute temperature
tex	[g/1000m]	Yarn weight concerning as 1000 m (linear density)
T_g	[°C]	Glass transmission temperature
t_{st}	[s]	Stitching time
$\underline{\underline{T}}_{\varepsilon}$	[%]	Three dimensional strain transformation matrix
$\underline{\underline{T}}_{\sigma}$	[MPa]	Three dimensional stress transformation matrix
U	[V]	Voltage
$\underline{U}$	[-]	Displacement Vector
$\underline{U}$	[-]	Generalized node displacement
U	[V]	Electric potential
v	[-]	Volume fraction
V_f	[%]	Fiber volume content
V_{st}	[SPM]	Stitching velocity
W	[mm]	Specimen width (SEN-T specimen)
X_i	[-]	i^{th} result
$\bar{x}$	[-]	Mean value of the values

Abbreviations

Abbreviation	Description
1k, 6k	1000 or 6000 single filament in carbon fiber rovings
2D, 3D	2 dimension, 3 dimension
AF	Aramid Fiber
ARTM	Advanced Resin Transfer Moulding
BMBF	German Ministry of Education and Research
BT	Bobbin Thread
CAD	Computer Aided Design
CED	Cohesion Energy Density
CF	Carbon Fiber
CFRPC	Carbon Fiber Reinforced Polymer Composite
CNC	Computer Numerical Control
CONH	Amide Bond
COO	Ester Bond
Co-PA	Co-Polyamide
Co-PET	Co-Polyester
DFP	Directed Fiber Preforming
DIN	German Norm
DPRTM	Differential Pressure Resin Transfer Moulding
EP	Epoxi Resin
F3P	Ford Programmable Preform Process
FE	Finite Element
FEM	Finite Element Modeling
FO	Fiber Orientation
FPA	Final Preform Assembly

FRPC	Fiber Reinforced Polymer Composite
GF	Glass Fiber
GMT	Glass Mat Reinforced Thermoplastic Material
IVW	Institut für Verbundwerkstoffe GmbH
IVW-CF	IVW Patented Carbon Stitching Fiber
KEVLAR	Description of p-aramid products of Company DuPont
LCM	Liquid Composite Moulding
LFI	Liquid Film Infusion
LFT	Long Fiber Thermoplastic Material
min	Minute
NCF	Non-Crimp Fabric
NF	Needle Fiber
P4	Programmable Powder Preform Process
PC	Personal Computer
PCL	Poly-Caprolactone
Par	Parallel
PEI	Polyether-Imide
Per	Perpendicular
PES	Description of PET Fiber Materials (textile technique)
PES	Polyether-Sulfone
PET	Polyethylene-Terephthalate
PVAL	Polyvinyl-Alcohol
PSU	Polysulphone
PZT	Lead-Titanate-Zirconate, Piezo Chrystal
QM	Quality Management
QS	Quality System
RIFT	Resin Infusion under Flexible Tooling

RT	Room temperature
RTM	Resin Transfer Molding
RTM6	Hexcel RTM resin system
SCP	Stitch-Cut-Process
SCRIMP®	Seeman Composite Resin Infusion Molding Process
SEN-T	Single Edge Notched Tensile
SHM	Structural Health Monitoring
SL	Stitch Length
SLI	Single Line Injection
SMC	Sheet Molding Compound
SPM	Stitch per Minute
SW	Stitch Width
TFP	Tailored Fiber Placement
TP	Thermoplastic Material
TPC	Thermoplastic Polymer Composite
TR	Tailored Reinforcement
UD	Unidirectional
UT	Upper Thread
UP	Unsaturated Polyester
VARI	Vacuum Assisted Resin Injection
VARTM	Vacuum Assisted Resin Transfer Molding
VI	Vacuum Infusion
WF	Woven Fabric

Introduction

Polymer composites of improving properties are applied as structural materials in the most prospering fields such as the automotive industry and airplane production. The drive of this phenomenon is the increasing social demand to reduce the load on the environment but still keep the great extent mobility [1, 2, 3, 4]. Simultaneously, such high requirements arise in the industry that can only be fulfilled with the help of the consequent application of modern materials [5, 6]. The increasing demands on the reinforcing materials of load bearing polymer structural elements serve as an incentive for researchers to develop better composite structures of more favourable price. Fiber reinforced polymer composites are the indispensable materials of high technical value in the up-to-date technologies due to their favourable strength- and stiffness-weight ratio. Nowadays the high technical value can be achieved mostly by the commercially available carbon (CF), glass (GF) and aramid (AF) fibers and the combination of different polymer types [7, 8, 9]. These materials have to substitute metals in the structure, since this means weight reduction and the fulfilment of the necessary functions at high level.

Composites are the most modern class of technical structural materials. Their spreading takes place only in a moderate way, due to the lack of economic production technologies.

As opposed to the injection technologies, the method applied often to produce composite structures is the prepreg technology, which is relatively costly but engineers possess significant experience as a background in its application [10, 11]. Nevertheless the results from different research activities and industries demonstrate that LCM (Liquid Composite Molding) technologies offer economical and technical advantages over composite parts from a conventional prepregging route [12, 13, 14, 15, 16, 17]. A summary can list the following reasons why LCM technologies gain more and more attention by manufacturers in different branches:

- Good surface finish on both sides of the composites
- Selective reinforcement and accurate fiber management
- Ability to achieve fiber volume content up to 65%

- Uniformity of thickness and fiber loading, hence uniform shrinkage
- Inserts may be incorporated into moldings
- Low pressure processing
- Tight tolerances and ability to generate high quality surfaces which are to precisely oriented in space
- Possibility of making highly complex structural and hollow shapes and to fabricate multi component structures which were previously constructed with several individual parts
- High level of part reproducibility and consistency in assembly operations
- Ability to produce near net-shape moldings, hence low material wastage
- Ability to achieve from 0.1 mm up to some 10 mm laminate thickness

The parts used in the automotive industry are predestinated to injection technologies (LCM, Liquid Composite Molding) considering their size, complexity and the number of pieces maximum in middle series (S_{item}/a, approx. 50,000 item/year) [18, 19]. Nevertheless, this LCM process involves an enormous development potential considering the reliability of the process, the tool construction as well as the preform technologies and matrix systems [20, 21, 22, 23]. LCM technologies are already present, and furthermore are developing rapidly in different industries. The reason for this significant spreading is that these technologies can substitute the conventional manual lamination and fiber spraying processes, and on the other hand parts of high technical value can be produced this way. The number of application fields increased and simultaneously the requirements on the applied fiber reinforcing structures grew. In case of liquid composite molding technologies, the required fiber orientation of complex shape parts can be provided with the help of the available preform technologies. However, the enormous potential of textile technology that can be used in LCM processes and the background experience is not available for manufacturers yet. The recent developments were aimed at finding and applying complex direct textile technologies for the production of complex composite parts [24]. The composite bicycle frames produced with Tailored Fiber Placement (TFP) [25], different L-, U- or Z-shape profiles manufactured with 3 dimensional weaving [26], and the knitted or looped nods for Space Frame Technique applications [27] are good examples for this trend. A similar solution is to manufacture 3 dimensional, bent

geometries with robot assisted braiding [28, 29]. These technologies have already been used in series production in some cases such as in airplane applications and in the production of longitudinal and cross directional load bearing structures of helicopters.

The application of stitching technologies in the industry based on already existing semi-products (Woven (WF) and Non-Woven Fabrics, Non-Crimp Fabrics (NCF) [30]) is predestinated to produce a preform of higher level and greater complexity as a combination of these materials. In order to assemble different subcomponents, another technological step, called preform-assembly had to be introduced. As a consequence, the characteristics of single preforms are defined by the semi-products of the textile industry built in the system and by the seam types applied in their fixation.

Besides stitching technologies, literature details other textile technological processes that can be applied in the production of preforms for composite parts. Processes like this are the different weaving, braiding and TFP (Tailored Fiber Placement) technologies [31, 32], as well as loop forming methods [33] such as knitting or circular knitting [34]. The object of these examinations is not only the applicability of technologies in a flexible production process, but also the examination of the influence of technological parameters, such as fiber orientation, auxiliary materials for processing [35] or the formability and flexibility properties of the product.

The development fields mentioned in the literature are often aimed at the applicability of stitching technologies in the assembly of preform components, so-called sub-preforms. Emphasized fields are the development of new engineering solutions, e.g. fixation of single side seam reinforced preform subcomponents in places that are difficult to reach [36, 37] or the development of special devices for the assembly of large preforms, for instance the total reinforcing system of an airplane wing surface [38]. The relations between the stitching parameters and the mechanical properties of composites built up of stitched preforms were only limited to the examination of the impact and position of nods in the seam until now [39, 40, 41, 42, 43]. In case of the two dimensional, sheet-like composite parts, fixing the layers by stitching has already been a well-known method for a long time [44], and its influence has already been

studied, but the extent of the impact and the relation of the stitching parameters is rarely mentioned in the literature.

The already completed research and development work verifies that the application of preform technologies improves the automation degree of liquid composite technologies to a great extent. The optimization and fitting of preform technologies to liquid composite methods should involve both technological and economic arguments. If the series size of LCM technologies is considered, it can be concluded that the preform technologies should be very flexible. In case this aim can be realized, the potential hidden in the LCM technologies could be utilized to a greater extent and its application can be more economical. Increasing the number of functions of the applied seams, the exploration of possibilities, the examination of three dimensional preforms and the further development of technologies should be the emphasized fields of stitching assisted preform technologies.

Objective of the dissertation

The aim of the investigations mentioned in the proposed dissertation is to reveal the possibilities of the preform technology. The primary objective is to investigate the applicability of stitching technology in three dimensional preform production and FRPC part manufacturing. Secondarily, the purpose is to map the potentials of the seam types and materials applied in preform technology and the assignment of supplementary functions to stitched preform technologies.

Hence, the investigation of stitching threads with low melting point, used in three dimensional, shape preserving preform production, had to be carried out. Based on these results, the solubility of stitching threads of low melting point had to be examined in different polymer matrix materials. The aim of the solubility examinations is to reduce the stitch holes formed due to stitching in a way that the threads are dissolved in these holes during injection. Owing to the dissolution of threads, the stitch holes close partially or completely, and hence the mechanical properties of composite parts improve significantly.

The reinforcing function of seams can be studied if the metal load carrying elements fixed by stitching during a preform technology and built in the reinforcing structure are investigated. The aim of the production and mechanical investigations is to examine the loadability of inserts in case of different embedding and stitching reinforcing methods. The results of these experiments should reveal the applicability of reinforcing by stitching and serve as a base for FE simulations.

The aim of simulations is to model the given composite-insert relation and to get to know the emerging load as well as strains, and to create a simulation tool that models reality with a good approximation. The task with this simulation tool is to work out the geometry of a metal insert developed further for incorporation by stitching.

Based on the investigations of the embedded, metal force transmission elements, the base of a monitoring system should be worked out in the final part of the dissertation. The sensors of this system that detect fracture damage could be carbon fibers. The investigations have to reveal whether these principles work, and the results should provide a basis for a cost efficient monitoring system.

1 Preform technique for liquid composite molding technologies

Several variants were developed within liquid composite molding (LCM) technologies, and hence different symbols evolved due to identification and patenting purposes [19]. A common basic characteristic of all technologies is that a liquid –the polymer that functions as the matrix in the composite structure later– is injected into a porous material, the reinforcing structure. The difference among the methods lies in the flow direction (2D, 3D flow) relative to the position, the injection pressure difference (vacuum and/or injection pressure) and the process itself [45]. The classical RTM (resin transfer molding) technology (Figure 1.1), i.e. injection under pressure, used for producing medium complex structures, belongs to the liquid composite molding (LCM) technologies. Primarily the RTM procedure is adopted for small and medium series manufacturing of large composite components with complex geometries. This technology is suitable for manufacturing sandwich structured components, as well as for those with localized toughening elements, e.g. metallic inserts. With this procedure, the finished product obtained will be of good surface quality. This technology, due to its full automation, has recently been used in the automotive and aerospace industry [46].

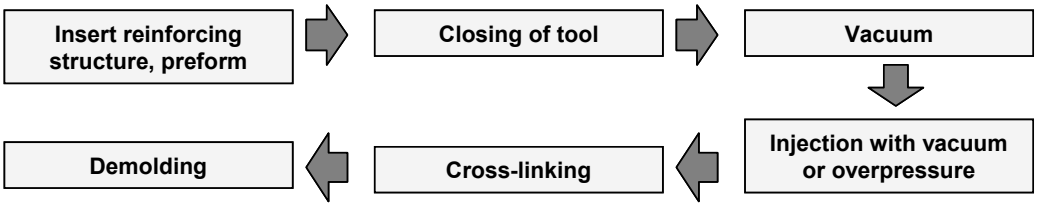

Figure 1.1: RTM technology, flow diagram

VARTM, Vacuum Assisted Resin Transfer Molding processes or Scrimp® (Seeman Composite Resin Infusion Molding Process) and processes similar to Scrimp®, which are vacuum or partially pressure assisted production processes where the main flow direction of resin is characteristically perpendicular to the shell shaped reinforcing structure, are also classified into this group. Besides these, combined technologies, such as Resin Infusion under Flexible Tooling, RIFT [47], a Differential Pressure Resin Transfer Molding, DPRTM [48], or Single Line-Injection, SLI [49] are also applied.

The excellent properties of fiber reinforced polymer composites can be utilized to the greatest extent if the fibers can be oriented in a given direction within a composite. This orientation makes it possible to obtain the outstanding strength properties in the structure only in the required directions utilizing the anisotropic properties of the composite. Orientation can be provided with different textile industrial processes, so-called preform technologies, during composite production.

In case of injection processes, the formation of three dimensional structures may be hindered since it requires complex design considering the build-up of the reinforcing system. Nevertheless, the vast range of materials used as reinforcement in the industry and their several ways of processing verifies the great attention in composite part design.

1.1 Three dimensional preforming by means of stitching technologies

During industrial application the parts made of composites are usually subjected to complex, multilateral loading. This aim can be realized by the orientation of fibrous reinforcing structures in composites. When applying injection molding processes, a significant step of production is to prepare the reinforcing structure and place it into the mold.

The net-shape, ready to impregnate semi-finished products manufactured by preform-technologies are the advantageous features of the RTM technology [50]. The preforming process reduces the total production time of fiber reinforced polymer composites (FRPC) and improves the quality assurance of the complete part [51]. The assembly of 2D preform components, so-called “sub-preforms”, is in an early development stage. The main focus of investigations is the optimization of the machine technique, for example a one-side-stitching technique to fix preform sub-components on one side accessible reinforcement [36, 37, 52]. The relation between the stitching parameters and the mechanical properties of stitched FRPC structures concerning the position of knots in the structure, especially by using a double lock stitch, was already explained in the literature [40]. In case of the double lock stitch, the loop is formed by the needle and the rotary hook uses two fibers (Needle Thread (NT) and Bobbin Thread (BT)). The needle leads the upper thread through the fabric, then the rotary hook crosses the loop formed this way with the lower thread located

in the bobbin. This way a knot is formed from the bobbin and needle thread (Figure 1.2). The presser foot compacts the fabric in the moment of stitch formation, and the transporter forwards it and this way defines the stitch length. Both the force exerted by the press foot, and the force of the bottom and upper threads influence knot forming, seam quality and the mechanical properties of composite parts [53].

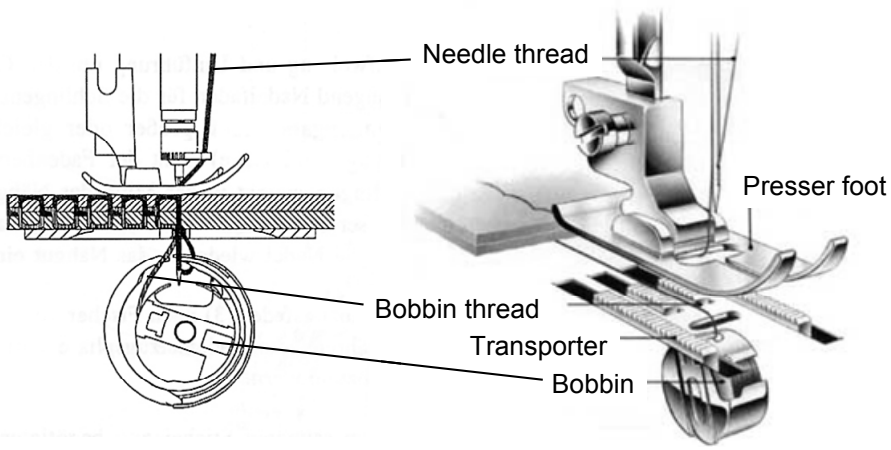

Figure 1.2: Shematic set-up of the double lock stitch

Double lock stitch is the most widespread stitching preform technology to form seams of two dimensional preforms. The advantages of this seam type are that different threads can be used as bottom and upper ones, the great holding force, hence large degree of compacting in the preform, and that the parameters can be set in an easy and exact way. Its disadvantage is that a greater thread slip can be formed in the fabric at the stitch holes, due to the structure of the seam. The investigation of stitched composite parts revealed that the seam influences the mechanical properties of composite parts least in a negative way if the knot formed by the upper and lower threads is located on the lower or upper part of the textile and not in the stitch holes [54].

A good illustration of 3D preform technology assisted by stitching is the production technology of the complex U-profile stiffener built up of modules (Figure 1.3) [55]. The task of the framework is to improve the stiffness of an aluminum profile. In case of the stiffening structure, the application of carbon fiber reinforced composites is necessary because the small own weight besides the excellent mechanical properties can provide outstanding stiffness in the system.

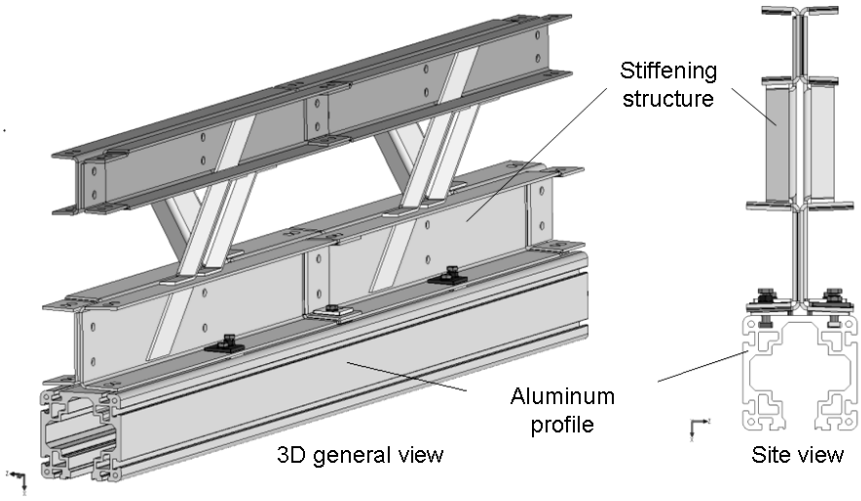

Figure 1.3: 3D CAD modell of the aluminium load-bearing console with FRPC-stiffener structure in X assembly

The three dimensional CAD model of the stiffening system can be prepared based on strength dimensioning, the characteristic mechanical stresses and the production technology. The fiber orientation of the composite system is defined in this model in the design phase. A two dimensional lay-out, in which the layer order of the components can be determined, is generated from the model. The layer order can be defined based on the loading and the available reinforcing systems.

Simultaneously the number of preforms necessary for the production of the final preform has to be defined. It is often impossible to create the final preform in one step. In those cases it can be created from simple modules, so called tailored reinforcements (TR), from which the complex final preform can be manufactured. In practice a multi step preform technology is necessary, hence from the single TRs, first a sub-preform is created, and more sub-preforms will finally make up the final net-shape preform that is ready to impregnate (Figure 1.4).

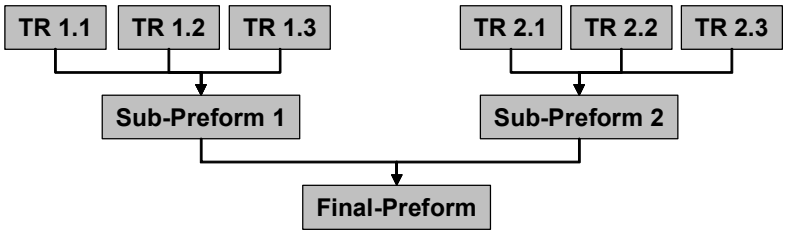

Figure 1.4: Preforming concept

After the determination of the single preform levels, and hence the necessary steps, the stitching and cut-out patterns of TRs can be planned based on the CAD drawings. These plans include all the seam and cutting contours necessary for the production of the preform. There are three different seam types for preforming.

The seams of essential importance in composite structures are defined as *structural stitches*, such as the interplain ("Z"-direction) reinforcement formed from high performance fibers or the fixing of different load transmission elements in composite structures.

The aim of the so-called *joining* or *preforming stitching* is to bind the single fabric layers to each other. These seams are applied as rasters when creating TRs, and they increase the friction between the layers besides their compacting function or they are applied to define the contours of TRs. This way TRs become easier to handle and more stabile. The contour lines are typically double seams that run parallel in a distance of 3-5 mm along the contour, and the real cut contours of the TR are located between these seams. This way the cutting edge remains regular. The seams on the two sides keep the reinforcing fibers fixed, and hence prevent fringing and aid cutting by fixing the threads.

The third type of seams is *assembly stitching*, the task of which is to fix the single TRs and sub-preforms together, and hence create a preform of higher level.

In case of the FRPC stiffener structure, the two dimensional CAD model was created with the help of the AutoCAD software (supplier: Autodesk Inc.), and the stitching as well as cutting contours were saved as *dxf* files. The *dxf* file format can be processed by the driver program (SNA Programmbetrieb, supplier: Parker Hannifin GmbH & Co. KG) of the programmable Hauser stitching machine (supplier: Parker Hannifin GmbH & Co. KG). With the help of the PC module of this stitching machine the parameters of the seam types can be defined. The stitching patterns and nesting can be modified with the help of this software in order to increase material yield. Cutting contours are processed with the PrefromCAD software developed for the programmable Bullmer cutter (Assyst Bullmer Procut L 5001 LV; producer: Assyst-Bullmer Spezial-Maschinen GmbH & Co. KG) (Figure 1.5). The software was developed in the cooperation of ProCom (ProCom Ingenieurunternehmen für computergestützte

Produkte GmbH) and IVW (Institut für Verbundwerkstoffe GmbH) in the framework of a „Pro-Preform RTM“ project (Prozessentwicklung und ganzheitliches Leichtbaukonzept zur abfallfreien, durchgängigen Preform-RTM-Fertigung, Förderkennzeichen: 02PP2476) supported by the BMBF (Bundesministerium für Bildung und Forschung) [55].

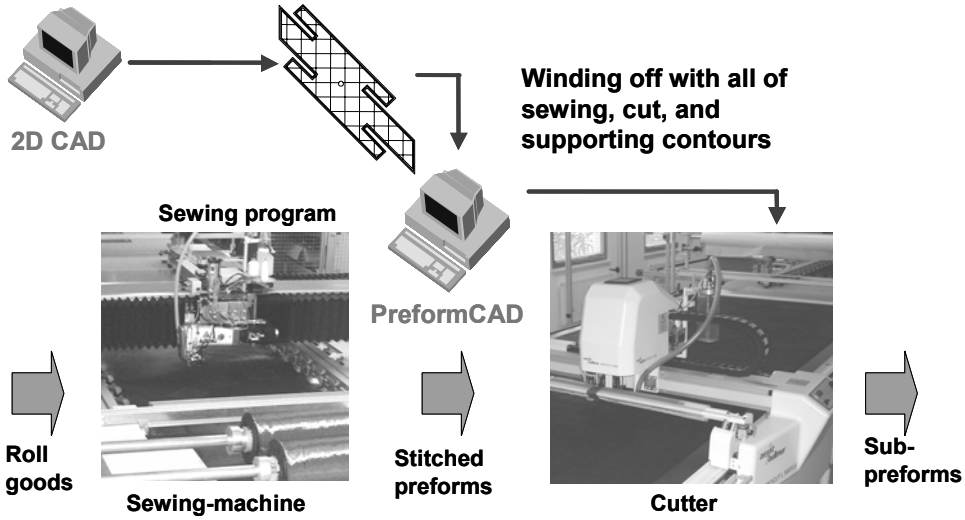

Figure 1.5: Shematic process flow for the preform manufacturing by means of stitching

The stiffening structure is modular, hence can be fitted to load bearing structures of different dimensions. The length of the module is 1000 mm, and the construction is built up in a way that one type of module of the same geometry forms the whole structure as a repetitive element. In this case the two parallel modules were turned towards one another and this way an I-profile truss was created from U-profile elements, and hence the stiffness of the construction improved as well. The elementary module is of “Z” arrangement and is composed of two horizontal “U” profiles of different size but of similar geometry and a connecting element located in 45°. The whole module was injected in one step, hence its mechanical properties did not deteriorate and there is no need for additional fixing elements that would increase the mass. Owing to the geometry of the module, the ready-to-impregnate, net-shape final preform of the total module is composed of three sub-preforms (Figure 1.6). The construction is built up in a way that the fiber orientation and the layer order of the single sub-preforms in the module is the same, hence production is cost effective and preforming is simplified.

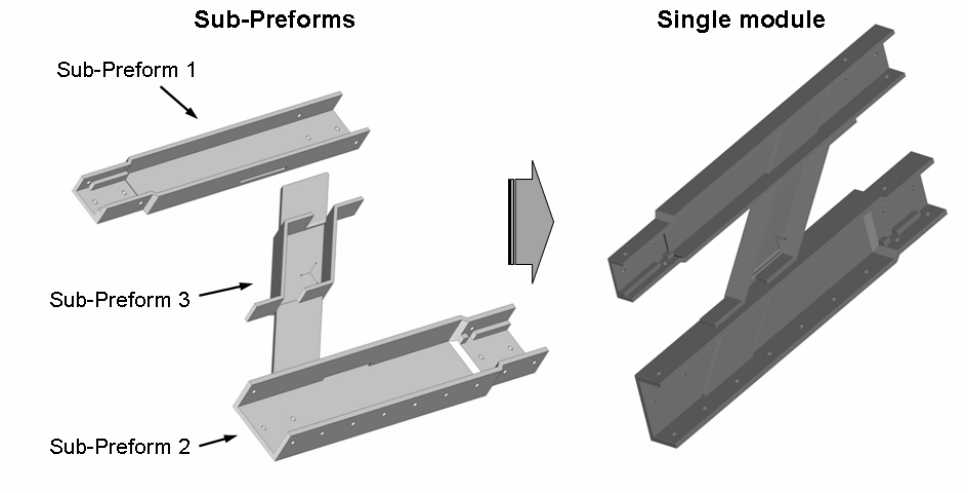

Figure 1.6: Preform concept for a single module of the stiffening structure [55]

The thickness of the single sub-preforms is around 5 mm. The difference between the external and internal radii of the bent elements results in the different extent slip of the layers. Hence the preform does not fill the mold totally along the edges, and those parts will only be filled with the matrix material during injection. Furthermore, the holes created during preforming would distort significantly. In order to prevent this phenomenon the sub-preform was divided into three TRs. The TRs are of different widths (the value of difference is given), hence if they are laid on each other and the side walls are folded up, the edges of the U-profile become of regular shape, and the holes of the TRs will be on the same axis (Figure 1.7).

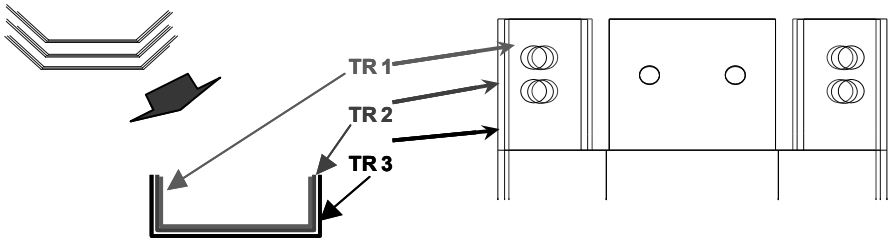

Figure 1.7: Gradual composition of the Tailored Reinforcements (TRs)

The TRs are built up in a way that they can be formed from the same pre-product (CF-NCF). As the TRs are laid on each other, a symmetrical layer order is formed in the sub-preform. This is necessary due to mechanical considerations, since the loadings in the asymmetric layer order would result in a torsion type distortion, and this way the stiffening module would warp. One TR is built up of two asymmetric CF-NCF layers of ± 45° orientation so that the specific weight of the fibers in the +45°

direction is 2 x 625 g/m^2, while that of fibers in the -45° direction is 2 x 156.7 g/m^2 (Figure 1.8). This asymmetric structure provides the necessary orientation of fibers in the single module that can take the arising load.

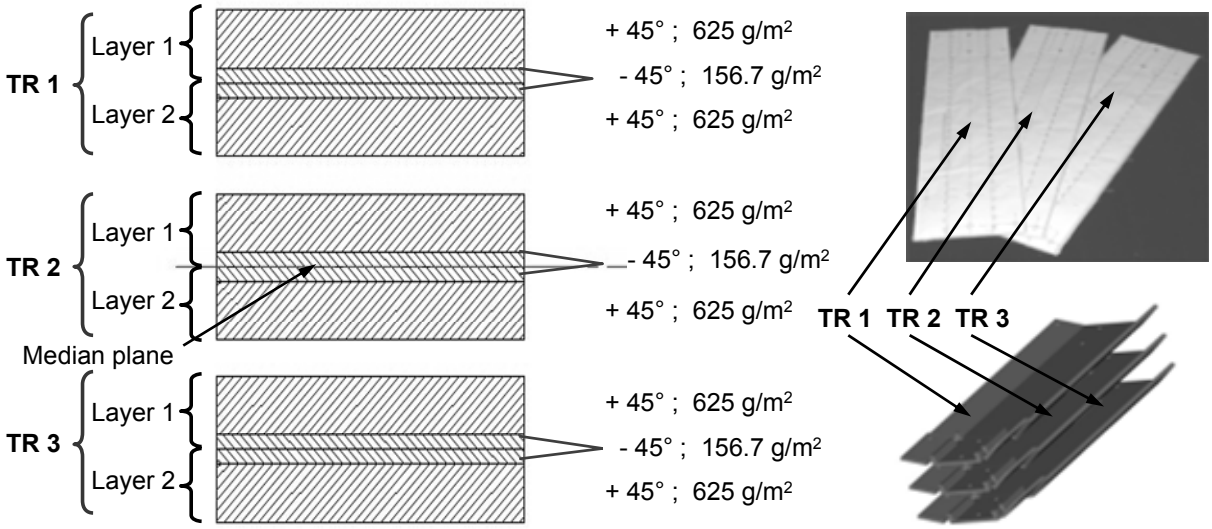

Figure 1.8: Set-up of the Tailored Reinforcements

The ±45° orientation in the single NCF layer is formed owing to the production technology. The reinforcing fibers are laid in the ±45° direction during production. Hence the 0°-90° fiber orientation required in the sub-preforms can be achieved if the TRs in the stitch field are rotated by 45° in a way that the direction of +45°containing more fibers would correspond to the 0° direction of the TRs, i.e. they should lie parallel to their longitudinal axis in the material. Since the TRs are built up of the same layers, the seam that belongs to the total single module can be taken on the two layers of CF-NCF pulled in by the stitching automate. The 2430 x 900 mm stitching pattern contains three times three samples of TR, i.e. 9 TRs that belong to the three sub-preforms (Figure 1.9). Firstly, a preforming stitching of 0°-90° orientation was created on the stitch field. The main aim of this stitching or raster seam is compacting, while it also helps the handling of TRs, and prevents the slip and distortion of parts. In the next step double seams that define the cutting edges, i.e. the contours of the product are created. The theoretical contour line of TRs, hence the cutting edge, is located between these two seams. Since the incisions necessary for the assembly of the stiffening module holes and the sub-preforms are

already created during preforming in the reinforcing structure, their contours are also fixed by the double contour seams.

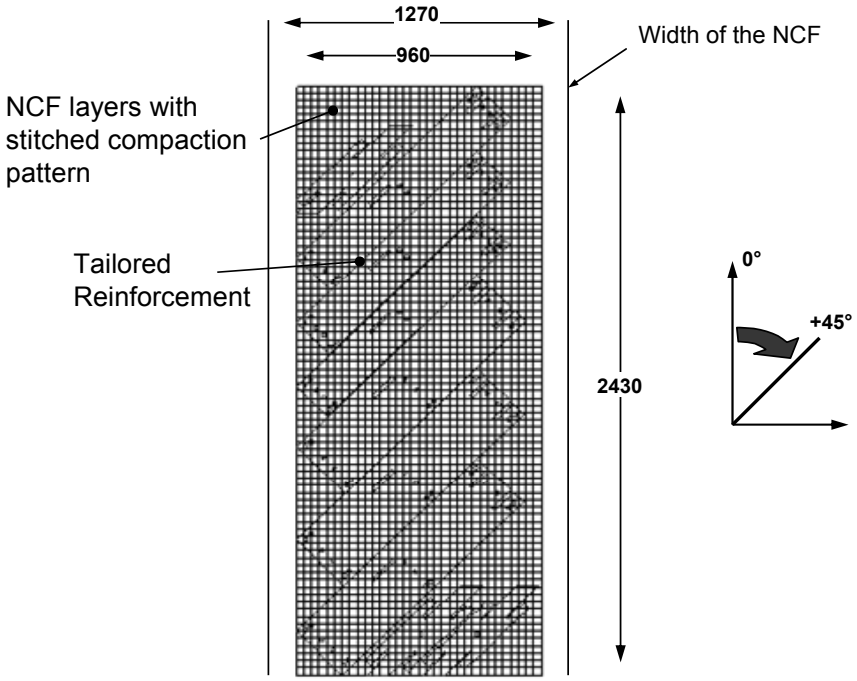

Figure 1.9: Position of the Tailored Reinforcements (TRs) in the stitch field

During stitching preforming it is possible to create additional auxiliary seams. With the help of these auxiliary seams reference points that can help the positioning of the cutter in the next step can be formed in the stitch field (Figure 1.10). It is possible to define a tighter seam raster during program planning, and this way a better stability can be provided for the areas that are loaded in a greater extent during cutting and when putting into the mold.

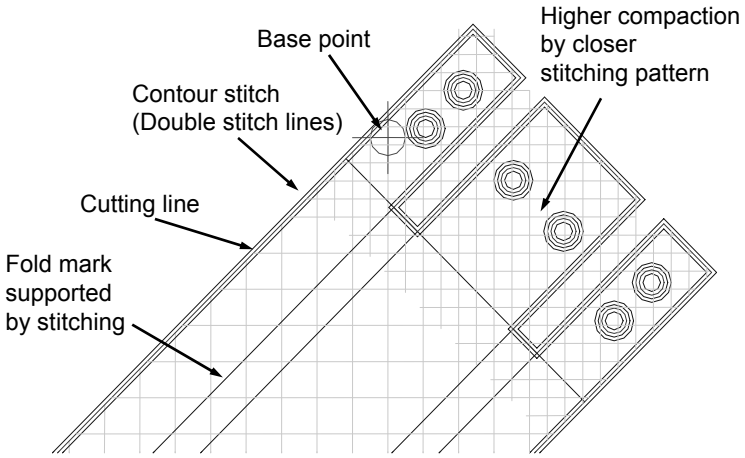

Figure 1.10: Stitch types on the stitching field

The tighter raster seam can result in a greater extent compacting, and hence can ease the fitting of critical preform parts into the injection mold and the mold closure.

After forming the whole seam structure, the stitched field is transported further to the cutter synchronized with the stitching machine. The table of the cutter is a vacuum table and a transporter belt in one. A layer of air-permeable paper is laid on the surface of this table, and then the stitched fabric is placed on it. Fixing the fabric with vacuum is aided by the thin foil placed on the surface. With the help of the foil, the vacuum affecting a large area holds down the stitched NCF to be cut efficiently. The applied cutter has an offline camera matching system with the help of which the reference point of the cutting head can be positioned exactly; hence the pre-programmed cutting contour can be matched exactly with the real contours. This positioning ensures that the cutting contours are located exactly between the double seams bordering the contours. Fixing the reference points can be achieved with the help of the already mentioned auxiliary stitches or the characteristic peaks of the stitched field (Figure 1.11). Camera matching is enhanced because the textile can be enlightened by UV waves in the visibility range of the camera. This way the auxiliary threads or the UV-active, optical by bright stitching threads help the identification of the reference points and the number of disturbing optical phenomenon can be reduced.

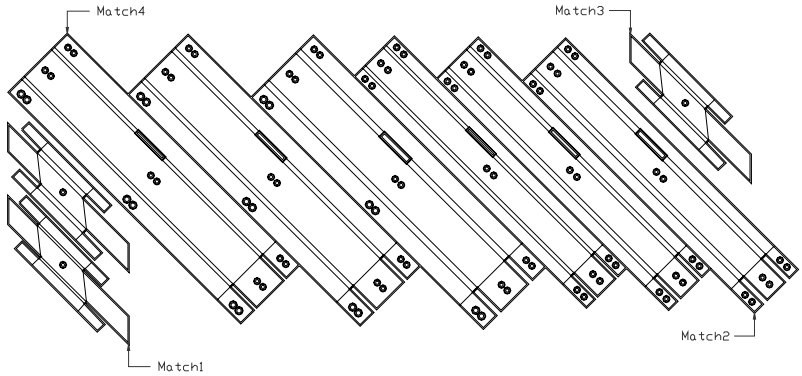

Figure 1.11: Cut contour with matching points for the visual re-adjust of base points

The preforms are cut out with the already mentioned programmable cutter. Cutting is carried out with a rotatable steel flying knife. This is the most common cutting method in preform technology. Cutting can also be done with laser or ultrasound, or with punching in case of simple, unchanged geometry and large scale production. Due to

their small diameter the holes are created with rotating tubular cavity tools. Cutting out the small diameter (<20 mm) holes with a flying knife would deform the fabric strongly and fibers would slip.

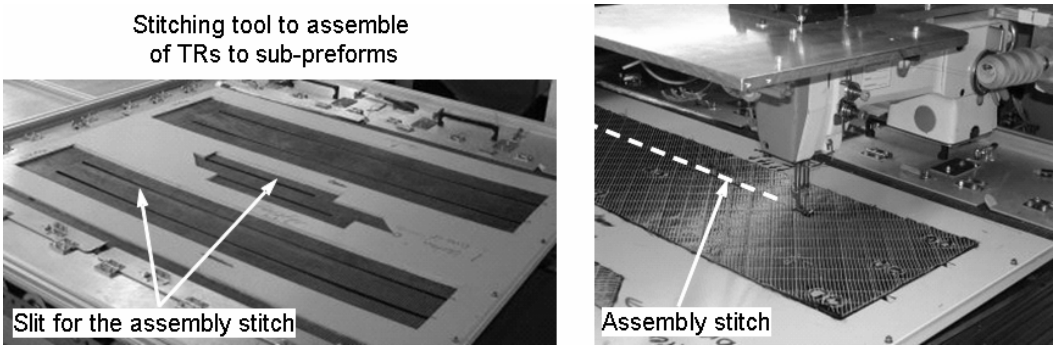

Figure 1.12: Seam supported assembly of the Tailored Reinforcements (TRs) to Sub-Prefroms

After cutting, the assembly of the nine tailored reinforcements is completed using a stitching template. The TRs belonging to the single sub-preforms match the cascading sockets of the template. This way the relative position of the TRs is defined. The TRs are only stitched together with an assembly stitch along the folding edges of the sub-preforms, hence the side walls of the U-profiles can be folded without the distortion of the TRs. The function of the assembly stitches is to define the folding edges and to join the TRs. The base plate of the stitching template has longitudinal incisions to aid stitching, and through these incisions stitches are formed with a programmable stitching machine fixed on a console (supplier: KSL Keilmann Sondermaschinenbau GmbH) (Figure 1.12).

After this stitching assembly, the further assembly of the sub-preforms is not necessary, since that would result in a too large and complex preform, the handling and placing of which into the injection tool would be more difficult. Furthermore, the joining surfaces do not have to be stitched together (structural stitching), and hence the mechanical properties do not have to be improved, since the large joining surface of the single preforms provides the sufficient stability after injection.

The exact positioning of the preform in the injection mold is aided by the holes and pins, which define the exact size of the holes, created during preforming (Figure 1.13). The two longitudinal beams (sub-preform 1, 2) are placed into the mold

followed by the joining element (sub-preform 3). The horizontal joining surfaces of the joining element are lead through the corresponding incision of the longitudinal element. In order to form the holes on the side surface of the U-profile, cores that involve the pins are needed in the mold.

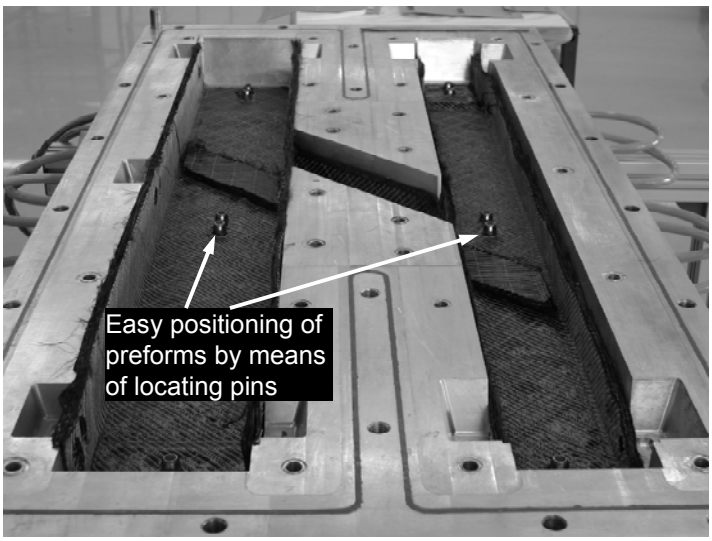

Figure 1.13: Laid net shape preform in the opened lower RTM tool

Hence the mold becomes more complex, however this way net-shape production technology can be achieved, and as a result there is only need for deburring and not for remachining (Figure 1.14).

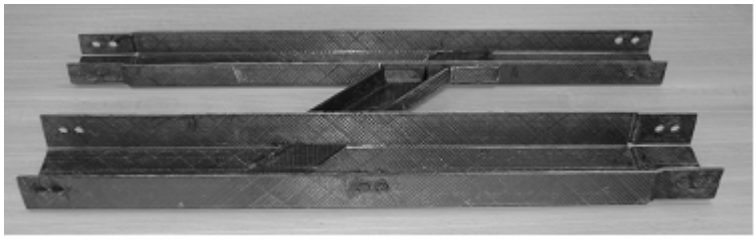

Figure 1.14: Trimmed net shape-RTM part [55]

Preform technology aided by automated stitching provides an alternative for the production of complex, 3 dimensional preform production as revealed by the example above. It can be seen that the computer aided process makes it possible to produce preforms efficiently, and that is inevitable when applying large scale RTM technologies.

Obviously, during planning the technology and the adequate preform level have to be determined, i.e. the necessary preform steps have to be defined (Figure 1.15).

Preforming above the necessary level makes a process more expensive due to the derivative technological steps. On the other hand, if the preforms are not prepared adequately, it makes placing into the mold difficult, hence this step will be more time consuming, and the whole production will be more costly. Furthermore, during planning it has to be decided whether absolute net-shape technology should be applied when producing the part. In some cases, the final shape can be achieved with remachining (e.g. drilling, milling) in a more cost-efficient way than with the application of complex injection tools and a multi-step preform technology.

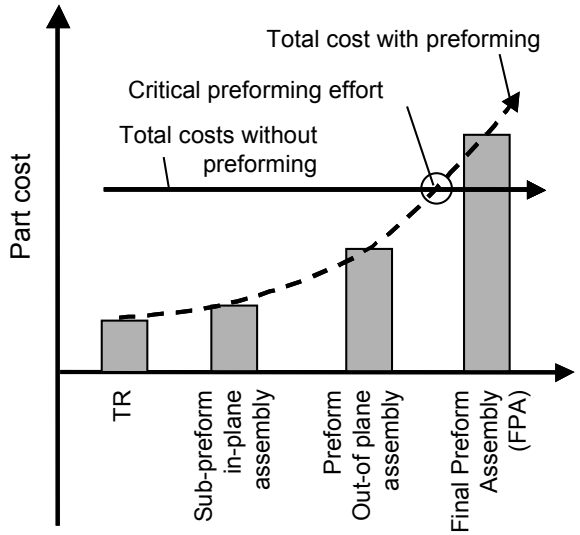

Figure 1.15: Relation between manufacturing cost reduction and preforming effort [51]

1.2 Philosophy of the stitching supported preform-LCM process chain

Quick placement of the preform into the mold, easy mounting, and fault free single shot resin impregnation is an economical method of FRPC manufacturing. Preforms manufactured within the mold tolerances reduce the mold placement time and also avoid the possibility of resin channel formation. If the preform manufacturing is performed by keeping the actual mold geometry and the tolerances in mind, then the next process tasks are easier and quicker than the conventional methods. Starting from the selection of textile material to the assembling of 2D preforms reduces the total molding time. As the preforms are cut to the exact shape, fiber setting between the molds can be avoided, thus there are limited difficulties in the mold closure. Again the inserts and other locally strengthening or toughening elements can be placed at

the exact position and fixed by means of stitching. It takes less time to position those elements in the mold. Figure 1.16 shows the continuous chain from textile selection to the product manufacturing which helps to manufacture 3D parts with required fiber orientation at different sections. The flow diagram shows also the specific benefits of the single process steps [50].

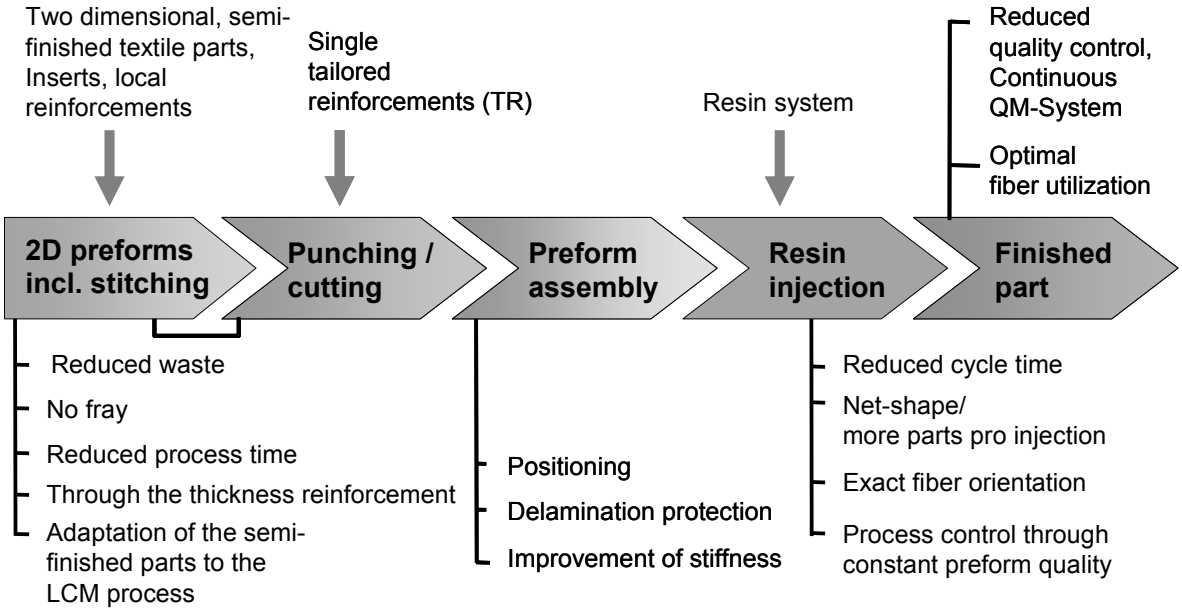

Figure 1.16: Preform-LCM process chain

2 Application of soluble bonding yarns to assemble 3D preform structures

Sometimes the predefined position and fixation of two dimensional reinforcing structures cannot fulfill the requirements and the production of fixed 3 dimensional preforms may also be necessary. Hence the preform design and the way it can be handled and placed into the mold are important features. Placing into the mold enhances a technological step if the size and geometry of the mold is the same as that of the preform placed into it. These three dimensional pre-products can be manufactured with three methods:

- direct preforming technologies
- with thermosetting or thermoplastic binder
- assembly and compaction using stitching technology

Direct textile technique processes, such as the Ford Programmable Preform Process (F3P) [56], or the Programmable Powder Preform Process (P4) [57] can be applied to manufacture preforms directly from fibrous reinforcing materials without any intermediate textile industrial process [58]. The essence of the process is that the fibrous material in the form of a roving is cut with a cutter-sprayer and mixer head. The short fibers formed this way are mixed with the binder powder or fluid and are pressed to the surface of the heated preform mold. The short fibers mixed with the binder are kept on the surface until complete melting and cooling with the help of air vacuumed through small capillaries in the mold. When the fibers fixed this way are removed from the surface of the preform mold, a three dimensional preproduct that provides a non-oriented, short fibrous reinforcement for composite parts can be obtained.

When a thermoplastic powder binder material of low melting point is used, it is spread on the surface with a roll or a spray jet. In case of thermosetting materials, there is a possibility to spread the material evenly in the form of a solution. The treated woven layers are put on each other and are heat treated; hence the binder material is molten and cooled down. This is how the layers are adhered to each other. This method makes it possible to shape textiles in three dimensions, since they keep the original shape after cooling.

The third possibility to produce spatial preforms is the application of the stitching technology already detailed in the first chapter. During stitching preform production threads that melt at low temperature are necessary because then the two dimensional sub-preforms can be fixed in a three dimensional form in a thermoforming process and this way the step of placing the preform into the mold is made significantly easier and quicker.

2.1 Application of bonding yarns in 3D preform manufacturing

The application of yarns made of fibers that melt at low temperature is already widespread in the textile industry. The following experiments were carried out using co-polyamide and co-polyester yarns of different melting points produced by EMS Griltech (www.emsgriltech.com).

Thermoforming tests were completed on a biaxial ± 45° CF-NCF material, the specific weight of which was 50 g/m^2 (producer Saertex GmbH & Co. KG). Stitching was carried out with a co-polyester yarn type Grilon KE-60 of 60°C melting point and 167 dtex linear density. The specimen in Figure 2.1 is composed of two 220 x 180 mm units that were fixed to each other with a 5 x 5 mm compacting seam.

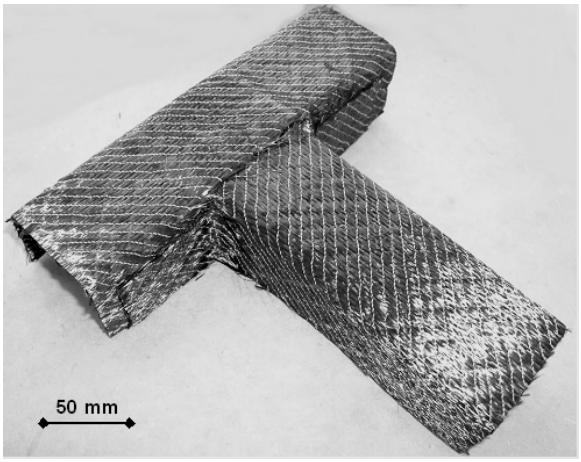

Figure 2.1: Bonding thread stitched and thermoformed specimen (dry preform)

Compaction was carried out on a programmable stitching automat. The yarn strength of the bobbin as well as that of the upper yarn was reduced significantly due to the unfavourable mechanical properties of the yarn. Then a “T” shape was created by cutting the two dimensional textile at the appropriate places. The preproduct composed this way was heated after having been placed on a mold of adequate

geometry and closed by a vacuum foil. With the help of the vacuum, the foil pressed the preform onto the mold and the stitching threads melted at around 70°C hence were distributed as an adhesive among the carbon fibers (Figure 2.2). After cooling, the foil was removed from the material and the result was a three dimensional, easy to handle preform that can keep its shape. This 3D preform production experiment verified that the commercially available binder stitching yarns can be applied in the production of three dimensional preforms well and cost efficiently due to their low melting temperature.

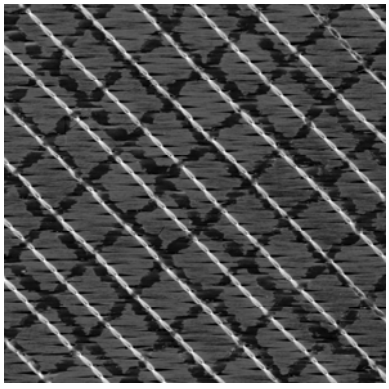

Figure 2.2: 5x5 mm stitching pattern on a CF-NCF reinforcing structure (after thermal treatment)

2.2 Testing of the perform mechanical properties

The majority of composite parts consist of a certain stacking sequence which is then repeated n-times. This basic sequence will be called “unit cell” throughout this dissertation. The sequence for the unit cell used in this study is from the top towards the bottom [0, 90°, +45°, -45°] (Figure 2.3, Figure 2.4). The unit cell is assembled by stacking two biaxial CF-NCF layers (+45°, -45°) each with an area weight of 250 g/m^2 (supplier: Saertex GmbH & Co KG).

The stitching was introduced by a Pfaff 1421 stitching machine, which performs a double lock stitch (Figure 1.2). The bobbin thread force (F_{BT}) was set to 53 cN, while the needle thread force (F_{NT}) was 260 cN. The ratio of the needle and bobbin thread defines the position of the knot.

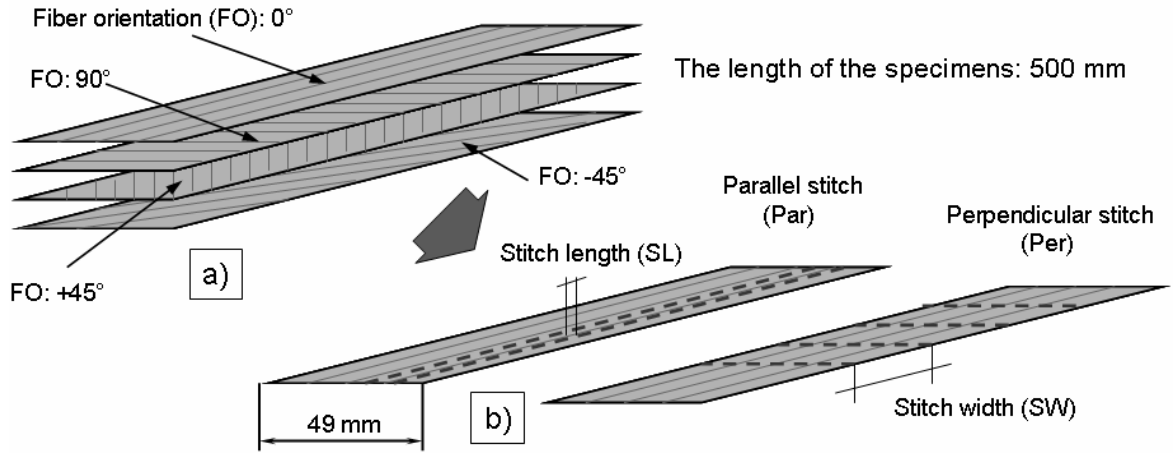

Figure 2.3: Specimen set-up for preform stiffness testing (DIN 53362)

In the specimens the knot was formed on the -45° layer facing the operator. The reason for this choice lies in the nature of the stitch formation and the intended bending direction. Any kind of stitch will generate a more or less elliptical cone wich decreased its cross-sectional area towards the knot of the stitch. If the unit cell material is bent appropriately at a later stage, these stitch holes will partially close. The bonding yarn that was used as a bobbin as well as a needle thread in this experimental investigation is EMS-Grilltech Grilon K-140. This bonding yarn is a co-polyamide with a melting range of 130-145°C. The yarn itself consists of 23 filaments with a total titer of 167 dtex and 100 twists per meter in z-direction.

The parameters that are modified for the sample preparation are displayed in Figure 2.3b, which are the stitching length (SL) and the stitching width (SW). Besides these parameters only the number of the unit cells that are stacked on top of each other is modified.

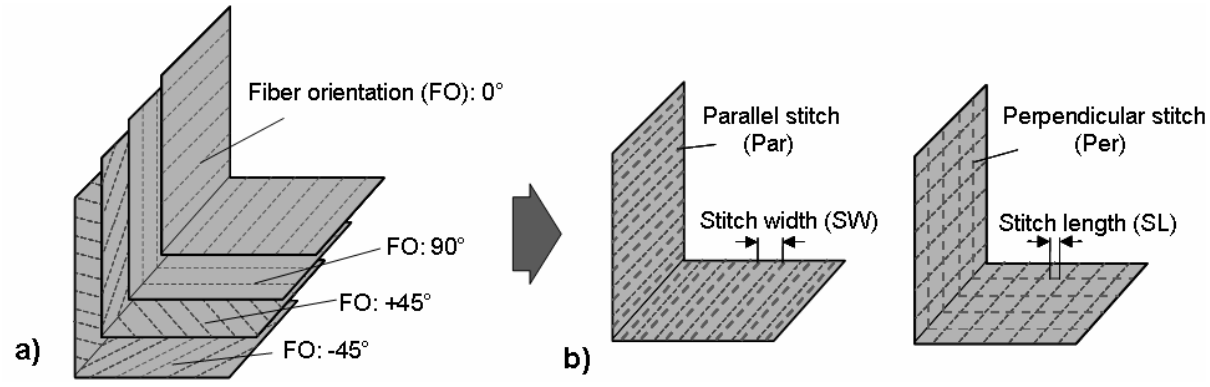

Figure 2.4: Nomenclature of the specimens for spring-back testing

To develop their adhesive effect the yarns need to be brought into the melting range of the thermoplastic yarn. For the purpose of maintaining a constant compaction pressure as well as a repeatable temperature profile to melt the yarn, all thermal treatments have been performed with the set-up displayed in Figure 2.5.

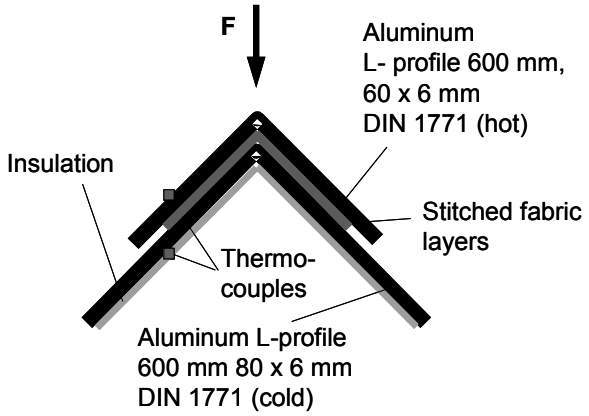

Figure 2.5: Set-up for the thermal consolidation of the stitched samples

The thermal treatment consisted of placing the unit cells on top of the larger L-profile and prefixing them there with small stripes of adhesive tape. Then the top portion, the square block and the small L-profile are taken out of the 250°C hot oven and are placed on top of the unit cells (stitched layer fabric).

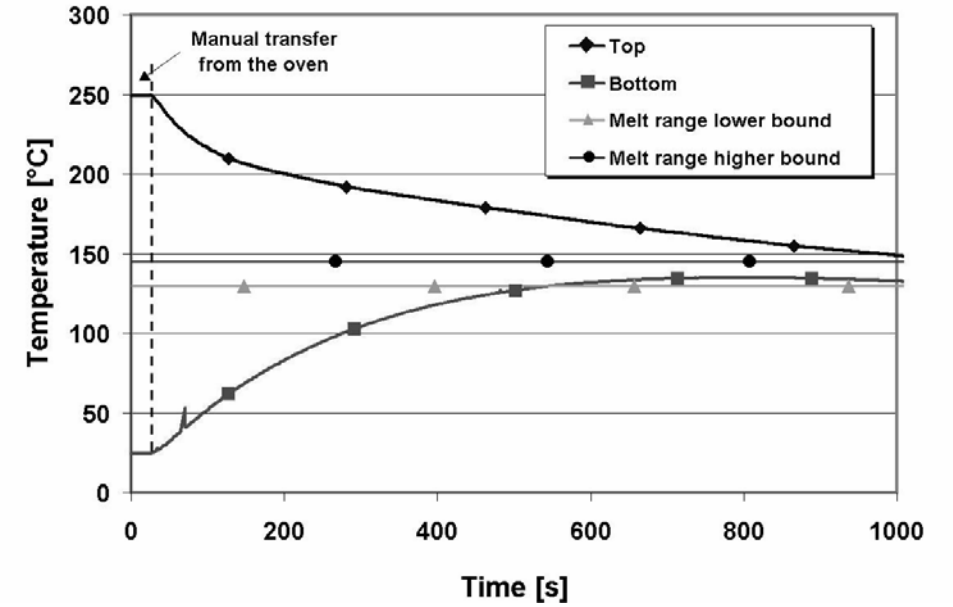

Figure 2.6: Thermal process of the consolidation

The temperature profile for the thermal treatment can be seen in Figure 2.6. It is evident that the complete stack reaches a temperature above the lower melting

range of the bonding yarn, since the thermocouple is positioned on the outer side of the L-profile, covered by the insulation.

2.3 Experimental procedure

The aim of the experimental procedure was to investigate the influence of the stitching process parameters on the characteristic of the preform. Firstly the preform characteristic is defined by measuring the perform bending stiffness, the spring back angle, and the restoring force for stitched an unstitched CF-NCF (Saertex).

2.3.1 Bending Stiffness

The bending stiffness for this type of material was determined by a cantilever test, according to DIN 53362 (German Standard) [59]. The specimens were cut in stripes of 49 mm width and 500 mm length using an accordingly shaped rectangular punch (Figure 2.3). Then the stripes were placed carefully into the measurement device and covered with a ruler. The beginning of the scale of the ruler was leveled with the front edge of the fabric facing the slope. By slowly pushing the ruler to extend over the edge, the fabric underneath was effected by the gravitation, hence bent towards the 138.5° plane of the apparatus schematized in Figure 2.7. The experiment is stopped, as soon as the free front edge touches the sloped plane. The result is the free length $l_ü$ wich is required for the calculation according to the formula of the bending stiffness provided in Figure 2.7.

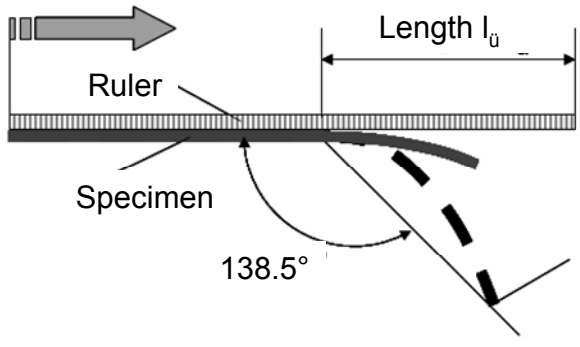

$$G = \frac{g * m}{b * l}\left(\frac{l_ü}{2}\right)^3$$

G= Specific bending stiffness [mN*cm]
b= Width of specimen [mm]
l= Length of specimen [mm]
g= Gravitational constant [m/s²]
m= Mass of specimen [g]
$l_ü$= Free length of specimen [mm]

Figure 2.7: Schematic set-up for determination of the bending stiffness according to DIN 53362

In a first step six configurations were tested with 5 repetitions each. These configurations were:

- Unmodifed biaxial CF-NCF [0°,90°]
- Unmodifed biaxial CF-NCF [+45°, -45°]
- 1 unit cell [0°,90°,+45°,-45°], stitching length 2 mm (SL2), stitching width 5 mm (SW05), without thermally treatment
- 1 unit cell, stitching length 4 mm (SL4), stitching width 10 mm (SW10), without thermally treatment
- 1 unit cell, stitching length 2 mm (SL2), stitching width 5 mm (SW05), thermally treated
- 1 unit cell, stitching length 4 mm (SL4), stitching width 10 mm (SW10), thermally treated

The results of this baseline test are displayed in Figure 2.8. It is obvious and easy to understand that the bending stiffness of the biaxial CF-NCF [0°,90°] is superior to the biaxial CF-NCF [+45°,-45°], since the fibers of the 0° direction extend parallel to the 500 mm edge. Once two layers of biaxial fabrics are stitched together to form a unit cell, the bending stiffness shows an effect concerning the combination of stitching length (SL) and stitching width (SW).

The combination of SL2 with SW05 is exceeding the measured values of the SL4 SW10 combination. The tension of the stitch information is locally “binding” the fiber stacks together, thus restraining the movement of the fibers relative to each other, and hence a higher bending stiffness arises. Additionally, the number of seams per width of the samples supports the development towards higher bending stiffness.

The third part of columns in Figure 2.8 reassembles the result of the bending stiffness after the stitched unit cell samples were thermally treated as mentioned previously. Therefore, the thermoplastic thread has molten and adhered to the carbon fibers surrounding the thread. The reason for the decrease in the bending stiffness compared with the results of thermally untreated samples can be explained by the fact that a part of the thread tension has been relieved during the melting process. Obviously, the thread tension was higher than the compaction pressure applied during the thermal treatment.

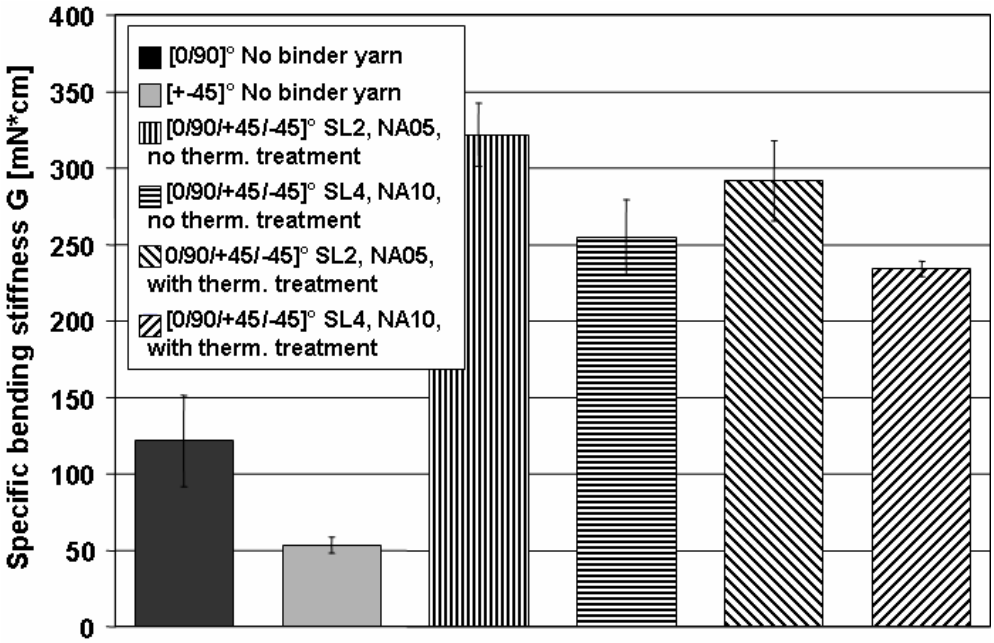

Figure 2.8: Specific bending stiffness of one unit cell according to DIN 53362

As expected the specific bending stiffness increases with the ascending numbers of unit cells per layer. Additionally, the bending stiffness of the high stitch density (SL2, SW05) exceeds the bending stiffness of the low stitch density (SL4, SW10). This can be explained by the amount of bonding thread per unit area. By increasing the stitch length and the stitch width, the amount of bonding thread per sample could be noted. The origin of this, failure could be located in-between the individual layers of the exterior unit cell of the stitching process, only the top and the buttom layer is encompassed by a thread (needle and bobbin thread) directly. Each layer between the top and bottom is only in contact with a droplet of adhesive coming from the bonding thread. This fact explains the location of the failure.

2.3.2 Spring back angle

Next, the evaluation of the spring back angle was performed. When the shape of the preform is modified, i.e. it is bent to comply with a certain shape, this deformation comprises of two components, a plastic and an elastic part. The spring back angle is the result of the elastic portion of the deformation. To produce manageable preforms that maintain their predefined shape is one of the ultimate goals of the preforming process. Therefore, the spring back angle and knowledge on how the introduced bonding yarn affects the spring back angle is of high interest. The definition of the spring back angle is defined throughout this work is introduced in Figure 2.9. The

deviation of the original geometry, which was a right angle, can be seen in the schematic graphic.

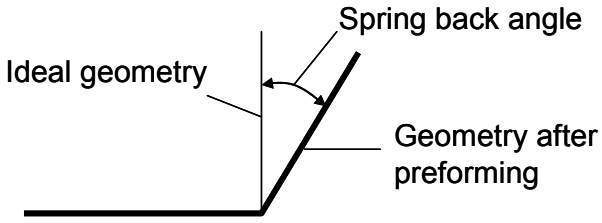

Figure 2.9: Effect of spring back after the pre-compaction step

The results of the investigations of the spring back angle are shown in Figure 2.10. The first important result is when the amount of unit cell is kept constant, there is a significant difference between the perpendicular and parallel stitching direction for all samples and stitching parameters.

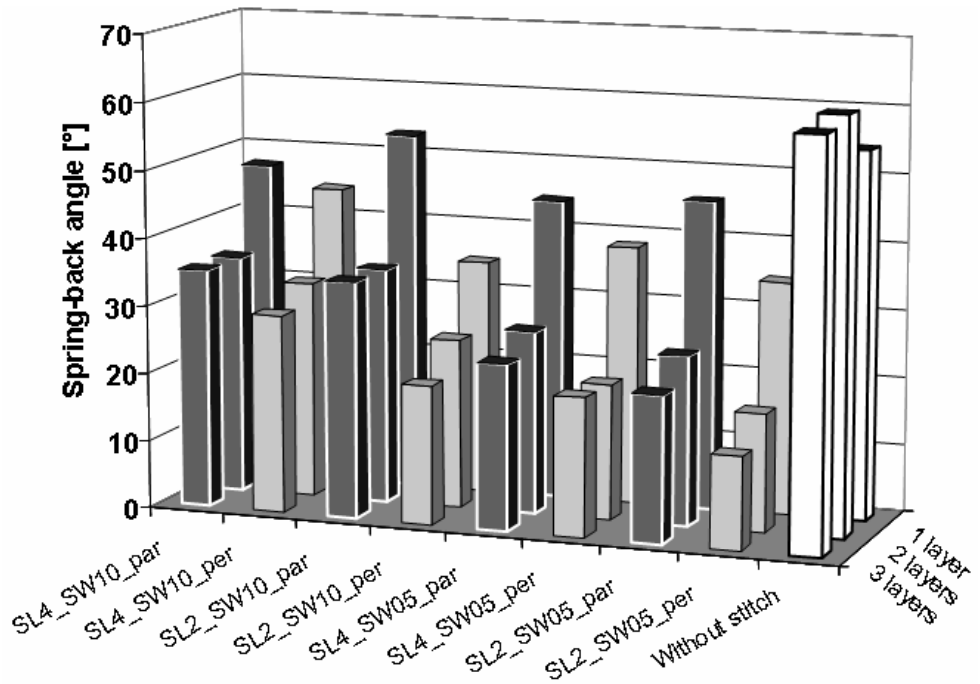

Figure 2.10: Influence of the number of unit cells per preform on the spring back angle

The perpendicular stitching direction, which is the bending line of the L-shaped geometry (Figure 2.4), always exhibits smaller spring back angles than the parallel direction. If the number of unit cells are kept constant and only the stitch length between two identical patterns is varied from 4 mm to 2 mm, the spring back angle is also reduced in every case. Similarly, the reduction of the stitching width from 10 mm

to 5 mm results in a reduction of the spring back angle. The increase of the amount of unit cells per sample also affects the spring back angle positively. This is reasonable, since the stitching between the unit cells provides a possibility to transfer the existing shear loads from the one layer to the next, and this was not possible before.

2.3.3 Restoring force

This experiment helps to define the restoring force required to eliminate the spring back angle. The same specimens was taken which were used for the spring back testing were examined in the following tests. The experimental set-up of the restoring force testing is shown in Figure 2.11. One side of the L-shaped specimen is fixed on the base plate with a metallic clamping. With help of a guide roller - which guides the thin PA fiber fixed on the free site of the specimen - and the sensitive spring scale it was possible to measure the restoring force required for the elimination of the spring back angle of the specimens after thermoforming.

Figure 2.12 shows that the preforms with 2 mm stitch length and 5 mm stitch width, i.e. the specimens with the highest stitch density, need the highest restoring force. It is also observed that the preforms with perpendicular stitch are more stable or stiff, than the parallel stitched specimens with the same stitch density.

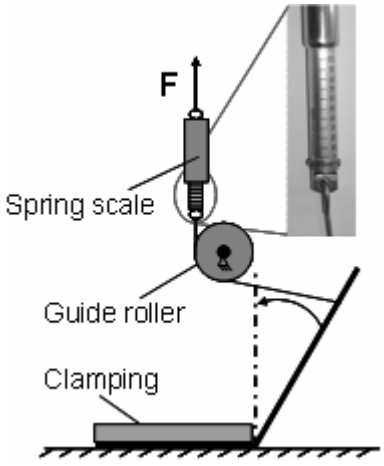

Figure 2.11: Experimental setup for the measurement of restoring force on compacted layers

Therefore the parallel stitched specimens with 4 mm stitch length and 10 mm stitch width, i.e. with the lowest stitch density, need the lower force to bring it back to the

right angle position. Additionally, it is clearly observed that the specimens with three layers are in all cases stiffer than the specimens with two layers.

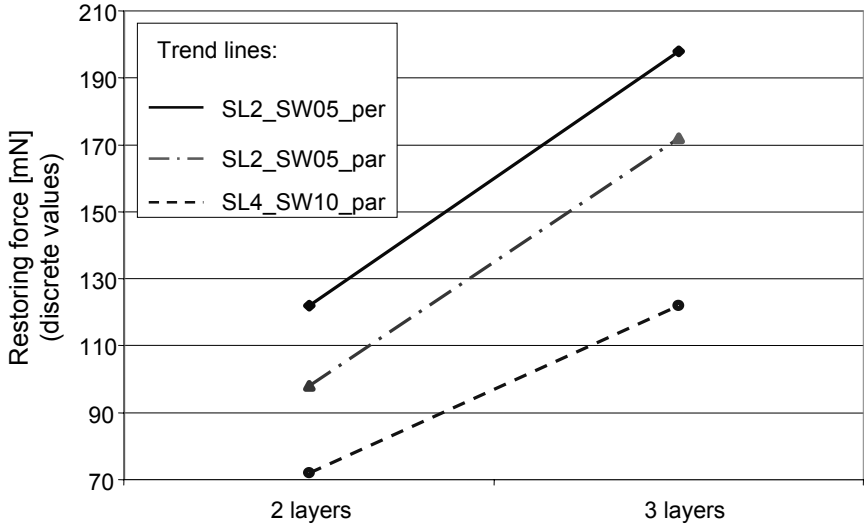

Figure 2.12: Experimentally determined restoring force of compacted layers

Quantitative measurement methods were worked out to reveal the mechanical properties of the fusible thread stitched three-dimensional preforms. These measurement methods indicate the effect of the orientation and density of the stitching in the reinforcing structure after thermal treatment. The three basic properties of the thermoformed preforms (specific bending stiffness, spring back angle, and restoring force) are important to evaluate the processability and handling of the preforms. In case of ideal properties the specific bending stiffness is high, the spring back angle and the restoring force are low.

2.4 Solubility tests of Grilon threads in different resin systems

The next important topic of the investigations is to examine the solubility properties of different stitching yarns for 3D preforming. This property of the stitching thread is necessary because the presence of thermoplastic stitching yarns can influence the mechanical properties of thermoset composites in case they are prepared with the stitching technology (Figure 2.13). Furthermore, the size of the stitch holes produced during stitching also has an impact on the mechanical properties but this unfavourable effect can be eliminated if the stitching yarns are dissolved.

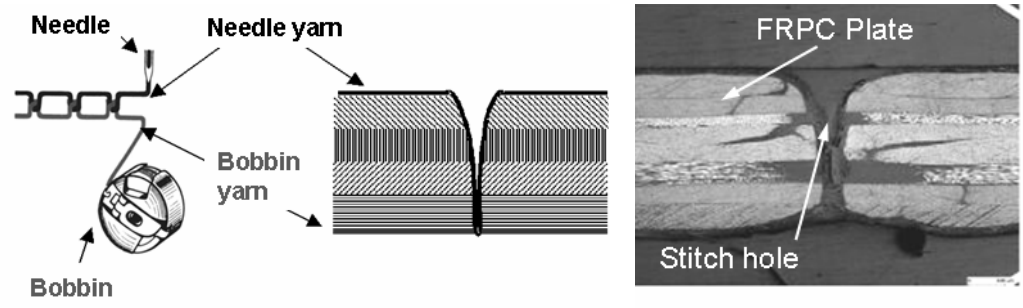

Figure 2.13: (Built) Stitch hole in the composite structure

If the stitching yarns taken into the system in the preform production technology fulfill their fixing function, ease the handling of the preproduct and disappear from the system, they will not influence the mechanical properties later. Thermoplastic polymers may have a favourable impact on the toughness of the composite.

The main aim of the examinations is to find stitching yarns that melt at low temperature (below 100°C) and also dissolve in the matrix material. Epoxy matrix (EP) is applied most often in the industry, hence the solubility in this material was examined primarily, but comparative experiments were made with unsaturated polyester (UP) resin matrix as well.

In order to be able to estimate the expectable results, the basic boundary conditions of the solubility of thermoplastic polymers have to be reviewed first [60, 61, 62]:

- It is necessary for solubility that the solvent and the polymer to be dissolved have approximately the same solubility parameter.
- The smaller the molecular weight of the polymer is the better solubility it has.
- The polymers to be solved should be amorphous to a great extent since the crystals are difficult to dissolve. The degree of crystallization in polymers is an important factor since the crystals should be destroyed during dissolving.
- A thermodynamical interaction should take place between the polymer and the solvent to initiate dissolving. In case of chemical interaction between the solvent and the polymer, dissolving may take place easier.
- Before the polymer starts to dissolve, it swells and the molecular structure will fall apart only later. In case there are holds together by hydrogen bonds or cross-linking, the solvent can not easy break them.
- Polymers usually dissolve in their own monomer or a similar solvent.

- Since epoxy resins and especially their hardeners are strongly polar, the TP polymer to be solved should also be polar. There are some suitable materials such as PEI (polyether-imide), PES (polyether-sulphone) and PSU (polysulphone) [63, 64, 65, 66, 67, 68, 69, 70, 71]. The disadvantage of these materials is that their glass transition temperature (T_G) is high (ca. 200°C). This effect is negative for the 3D performing applications because the sizing of the reinforcing fibers can be degraded at this temperature. This materials cannot be applied as binder yarns due to the economical reasons.
- Since Co-PA and Co-PET are used as binder yarns commercially, a strongly polar resin system is necessary for solubility.
- The RTM6 system often applied in composite technologies has an acid anhydride hardener (producer: HEXCELL, T_G ca.: 210°C). A similar system is commercially available now with amine hardener which is of stronger polarity, hence Co-PA and Co-PET fibers are more likely to dissolve in them. The disadvantage of the amine hardener resins is that their T_G is lower, around 136°C.
- The examinations can be extended to the range of biodegradable polymers of low melting point because they have CONH (amide) and COO (ester) bonds, which even are polar. Therefore, the related polymers can be dissolved in the resin matrix more smoothly. Such materials are e.g. polycaprolactone or polyvinyl-alcohol.

Since a basic criterion of dissolving is that the solvent and the material to be solved have almost the same solubility parameter, the first step is to examine this condition.

2.4.1 Solubility of polymer materials

The interaction between amorphous polymers and liquids is similar to that between two liquids. It is known that the free enthalpy, i.e. the Gibbs potential (G) has to decrease in natural processes. Solubility is also present if the free enthalpy of mixing, ΔG, is negative.

It is known from thermodynamics [72] that

$$\Delta G = \Delta H - T\Delta S \qquad (2.1)$$

where H [J] is enthalpy (U + PV), T [K] is absolute temperature, and S [J/K] is entropy. The U [J] is internal energy, P [Pa] is pressure, and V [m^3] is volume.

The entropy of mixing is positive in non-water systems; hence the sign and value of ΔG are determined primarily by ΔH, the heat of mixing. If there is any exothermic interaction between the liquid and the polymer, ΔH is negative, the system warms up and the polymer dissolves. If the chemical interaction is endothermic, ΔH is positive, the system cools down, and the value of ΔH determines whether the free energy calculated from Equation (2.1) is positive or negative, i.e. whether dissolving takes place. Polymers dissolve in two steps. Firstly, the solvent diffuses into the polymer that swells as a result, then the molecules have to diffuse out of the polymer and dissolving takes place [73].

2.4.2 Solubility parameter

If the interaction between the polymer and the solvent is only a result of dispersion forces, ΔH is positive and its value determines whether dissolution takes place. According to Hildebrand and Scott (1950) the heat of mixing for a volume unit is [73]:

$$\Delta H = v_1 v_2 (\delta_1-\delta_2)^2 \qquad (2.2)$$

where v is the volume fraction, index 1 refers to the solvent and index 2 to the polymer, while δ is the solubility parameter, which is the square root of the cohesion energy density (CED). The equation reaches its minimum when the values of δ_1 and δ_2 are almost the same and in this case ΔG is maximal in absolute value. This means that the solubility parameter of the solvent and the polymer to be solved has to be approximately the same so that dissolution can start. Although the polymers used by us are copolymers, first of all the solubility parameters of basic polymers were considered. Table 2.1 contains the solubility parameters of polymers important in the experiments.

Table 2.1: Solubility parameters of polymers

Polymer	Solubility parameter δ [$(J/cm^3)^{1/2}$]
Polyethylene terephthalate (PET)	19.9-21.9
Polyamide (PA)	27.8-28.0

Polycaprolactone (PCL)	19.1-19.3
Polyvinyl-alcohol (PVAL)	25.8-29.1
Epoxy resin (EP)	23.3-24.9
Unsaturated Polyester (UP)	22.2
Grilon MS (Polyhydroxyether)	22,3

2.5 Results of the solubility tests

The tests completed at different temperatures are denoted by “X” in Table 2.2. Before the experiments the stitching threads were rolled on a 20 mm x 30 mm alumina frame except for the RTM6 technology. These bobbins were placed into a small holder filled with the matrix and resin was cured at the temperature shown in Table 2.2.

After curing of the resin, cross sections of the threads and resin were cut and light microscopic examination was carried out on them. The polished samples were investigated at different magnifications. The essence of experiments was to examine the interface of thermoplastic stitching threads and resin.

Table 2.2: Solubility test of Grilon threads in different resin systems

Binder polymer yarn	**Solubility**					
Resin (Curing temperature)	**UP**		**EP**			**RTM6**
	RT	**40 °C**	**RT**	**40 °C**	**80 °C**	
Grilon KE-60 (Co-PET)	X	X	X	X	X	X
Grilon K-85 (Co-PA)	-	-	X	-	X	X
Grilon K-140 (Co-PA)	-	-	X	-	X	X
Polycaprolactone (PCL)	X	-	X	-	X	X
Polyvinyil-alcohol (PVAL)	-	-	X	-	X	X
Grilon MS (Polyhydroxyether)	X	-	X	-	X	X

2.5.1 Solubility test of co-polyester (Grilon KE-60) polymer in different resin systems

Firstly, co-polyester type Grilon KE-60 was examined in unsaturated polyester (UP) resin (Figure 2.14). Figure 2.14 reveals that the filaments in the stitching thread partly fused in the resin. The reason for this phenomenon is the exothermic effect of the UP resin cured at room temperature. In case of partial melting, sharp borders can be found between the TP fibers and the matrix and that means no dissolving took place in the system. In Figure 2.14 the lighter spots in the middle of the molten fibers show

materials shortage, i.e. cavitations formed during sample polishing. The reason is the worse wear resistance of the TP material.

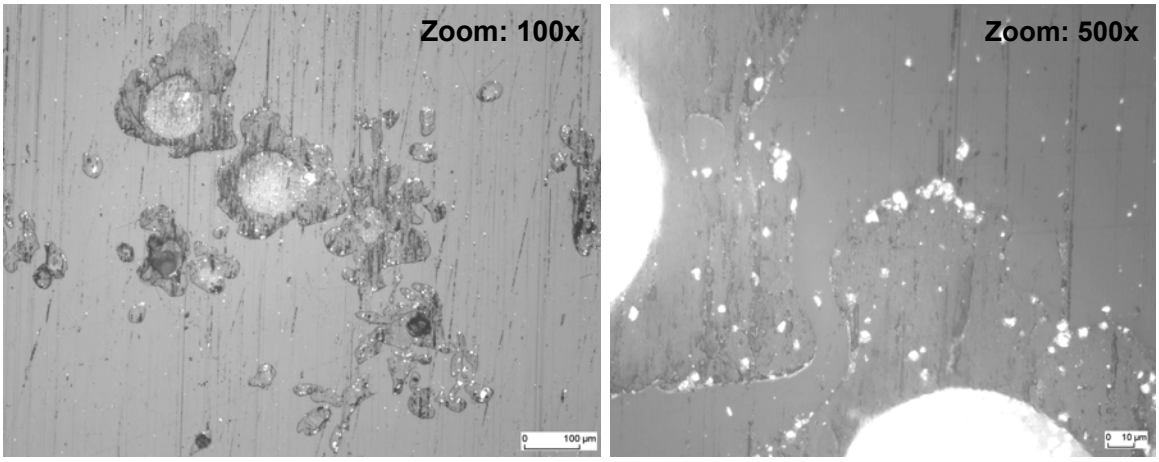

Figure 2.14: Solubility of Grilon KE-60 (co-PET) thread in UP resin at room temperature

In the following cases fiber type KE-60 was examined in unsaturated polyester resin at 40°C cross-linking temperature. Due to the repeated exothermic heat impacts the fibers melted to a greater extent in this sample and the ratio of not completely molten, pure TP fibers is smaller (revealed as white spots in the figures) than in the previous case (see Figure 2.15). The phase boundaries between the two materials can be distinguished well despite the temperature was higher and melting was more complete.

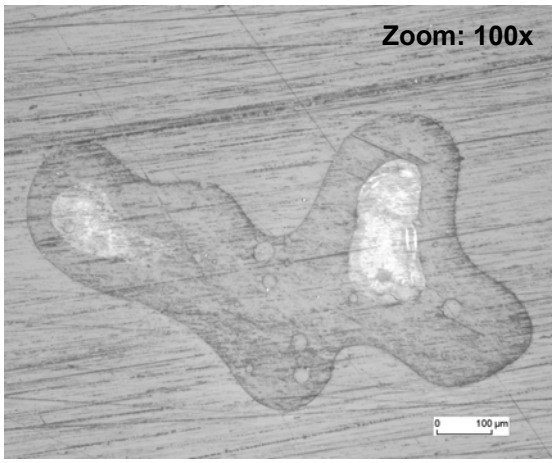

Figure 2.15: Solubility of Grilon KE 60 (co-PET) thread in UP resin at 40°C

Stitching thread KE-60 remained intact in the epoxy resin (producer Bakelite AG, Type: 4908) cross-linked at room temperature. At this temperature no melting, no dissolving occurred as it can be seen in Figure 2.16.

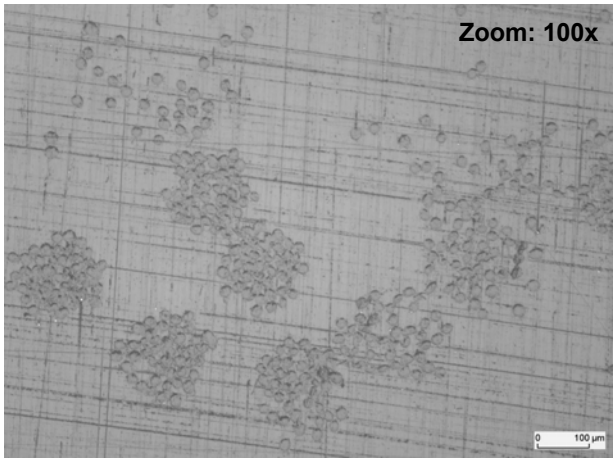

Figure 2.16: Solubility of Grilon KE 60 (co-PET) thread in EP resin at room temperature

Fibers of multifilament yarn arranged in groups in the resin like the stitching threads, and the phase boundaries can be distinguished well at every magnification.

The KE-60 co-polyester fibers in the epoxy resin cured at 40°C are completely molten, hence the phase boundaries are not visible between the thermoplastic stitching thread and the matrix material. Even examinations without a microscope verify that the fibers disappeared partially, i.e. dissolved in the matrix (Figure 2.17).

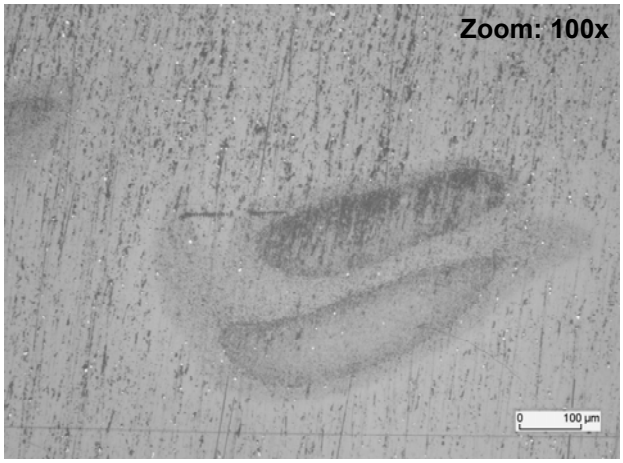

Figure 2.17: Solubility of Grilon KE 60 (co-PET) thread in EP resin at 40°C

Owing to the exothermic processes in the resin, the temperature may rise above the adjusted 40°C during cross-linking, and this way the melting point of material KE-60 (60°C) was approached.

When polyester fibers that melt at 60°C were placed in epoxy matrix cross-linked at 80°C all the fibers dissolved completely. In this case no evaluation can be made based on light microscopic investigation. According to the non-microscopic visual observations, only a refraction phenomenon experienced at a few spots in the matrix refers to the presence of fibers with a melting point below the temperature of cross-linking.

2.5.2 Solubility test of co-polyamide (Grilon K-85) polymer in epoxy resin

No signs of dissolving were experienced in fibers of 80°C melting point in epoxy resin (producer Bakelite AG, Type: 4908) cross-linked at room temperature. The single filaments arranged in groups correspondent to the stitching thread in the matrix. The sharp phase boundaries revealed that no swelling process that may refer to melting or dissolving started (Figure 2.18).

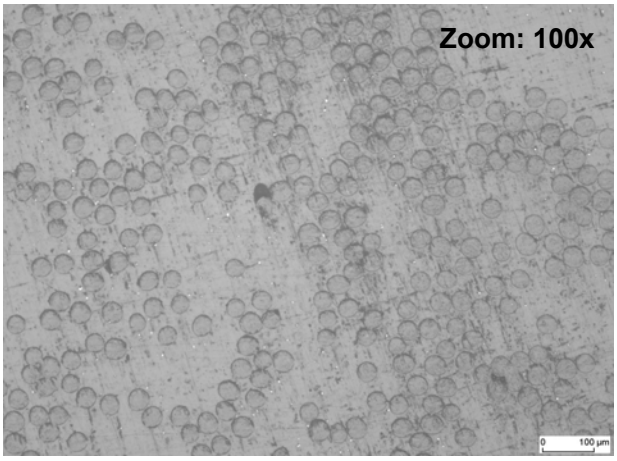

Figure 2.18: Solubility of Grilon K-85 (co-PA) thread in EP resin at room temperature

The filaments of these fibers fused in the resin cross-linked at 80°C and they arranged in spots, not in the form of fibers, in the matrix. The cross-linking temperature of the resin was the same as the melting point of the co-polyamide (K-85) fibers but the presence of sharp phase boundaries referred to the fact that no dissolving took place in the system (Figure 2.19).

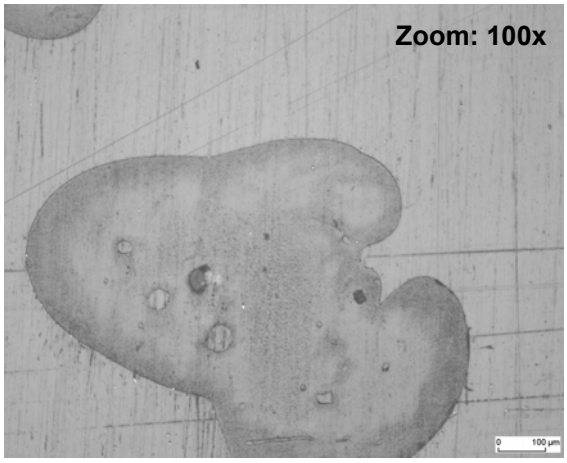

Figure 2.19: Solubility of Grilon K-85 (co-PA) thread in EP resin at 80°C

2.5.3 Solubility test of co-polyamide (Grilon K-140) polymer in epoxy resin

Solubility tests were carried out on co-polyamide fibers type Grilon K-140 in epoxy resin (producer Bakelite AG, Type: 4908) at room temperature and at 80°C which is the proposed curing temperature of the resin. The fiber Grilon K-140 (melting temperature: app. 140°C) shows no soluble properties in epoxy resin at room temperature and at 80°C. The fibers keep intact in the resin during the curing process.

2.5.4 Solubility tests of different polymers in RTM6 system

Co-polyester type Grilon KE-60 and co-polyamide type Grilon K-85 and Grilon K-140 fibers –already applied in previous experiments (see in Figure 2.1, and chapter 2.2)– were used as binder yarns in these examinations. The melting point of yarn K-140 was around 140°C and its mechanical properties (maximum tensile stress and elongation) were better than that of co-polyester (KE-60) of 60°C melting point. This property makes it a good choice for applications in preform technologies for aircraft applications.

For the following experiments a 2-layer NCF-CF (producer Saertex GmbH & Co. KG) reinforcing system of 250 g/m^2 weight per layer was stitched with TP stitching threads. After the injection followed by cross-linking, polished samples from more directions were made from the specimens. Injection was carried out with the VARI process the parameters of which are listed in Table 2.3.

Table 2.3: Parameters of the RTM6 process

Process	Parameter
Resin temperature for injection	90°C
Injection and tool temperature	120°C
Curing parameters cycle 1	160°C, 75 min
Curing parameter cycle 2	180°C, 120 min

This way the behaviour of stitching threads was studied in composites. A cross-sectional and a top view picture were taken of the CF-laminates prepared in an RTM6 process in both cases. Figure 2.20 reveals that the CF sheet stitched with a thread type Grilon K-140 produced gas during the process of injection and cross-linking and it was dispersed in the form bubbles on the surface of the laminate. The stitch hole ellipse formed by the stitching thread can be examined at 25x magnification well.

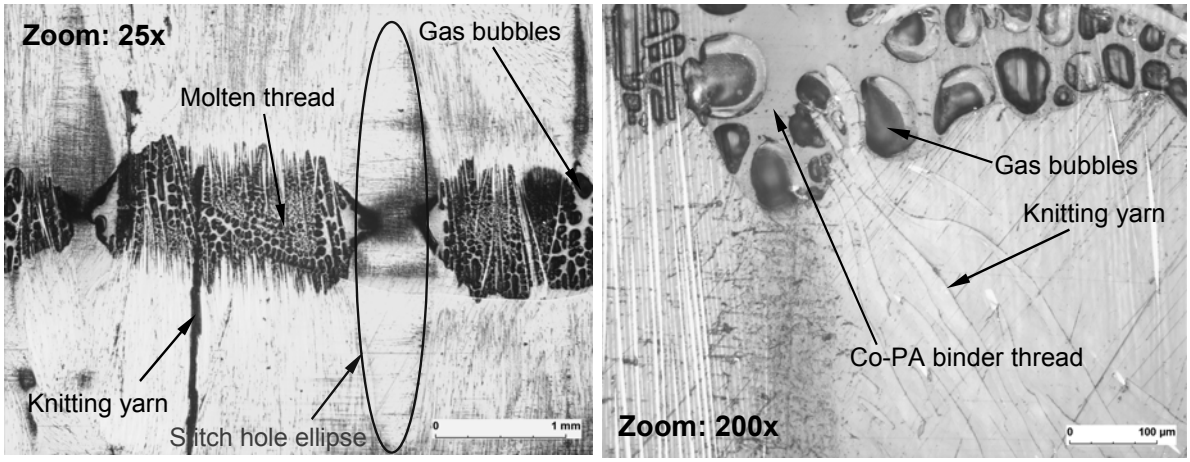

Figure 2.20: Solubility of Grilon K-140 (co-PA) thread in an RTM6 system (top view)

The black line on the left side in Figure 2.20 shows the polyester knitting yarns. Despite the dissolution of fibers, the higher magnification revealed the sharp phase boundaries of the TP fiber and the matrix yarn that was introduced to the system during the production of CF-NCF. The holes, i.e. stitching points, formed by the 2 mm long stitches in the reinforcing system are well visible in the sectional image in Figure 2.21.

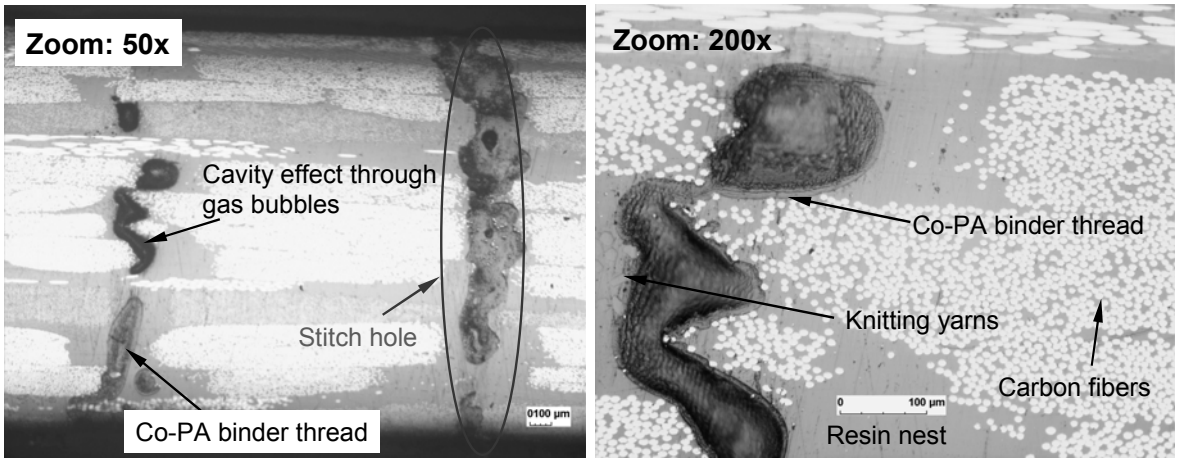

Figure 2.21: Solubility of Grilon K-140 (co-PA) thread in RTM6 system (cross section view)

It can be observed that the stitch holes are partially closed due to the dissolution of stitching threads. This phenomenon is considered to be favorable if the mechanical properties of composites are considered. The microscopic investigation of polished samples revealed that gas inclusions were formed in the material in the vicinity of the stitching threads and that the fibrous characteristic disappeared during the dissolution of stitching threads, hence TP is present in islands inside the composite. Despite the high injection and cross-linking temperature characteristic of the RTM6 systems, the phases are separated sharply on the sectional images meaning that no dissolution took place. Figure 2.22 shows the white light profilometry picture of the plate cross section at the stitch holes.

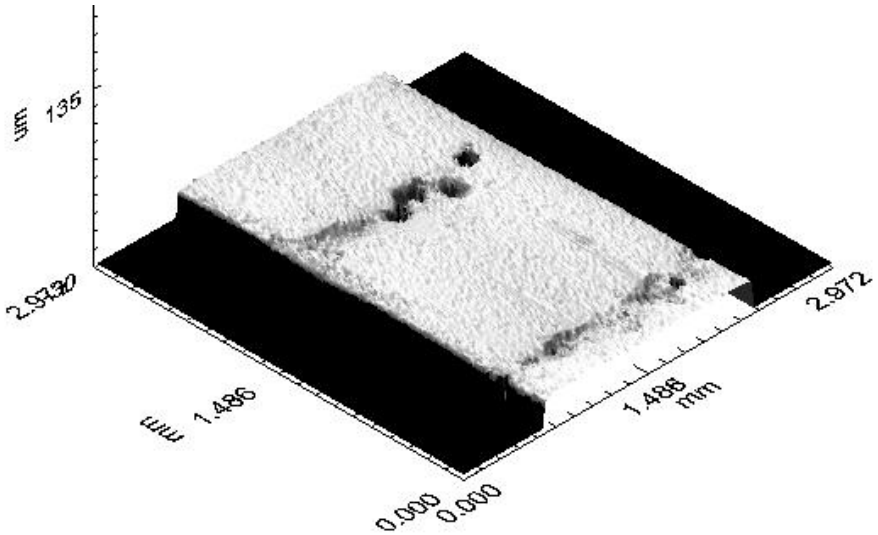

Figure 2.22: White light profilometry picture of the cross section (Grilon K-140 Co-PA in RTM6 system)

On the Figure 2.22 it can easy be observed the cavities of the above mentioned gas inclusions in the stitch holes.

In case of co-Polyamide, type Grilon K-85 complete fusion of the fibers was observable but dissolution is not to be observed. The micrograph pictures shown sharp phase surfaces between the co-Polyamide islands and the epoxy matrix material.

Co-polyester fibers type Grilon KE-60 were examined in the next step. The microscopic investigations were carried out again on composite sheets manufactured by stitching and injection.

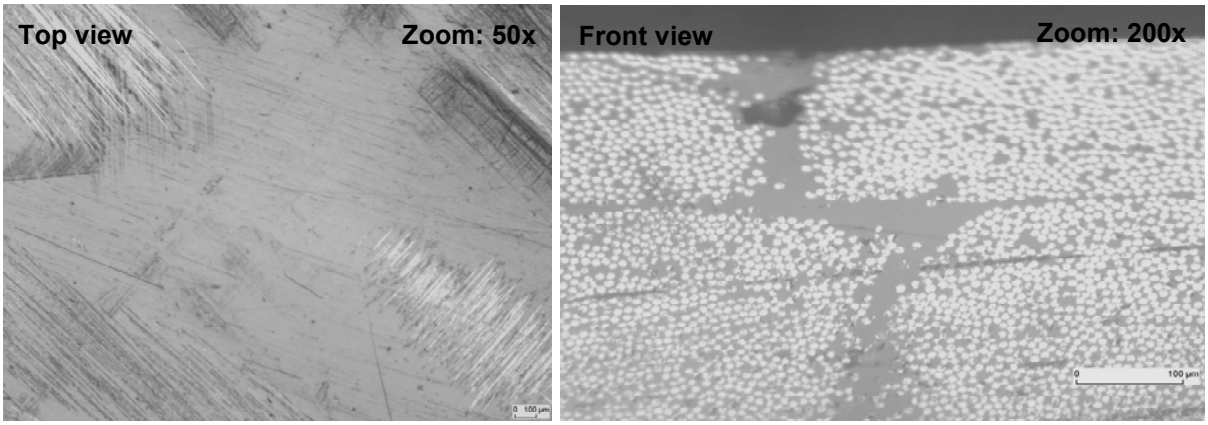

Figure 2.23: Solubility of Grilon KE-60 (co-PET) thread in RTM6 system

Figure 2.23 reveals that the resin pocket in the stitch hole does not contain sharp phase boundaries, hence the TP stitching thread and the matrix material cannot be separated. The differently oriented light lines reveal the carbon fibers that were brought to surface during polishing. The closing of the stitch hole can be seen clearly in the sectional image and this is again a result of the disappearance of the stitching thread. The section image in Figure 2.23 also shows that the TP stitching threads and the matrix cannot be separated in the resin pocket formed in the stitch hole, and there are no gas bubbles as well. The white spots denote the sectional image of polished carbon fibers. This reveals that the co-polyester fiber of very low melting point was dissolved in the matrix material completely. The stitching tests carried out during the production of specimens revealed that the co-polyester fibers (Grilon KE-60) of low melting point can be applied in composites to provide both functions:

Hence they can be binder materials and they can also dissolve in the resin in RTM6 systems at high injection temperature.

2.5.5 Solubility test of polycaprolactone and polyvinyl-alcohol (biodegradable polymers) in different resin systems

Solubility tests were carried out on two different biodegradable polymer materials (polycaprolactone, and polyvinyl-alcohol). It has been presumed that the polymers are soluble in epoxy resin because of their affinitative chemical structure to the epoxy resin. This analogy is basically the ester bond in the polymers and therethrough the polar property. After the observations the polymers are no soluble in the epoxy resin.

In case of polycaprolactone at room temperature in epoxy and in UP resin no solubility or swelling was observable. At 80°C in epoxy resin and in RTM6 resin at 120°C the polymer is temporarily swollen, and the color of the TP polymer is changed with the higher temperature but after cooling sharp phase interfaces were observable between the polycaprolactone and the cured epoxy polymer.

The polyvinyl-alcohol shows also no soluble properties in UP and EP resin. In this case no changes were observable on the polymer structure or color.

2.5.6 Solubility test of Grilon MS polymer in different resin systems

The examinations of the recently developed Grilon MS (matrix soluble) threads (supplier: EMS-CHEMIE AG) revealed their good solubility properties. Due to the low melting point (ca. 80°C) of the polymer (polyhydroxyether), it can be applied well in three dimensional preform technologies. Forming becomes economic this way since the heat treatment of the stitching threads does not require high temperature. Furthermore, stitching tests proved that the thread has the mechanical properties necessary for stitching technologies (tensile stress and elongation). Since the polymer has similar morphological properties to epoxy, our assumption was that the thread can be solved well both in epoxy and UP resins.
Primarily, the polymer was examined in RTM6 resins at 120°C. The Grilon MS thread was reeled on an alumina frame and was placed into a beaker filled with epoxy resin later (Figure 2.24). The resin started to cross-link at 120°C, and was completely cross-linked at 140°C.

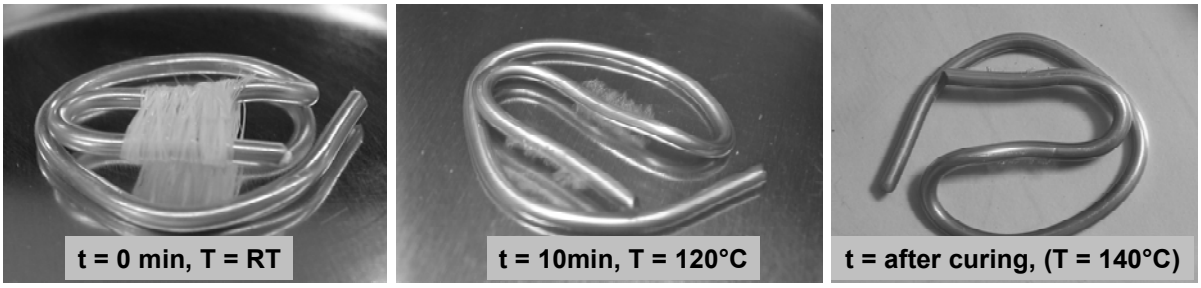

Figure 2.24: Solubility test on Grilon MS thread in RTM6 resin

It can be seen in Figure 2.24 well that the threads already revealed good solubility properties in the tenth minute, and after the complete cross-linking, no Grilon MS yarn was present in the resin. Simple optical examinations prove the good solubility of polyhydroxyether in epoxy resin at a temperature above the melting point of the polymer. This property could already be predicted since the solubility parameter of the material is very close to that of epoxy. The solubility tests of Grilon MS stitching threads revealed that it was not soluble in epoxy resin if injection took place at room temperature. In this case a carbon woven fabric was stitched with the thread, and solubility was examined on micrographs of stitch hole sections.
The section of the composite plate injected and cross-linked at room temperature exhibits the undamaged threads in the stitch holes as well (Figure 2.25).

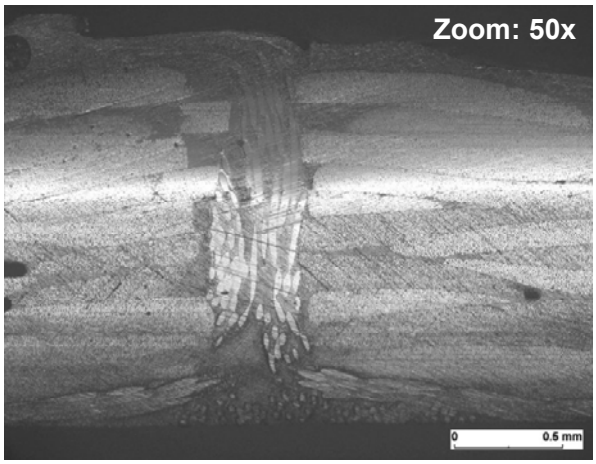

Figure 2.25: Micrograph picture of a stitch hole in a CF-EP composite structure (Grilon MS, injection temperature: room temperature)

The thread type Grilon MS shown no soluble properties in epoxy resin at 80°C. The stitching thread is partially melted, but no dissolution was observable.
The stitched CF woven fabric was also injected with RTM6 resin. The resin was cross-linked at 140°C after injection at 120°C. The section image of the composite

plate produced this way revealed that the stitch holes closed, hence the Grilon MS stitching thread dissolved in the resin (Figure 2.26).
The dissolved thread did not block the movement of the layers any more, hence the reinforcing structure took its original shape. This re-organization of layers makes it possible to eliminate the resin parts formed in the holes, to promote the efficient operation of the reinforcing system and to prevent the deterioration of mechanical properties caused by the stitch holes formed during stitching [39, 40].

However, besides the solution of threads and reorganization of the reinforcing fibers, gas bubbles (revealed by black spots in Figure 2.26) can also be observed in the stitch holes. Those gas bubbles only appear if injection was carried out above the melting point of the stitching thread. Further tests also proved that the thread itself emits gas above 200°C, even without the presence of epoxy resin.

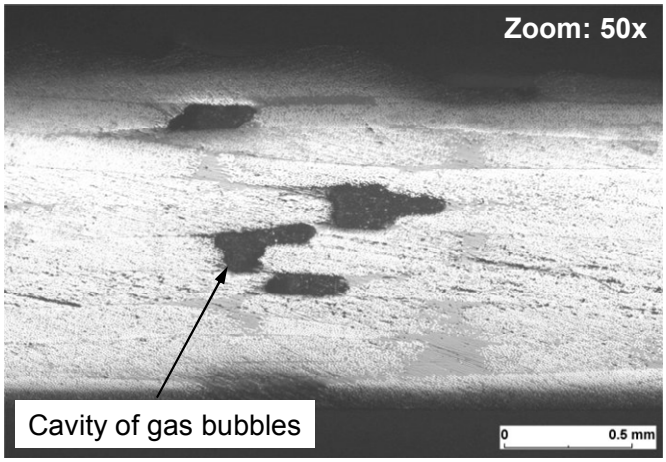

Figure 2.26: Micrograph picture of a stitch hole in a CF-EP composite structure (Grilon MS, injection temperature: 120°C)

Figure 2.27 shows the white light profilometry picture of the plate cross section at the stitching hole. It can easy be observed the cavity of the above mentioned gas bubbles.

According to the supplier (EMS-CHEMIE AG), gas formation at higher temperature can be caused by the sizing used in the production of threads. This oil-based sizing material may evaporate from the surface of the stitching thread at higher temperatures and in vacuum. This steam can be stuck in the injected structure, in the immediate environment of stitch holes. Hence if another type of sizing is applied, the

stitching thread can be used in 3D performs, and this way in the production of FRCP parts.

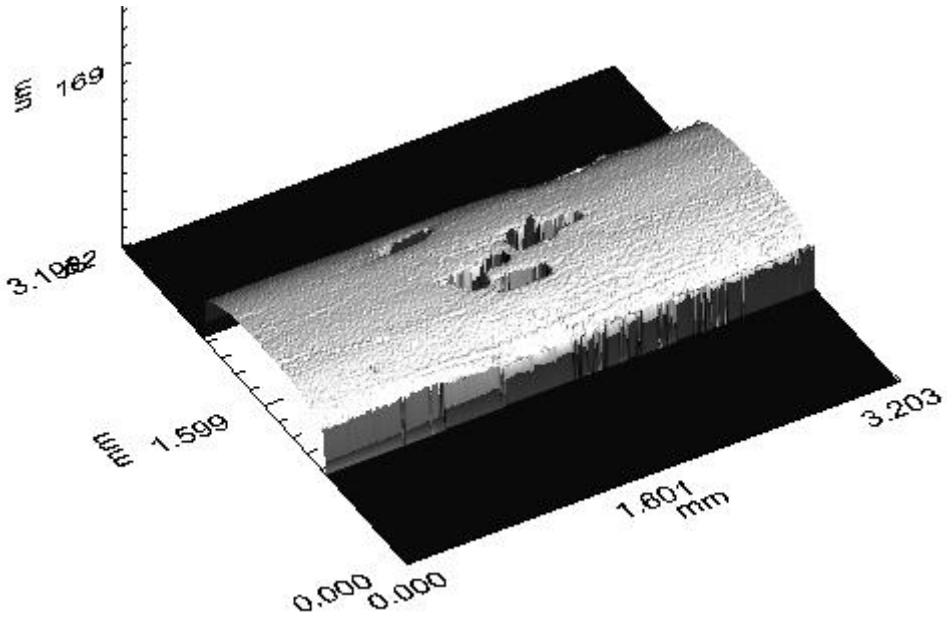

Figure 2.27: White light profilometry picture of the plate cross section at the stitch hole (Grilon MS in RTM6 system)

Since the solubility parameter of Grilon MS stitching thread (Table 2.1) is almost the same as that of unsaturated polyester resin, the following tests focused on the solubility in this material. Despite of this analogy the examinations revealed that the stitching thread cannot be solved in UP resins at room temperature. Although the exothermal cross-linking of the resin results in a higher temperature that can be enough theoretically for the solution of the stitching threads, this temperature is only reached after gelation of the resin that prevents the solution of the thread.

Table 2.4 summarizes the results of the observations during the experiments. The results show that using soluble binder stitching threads is most useful at high temperatures in RTM6 processes. Even in this case the application of polyhydroxyether and co-polyester fibers of low temperature is the best but its impact on the mechanical properties of composites after dissolution is not investigated within this dissertation. Hence the Grilon MS stitching thread can only be dissolved in epoxy resins around or above its melting point.

Nevertheless the most important result of the preforming and solubility investigations verified that it is possible to find a thermoplastic polymer yarn which can be used for 3D preforming through its low melting temperature and good solubility properties in epoxy resin. Through the dissolution of the stitching yarns the stitch holes can be closed in the reinforcing structure during the injection and this effect can improve the mechanical properties of the composite material.

Table 2.4: Solubility results of different TP polymers in different resin systems

Binder polymer yarn	**Solubility**					
Resin (curing temperature)	**UP**		**EP**			**RTM6**
	RT	**40°C**	**RT**	**40°C**	**80°C**	
Grilon KE-60 (Co-polyester)	No dissolution, the fibers melt partially*	No dissolution the fibers are fused*	No dissolution, the fibers are intact	Complete melting, the fibers are partially vanished	The fibers are mainly disappeared	The fibers are completely disappeared in the resin
Grilon K-85 (Co-polyamide)			No dissolution, the fibers are intact		Fusion of the fibers, dissolution is not to be observed, sharp phase surfaces	Complete fusion of the fibers, dissolution is not to be observed, sharp phase surfaces
Grilon K-140 (Co-polyamide)			No dissolution, the fibers are intact		No dissolution, the fibers are intact	No dissolution, the fibers are fused, but gas bubbles are observed in the stitch holes
Polycaprolactone (PCL)	No dissolution, the fibers are intact		No dissolution, the fibers are intact.		No dissolution, temporary bulking at 80°C, the polymer stay intact	Complete fusion of the polymer, dissolution is not to be observed, sharp phase surfaces
Polyvinyl-alcohol (PVAL)			No dissolution, the fibers are intact		No dissolution, the fibers are intact	No dissolution, the fibers are intact (crystalline PVAL)
Grilon MS (Polyhydroxyether)	No dissolution, the fibers are intact		No dissolution, the fibers are intact		No dissolution, the fibers are partially melted	The fibers are completely disappeared in the resin

3 Improvement in bonding of functional elements in the fiber reinforced polymer structure

The application of inserts in composite parts is often inevitable to be able to fix them to other structures. Owing to the mechanical characteristics of polymer composites, the integration of these inserts results in better strength properties compared to glued, screwed or riveted joints [74]. The mechanical properties of structures with inserts can be improved further, if they are stitched to the reinforcement instead of simple interlaminar embedding.

The fixation of fiber reinforced polymer component parts to others or to other metallic structures by gluing gives only low mechanical properties and may be the reason for the application of inserts [75]. Embedding metallic inserts into a preform raises new problems in the manufacturing chain. The load capacity of non-stitched inserts embedded in thin monolithic FRPC laminates has already been tested and FEM modeled, but this investigation was not extended to the stitched metallic inserts [76, 77 ,78 ,79 ,80 ,81 ,82 ,83 ,84.,85 ,86 ,87 ,88, 89, 90, 91]. The Aeronautical and Maritime Research Laboratory, Melbourne paid particular attention to the analysis and development of suitable methods for the life extension of aircraft components in particular airframes. Tests with a metallic insert bonded to a damaged zone were also done in the context of life extension investigations of FRPC parts [92]. The stitching technology is very suitable to join inserts to the textile lay-up because of possible improvements in the delamination resistance of the laminates [93]. To obtain excellent mechanical characteristics, the insert can be embedded into the reinforced structure during preform production, and the stitched sub-preform can be part of the main 3D preform structure. Stitching is a relatively new method for increasing the strength and damage tolerance of monolithic or sandwich composite panels. Few researches investigated the influence of localized through-the-thickness stitching to fix metallic inserts in FRPC sandwich structures [94, 95]. Static tensile tests carried out on Big-Head® (Bighead Bonding Fasteners Limited) inserts fixed with polyester yarns revealed that the mechanical properties of the composite insert connection can be improved to a great extent with the help of seams.

A polyester, twisted multifilament thread impregnates inadequately because of its tight structure. On the other hand, core spun threads have a more open structure, thus, they can be completely impregnated [96]. Therefore, during the experiments, the behavior of the used stitching thread was also analyzed in terms of thread matrix bonding, ultimate compatibility and contribution towards the strength. The finite element (FE) analysis was applied to cross check the theoretical and actual failure positions and modes of the bonded inserts.

3.1 Specimen development

As shown in Figure 3.1, Big-Head® inserts were applied as load carrying elements which are later embedded in polymer composites. A steel insert consists of a screwed bolt (M6) and a base metal plate (Ø38 mm) perforated in two circular rows with 6 and 12 holes. The diameter of the holes at the inner and the outer pitch circle is 4 mm and 5 mm, respectively, and the thickness of the base plate is 1.5 mm. The application of this insert made it possible to optimize the design and to carry out exact fracture mechanical experiments. Before embedding the metallic inserts were treated (washed) in acetone for the good bonding between the insert base plate and the resin of the composite.

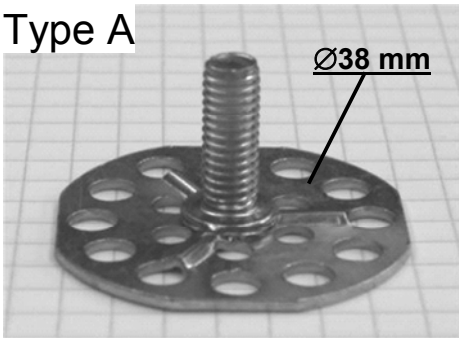

Figure 3.1: Big-Head® insert (Type A)

In all cases, the metallic inserts were embedded in glass fiber reinforced epoxy matrix composites. The matrix material used for RTM was a Rutepox VE 4908, a low viscosity (120 ±20 mPas) resin (producer: Bakelite AG). The reinforcing structure consisted of glass fiber non-crimp fabric of 894 g/m² specific weight and +45°/-45°/+45° orientation (producer: Saertex GmbH & Co. KG). The inserts were fixed to the fabric with and without stitching during the preform technology (Figure 3.2).

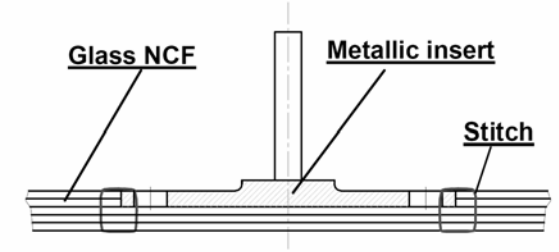

Figure 3.2: Stitched inserts

In the first part of the investigations, three layers of fabric were used as a preform base. A preform set consisting of two fabric layers with circular blanks (the diameter of the blanks corresponds to the insert base plate) was stitched on the fabric [97] (Figure 3.3). The thickness of these intermediate layers was the same as the insert base plate, hence it helped maintains an even surface and in all cases exact resin distribution over the insert base plates (Figure 3.4).

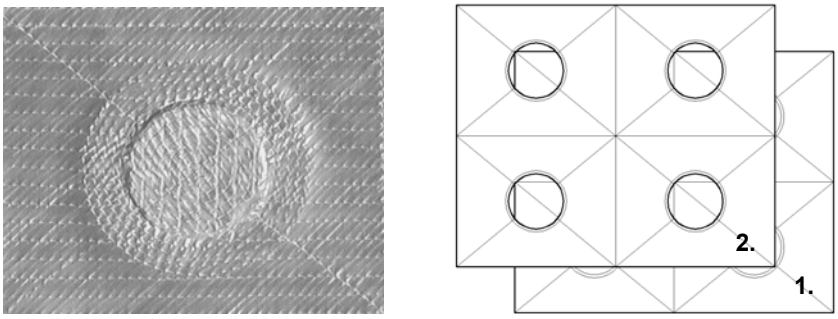

Figure 3.3: Base and intermediate plate

After incorporating the metallic insert into the reinforcing structure it was fixed by a specific stitching procedure. In the second part of the investigations, the base plate thickness of the preforms was altered by more layers, i.e. 2, 4 and 6 layers.

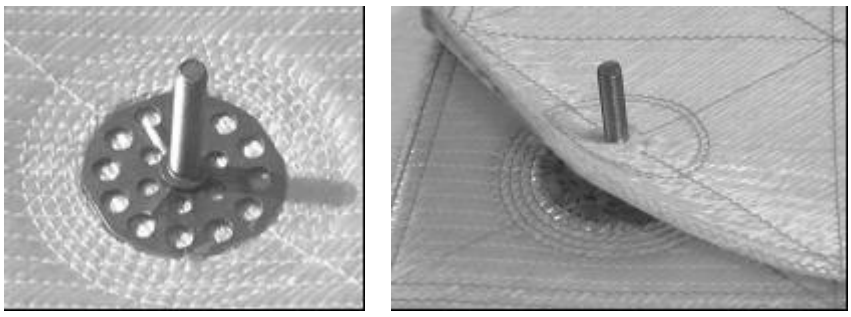

Figure 3.4: Unstitched (Type 1) and stitched metallic inserts with cover layer (Type 6) (insert type: Type A)

In order to carry out comparative measurements, specimens with the same assembly, without stitching were also tested. Furthermore, an assembly without stitching and with two further non-crimp fabric as a cover layer were also manufactured (Figure 3.5). The number of parameters was altered in order to find an ideal embedding of inserts to be applied in the composite parts. Accordingly, seven different specimens were manufactured (Table 3.1).

A multifilament polyester stitching thread, Serafil 80 (Amann & Söhne GmbH & Co. KG), was used for stitching in the first case. For the improved stitching technology a core spun polyester thread (Saba c50 type) was used (Amann & Söhne GmbH & Co. KG).

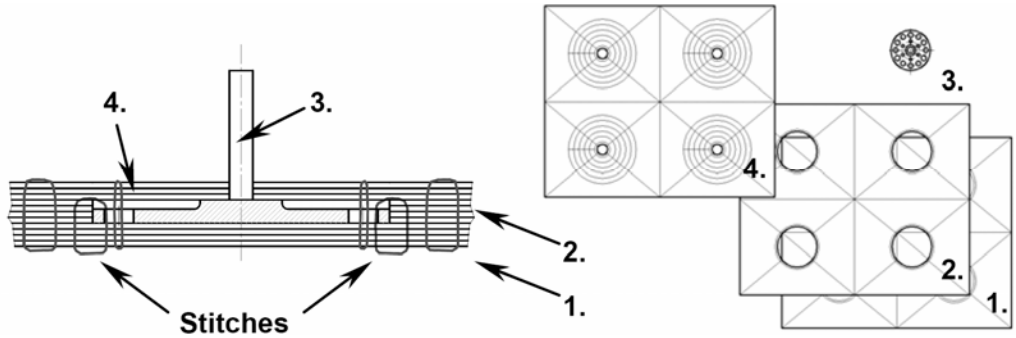

Figure 3.5: Preform with base plate 1), intermediate plate 2), insert 3), and cover layer 4)

During the production the inserts were fastened with 8 and 16 stitches per hole. This means that at the simple stitching type the number of stitching threads per hole were 8, hence, altogether 96 threads per insert (Figure 3.6).

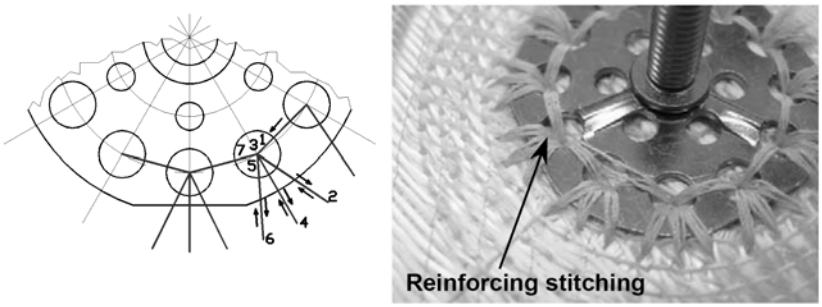

Figure 3.6: Stitching pattern for reinforcing stitching

For the improved technology the insert was stitched 16 times, thus 16 threads were applied per hole in a similar arrangement, this means one insert is held by 192

stitches. Furthermore, the stitch points were positioned 2 mm from the edge of the insert base plate compared to the previous volume of 4 mm.

Table 3.1: Specimen selection

Type of specimens	Stitches	Without cover	With cover
Specimen without stitching	0	**X** (Type 1)	**X** (Type 5)
Single stitching with Serafil 80 type PET thread	96	**X** (Type 2)	-
Improved stitching with Saba c50 type PET thread	192	**X** (Type 3)	**X** (Type 6)
Improved stitching with Saba c50 PET type thread, with 2, 4 ,6 base plates	192	**X** (Type 3)	-
Improved double stitching with Saba c50 type PET thread	384	**X** (Type 4)	-

Table 3.2: Specimen architectures

Specimen without stitching (Type 1)	Single and improved stitching (Type 2, 3, 4, and Type 8, 9, 10)*
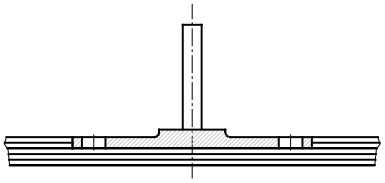	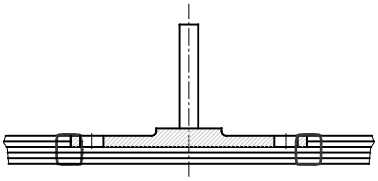
Specimen without stitching, with cover layer (Type 5)	Improved stitching with cover layer (Type 6)
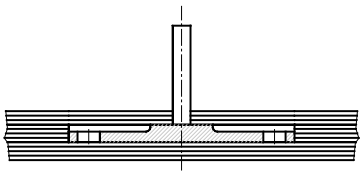	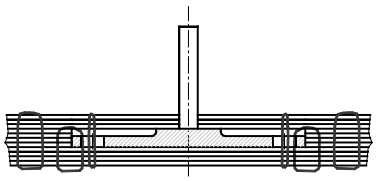
Insert without embedding Type 7	* = Embedded inserts, stitched with different threads: - Type 2: PET, Amann Serafil 80 - Type 3, 4: PET, Amann Saba c50 - Type 8: Kevlar®, Amann Kevlar® No. 50 - Type 9: Glass, Culimeta MN30 - Type 10: Carbon, 1K IVW CF thread (Tenax HTA 5641)
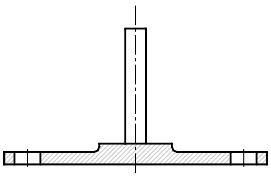	

The advantage of this technology is the smaller angle of thread pull which results from bonding of the insert with the base fabric. Again, the short span length of the

thread (2 mm) at the load bearing area does not allow easy elastic deformation of a thread at this specified stitch. This can help improve the tensile properties of the stitched insert.

The Saba c50 (67.2 tex) thread applied in the improved technology can be more easily wetted by the epoxy resin, and the adhesion between the resin and the thread is stronger compared to Serafil 80 (36.6 tex) [55, 96] (Table 3.8). In case of the double stitched inserts (using the improved technology) the double amount of stitching thread was introduced into the assembly. This means that 384 stitches hold the insert. Table 3.2 shows the type of the insert embedding and the specimen architectures.

The applied thread tension was identical in all cases (F_{NT} = 310 cN, F_{BT} = 100 cN) and hence modified lock stitches can be produced [98]. A semiautomatic stitching machine, Pfaff 3574 (Pfaff Industriemaschinen AG), was used for the preform production. During the stitching process the exact position of the inserts were fixed by adjustable insert holders.

After the preform was placed in the RTM mold the vacuum assisted resin infusion molding technique (VARI) was used for the specimen manufacturing. The screwed bolt of the insert was placed into the silicon rubber cartridge, which protects the screw from resin contaminations. All the VARI parameters, for instance, tool set-up, vacuum, type of resin, applied curing time, temperature etc. were kept the same in all cases (Table 3.3). The fiber volume content in the composite base plate was 50%.

Table 3.3: Parameters of the VARI process

Resin type	Temperature of injection	Vacuum of injection	Cure temperature	Cure time
Rutepox VE 4908	23 °C	5 mbar	80 °C	6 hour

3.2 Experiments and results

In order to compare different technologies used in the production, simple tensile tests were carried out [99]. During the experiment the force needed for specimen fracture was measured and the characteristic failure modes were observed. The specimens with a 75 x 75 mm GF/EP composite base plate were clamped by a 55 x 55 mm

frame to the machine (Figure 3.7). Measurements were carried out at 2 mm/min speed at room temperature. Figure 3.8 shows the acting forces on the specimen during the simple static tensile test.

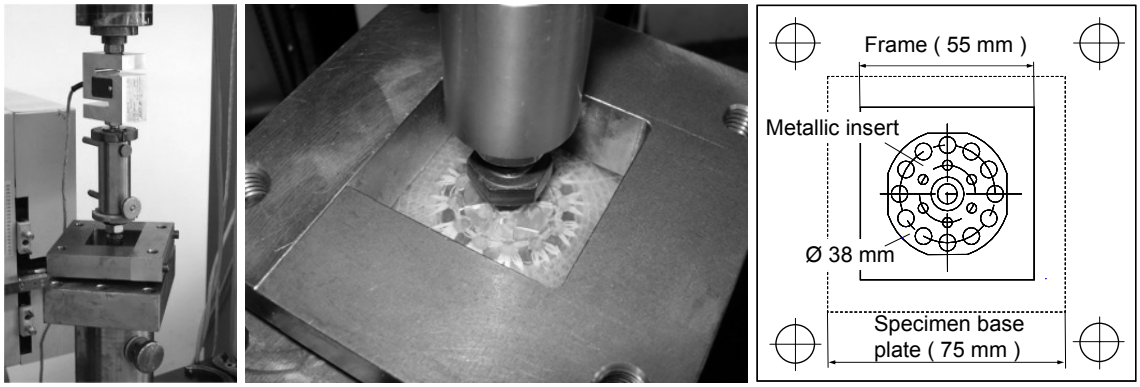

Figure 3.7: Static tensile testing configuration

In order to evaluate the obtained results a tensile test of pure metallic inserts was also carried out. The inserts were clamped onto the base plate with a frame having a 26 mm diameter hole. Zwick 1474 universal material testing equipment was used for tensile testing.

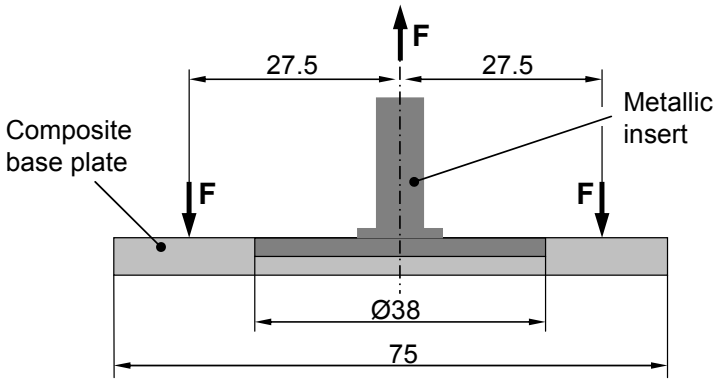

Figure 3.8: Acting forces during the static tensile test

From each type (see Table 3.1) seven specimens were measured. After eliminating the lowest and highest strength values the mean value and standard deviation were calculated with 95% confidence interval from the 5 results.

Standard deviation: $$SD = \sqrt{\frac{\sum_{i=1}^{n}(x_i - \bar{x})^2}{n-1}} \qquad (3.1)$$

Mean volume: $\bar{x} = \frac{1}{n}\sum_{i=1}^{n} x_i$ (3.2)

Were: x_i = i-th result n = number of results

As shown in Figure 3.9 even the simple stitching (Type 2) leads to a more than 100% increase in strength compared to the unstitched assembly. The technology improvement (Type 3) resulted in a further significant increase of strength (additional more than 70%) compared to the strength of the Type 2 embedding.

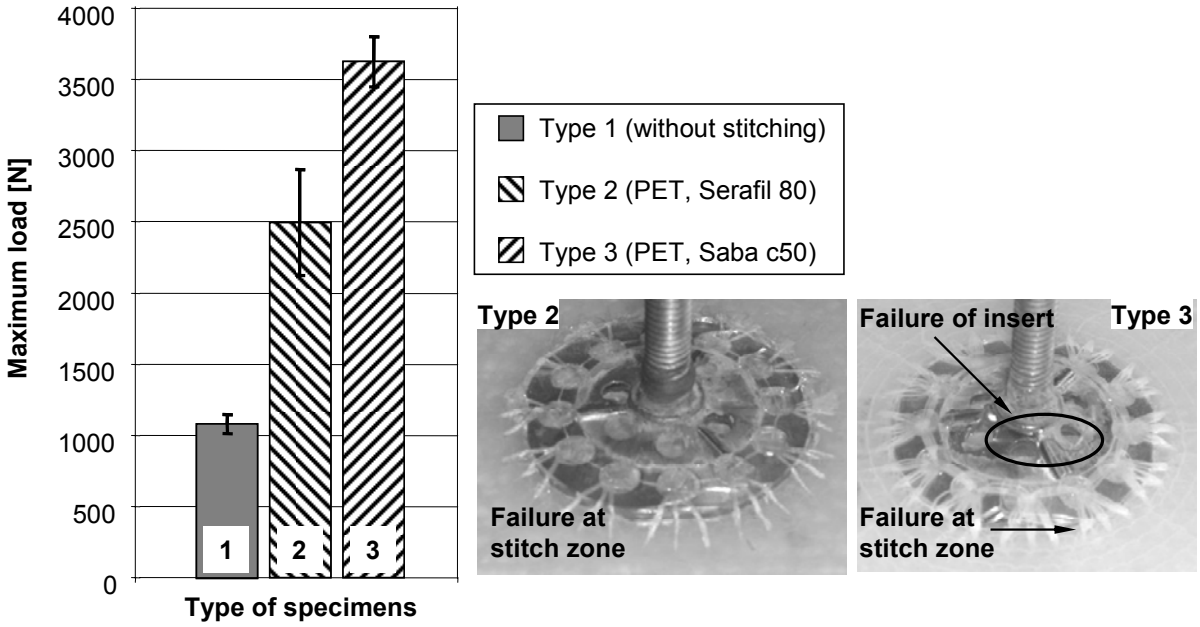

Figure 3.9: Results of the tensile tests on unstitched and two types of PET thread stitched specimens (Type 2 and Type 3, maximum load)

The pull out and breakage of the stitching threads was definitely observed in the Type 2 specimen, whereas, in case of the Type 3 specimen not only the broken threads but in few cases also the breakage of inserts in their weak points were observed. This can be seen as a characteristic failure mode in Figure 3.9. On all specimens the spherical distortion of the composite base plate during the tensile test was observable (Figure 3.10). Taking this phenomena into consideration, the focus of the investigations was placed on the influence of the composite laminate stiffness on the load carrying capacity of the structure.

In the next step, specimens manufactured with 2, 4 and 6 base layers and improved stitching types, i.e. 192 stitches/insert (Type 3) were tested and evaluated. It was

interesting to find that as the number of base layers increases the spherical distortion of the specimen under the clamping frame reduces.

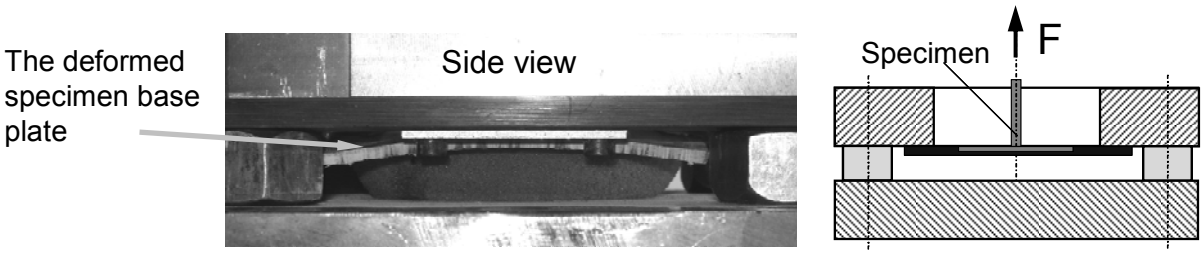

Figure 3.10: The deformed specimen base plate during tensile test

It can be seen clearly in Figure 3.12 that the structure strength did not change essentially, but the stiffness changed considerably. The visibility of first delaminations of the insert is specimen dependent. In case of 2 base layers the first delamination that appears always under the screwed bolt of the insert is not noticeable but in the case of 4 and 6 layers it is revealed (Figure 3.11).

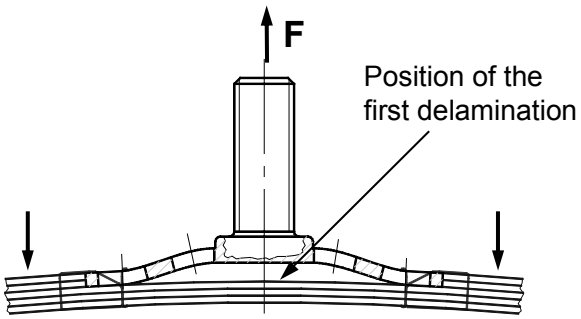

Figure 3.11: Position of the first delamination in the structure

Specimens with 2 layers could follow the spherical distortion during the tensile test, whereas, the specimen with 4 and 6 base layers do not show this phenomena. Therefore, the first delamination appears at a relatively low force range and it is well marked. The adhesive bonding between the metallic insert and the matrix material broke, as well as the resin layer sheared above the insert base plate at this force range. After this, the stitches take over the large proportion of load. The specimen undergoes irreversible damage, nevertheless the seams increase the load carrying capacity of the insert.

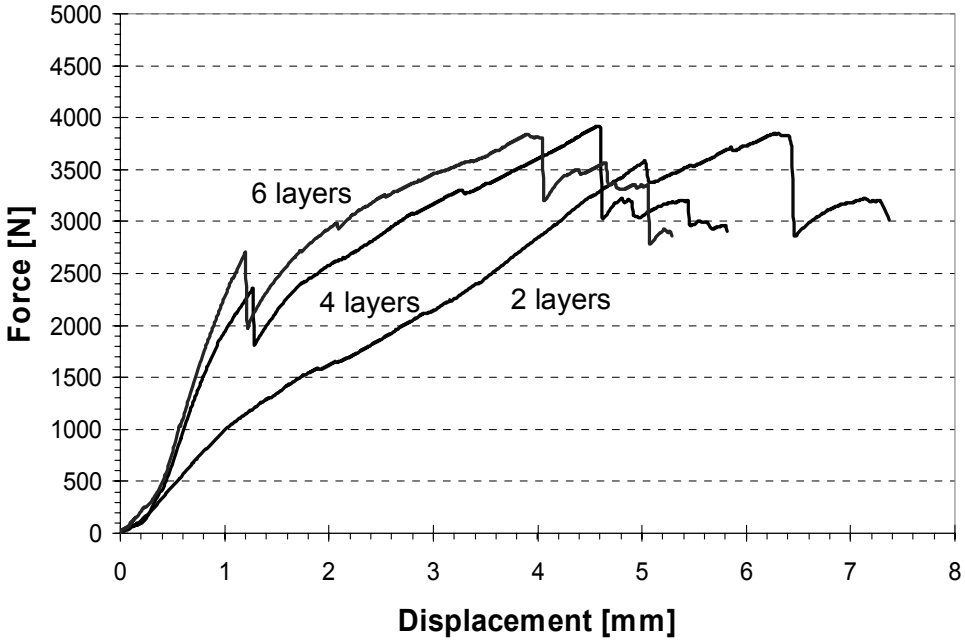

Figure 3.12: Change of the specimen stiffness in case of different number of base layers (Type of specimen: Type 3)

In case of specimen Type 4, where the inserts (Type A) were fixed with the improved double stitching, only the insert failure was noticed. The smaller range of deviation also reveals a homogenous failure mode. This implies that with this reinforcing stitching the limit value of the inserts' load carrying capacity was reached.

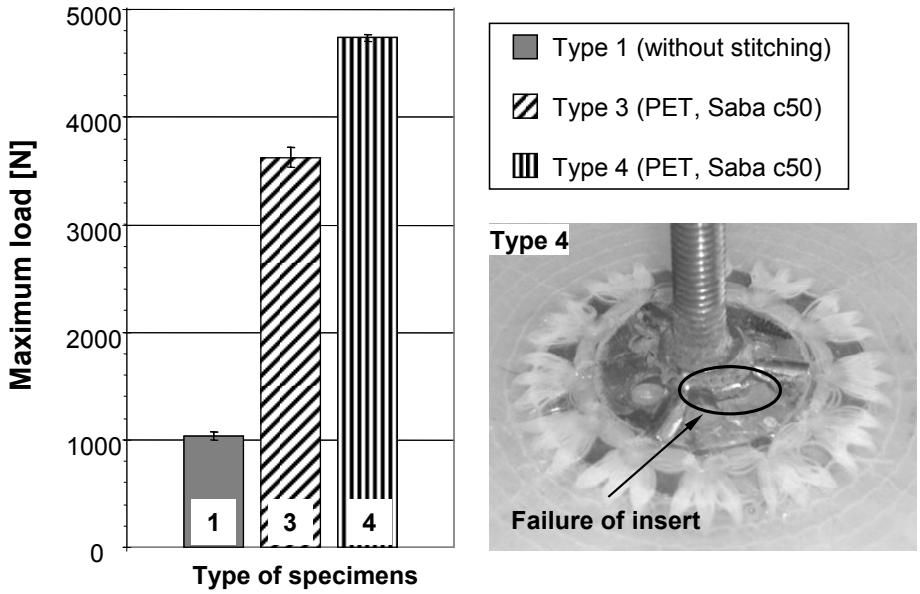

Figure 3.13: Results of the tensile tests and characteristic failure mode of the specimen Type 4 (Maximum load)

In this case, the stitches show almost no failure and the weak point of the system is shifted to the metallic insert Figure 3.13. With this type of stitching (Type 4) fivefold reinforcements can be achieved compared to the unstitched type (Type 1).

In case of specimen Type 5 the inserts were implemented without stitching but with a cover layer (Figure 3.4). The force - displacement diagram shows the higher stiffness of the specimen that arises from this construction (Figure 3.17, curve: Type 5). The result of this specimen type was distinguishable in all cases and the delamination between the cover and immediate layers could also be observed (Figure 3.14). This specimen type demonstrated a good reinforcing effect, but only with the larger standard deviation for strength values. The cover layer prevents the breakage of the inserts due to a reduced load per unit area acting on the insert. This is the reason for the further strength increase. This embedding type shows an improved performance compared to the stitched insert systems but the exact positioning of inserts is very difficult during the manufacturing process.

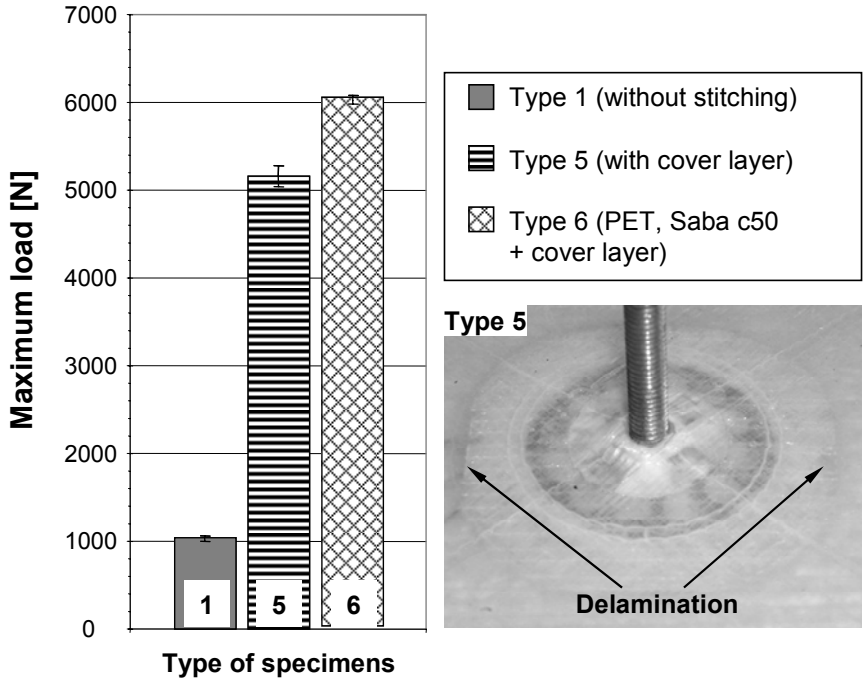

Figure 3.14: Results on the tensile tests of specimens with cover layer and the characteristic failure mode of the specimen Type 5 (Maximum load)

In case of specimen Type 6 stitching and covering were carried out simultaneously (Figure 3.5, Table 3.2) and a further significant increase in the delamination resistance has been observed (Figure 3.14). In this case the cover layer made the

insert failure mechanism more difficult and stitches prevented delamination (Figure 3.15). The range of standard deviation was much smaller than in the previous cases, hence, the higher reliability of this embedding type is demonstrated. The insert failure occurs at the inner pitch circle close to the bolt of the insert.

To cross check the above mentioned investigations, pure metallic inserts without embedding (Type 7) were also tested. In this case a testing frame built with a Ø26 mm cavity in the center was used as an insert holder. The metallic inserts were fixed with this holder frame to their base plates (Ø38 mm) during the tensile test. The result shows that the maximum value of the insert load carrying capacity varies from 80 to 130% of the embedded inserts (Type 4 and Type 6). Figure 3.15 shows the typical insert failure caused by tensile stress, and the resulting shear loading. During the tensile test, the metallic insert without embedding shows higher strength than the inserts stitched with the improved technology (Embedding types: Type 3 and Type 4). This may be the reason of the flexible clamping of the inserts, because in this case the base plate of the inserts is partially pulled out from the clamping frame. It has been observed that the plastic deformation of the insert base plates increase the breaking force of the metallic insert. The insert base plate was bell-shaped and, therefore, it took up most of the tensile stress, while at the embedded types transverse movement was arrested through the stitched base plate. Therefore, in the embedded case the insert base plate takes up the majority of shear stress.

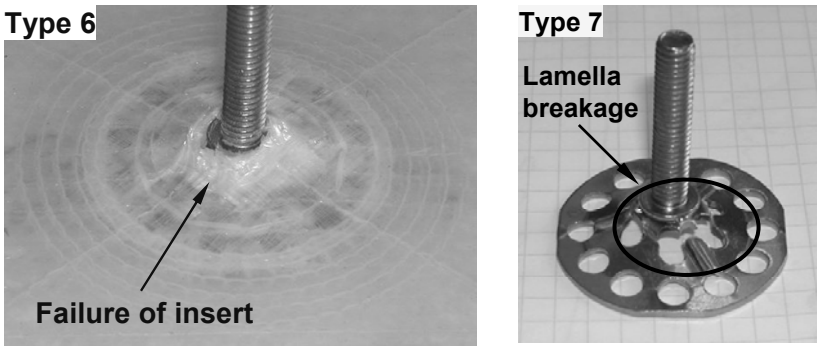

Figure 3.15: Fracture type of the embedded metallic insert (Type 6) and insert without embedding (Type 7)

The Table 3.4 shows the summarised mean values of the measured maximum forces and the standard deviations in case of the different specimens. Figure 3.17 shows the characteristic force - displacement diagrams of the different specimens.

Table 3.4: Test results

Type	Type of specimen	Stitches	Mean F (N)	SD
1	Without stitching	0	1084	67.3
2	Single stitching with Serafil 80 type PET thread	96	2496	373.5
3	Improved stitching with Saba c50 type PET thread	192	3628	175.9
4	Improved double stitching with Saba c50 type PET thread	384	4742	58.3
5	Without stitching, with cover layers	0	5155	242.1
6	Improved stitching with Saba c50 type PET thread and with cover layers	192	6022	101.1
7	Metallic insert	0	5203	280.5

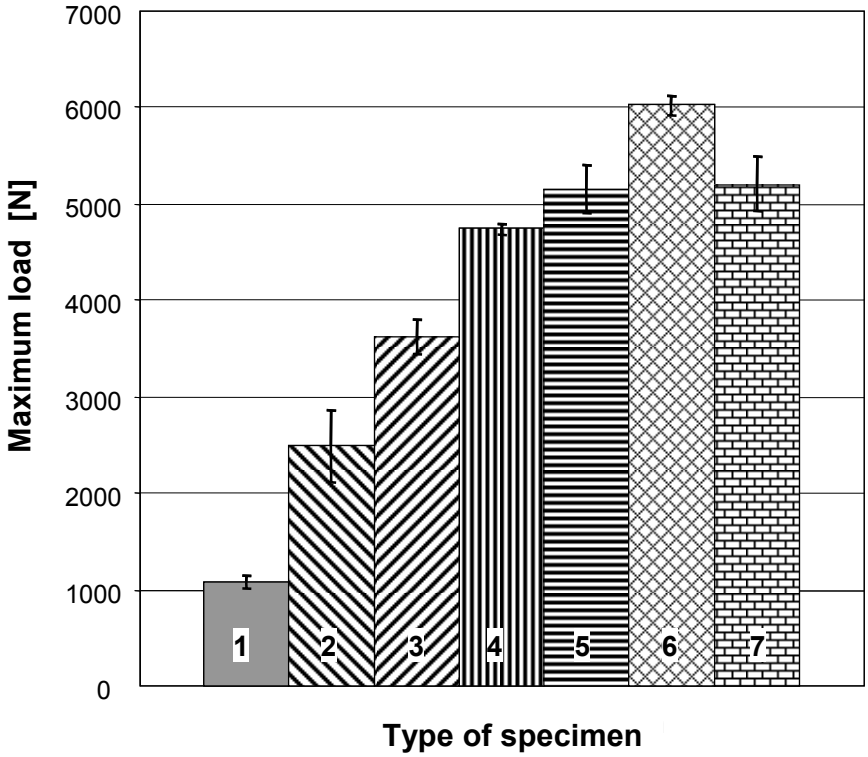

Figure 3.16: Comparison of differently stitched specimens (Maximum load)

To the extent that the economic aspect of the technology is concerned, the mechanical characterization of the metallic inserts can be improved by using stitching technologies and preforming techniques. At the same time the high performing costs must be considered as a disadvantage. Furthermore, manufacturing of different sub-preforms and assembling them into the net shape structure needs more time and manpower.

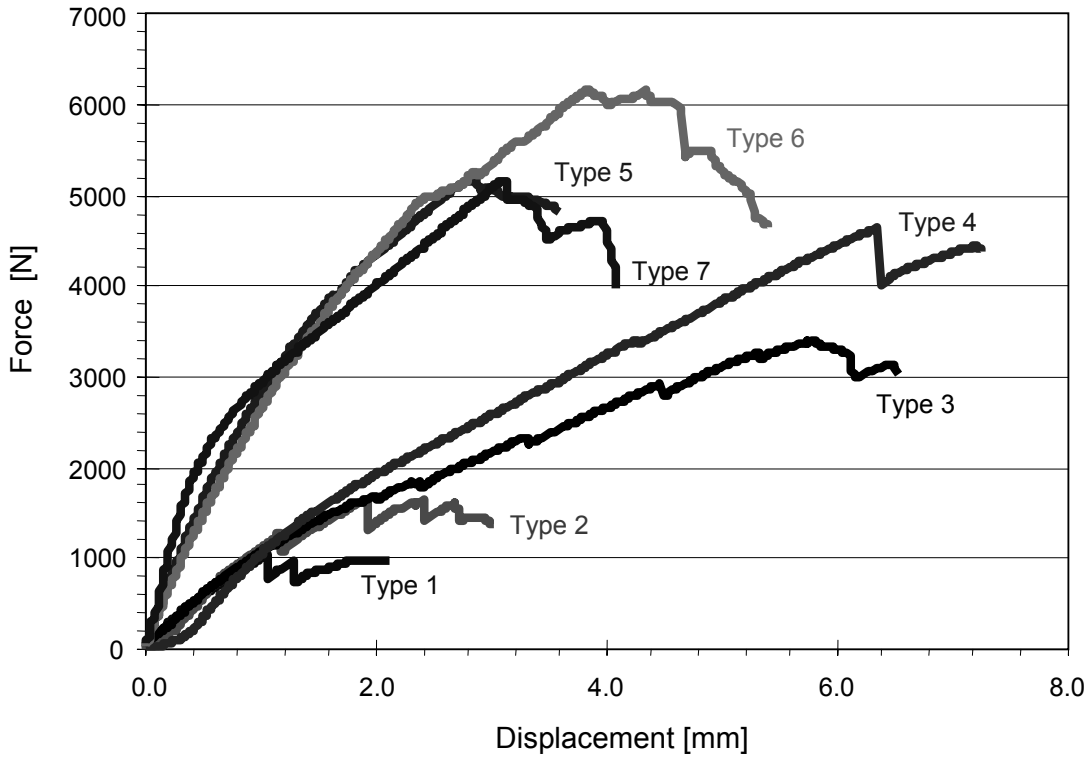

Figure 3.17: Characteristic force - displacement diagrams of different specimens

3.3 Investigations with high performance fibers

The aim of the following examinations is to study the applicability of high performance stitching threads in the fixing stitches of metallic inserts. Static tensile tests carried out on inserts fixed with polyester threads revealed that stitching improve the mechanical properties of the connection between the composite and the insert to a great extent [100]. The investigations below involve the evaluation of the mechanical investigations of metallic inserts stitched to the composite preform with high performance threads.

The above mentioned Big-Head® inserts were fixed in the preform of the specimens with high strength carbon, glass and aramid threads. The same stitching pattern and the same glass NCF was used to build up the specimens as applied in case of the investigation carried out on samples stitched with polyester fibers, hence the results of these two experiments can be compared properly.

After the first investigations with a core spun polyester (PET) thread (Saba c50) and Kevlar® spun thread (No. 50 7627 Amann & Söhne GmbH & Co. KG) a multifilament glass fiber, Culimeta MN 30 (Culimeta Textilglas-Technologie GmbH & Co.KG), and

1K CF fiber stitching thread (patented by the Institute für Verbundwerkstoffe GmbH) were used for the following experiments.

Table 3.5 contains the specimen selection. All the RTM parameters for specimen manufacturing, for instance, tool, vacuum, type of resin, applied curing time, temperature etc. were kept the same in all cases (Table 3.3).

Table 3.5: Specimen selection

Type	Type of specimen	Stitches	Without cover	With cover
8	Improved stitching with Amann No. 50 type Kevlar® thread	192	X	-
9	Improved stitching with Culimeta MN 30 type glass thread	192	X	-
10	Simple stitching** with 1K CF thread (Tenax HTA 5641)	96	X	-
** = Improved stitching with reduced stitch number				

Table 3.6 shows the mechanical properties of the dry stitching threads (without resin) applied for the investigations. The theoretical cross-section values are calculated from the material density and the specific weight values of the threads.

Table 3.6: Data sheet of the applied stitching threads

Thread type	Maximum Force F_{max} (N)	Specific weight tex (g/1000m)	Density ρ (g/cm^3)	Theoretical cross-section A (mm^2)	Elongation ε (%)	Theoretical maximal stress σ (MPa)
Amann Serafil 80	22	36.6	1.34	0.0273*	16	806*
Amann Saba c50	31	67.2	1.34	0.0501*	19	620*
Amann Kevlar® No. 50	76	61.5	1.44	0.0427*	4	1780*
Culimeta MN30	64/128*	139	2.60	0.0534*	4.8	2400
1K IVW CF thread (Tenax HTA 5641)	143*	67	1.78	0.0376*	1.4	3800
* = calculated values						

Based on the values shown in Table 3.6 the calculated theoretical total cross section and the maximum load force of the stitching threads are represented in the Table 3.7. The values show the theoretical maximum loadability of the stitched inserts in case of the different embedding types.

The examination of simple and double stitched inserts revealed that the reinforcing effect is not in direct proportion with the amount of fibers used. The reason for this phenomenon is that the thread already stitched in is damaged by the needle

penetrating it in the next step. Hence the thread can only fulfill its function partially. The extent of this damage is of course more significant in case of multiple stitched inserts.

Table 3.7: Theoretical total cross section and maximum force of the stitching threads per insert

Type of specimen		Stitches	Theoretical total thread cross-section A (mm^2)	Theoretical maximum thread Force F_{max} (N)
Type 2	Single stitching with Amann Serafil 80 type PET thread	96	5.2416*	4224*
Type 3	Improved stitching with Amann Saba c50 type PET thread	192	19.2384*	11904*
Type 4	Improved double stitching with Amann Saba c50 type PET thread	384	38.4768*	23808*
Type 8	Improved stitching Amann Kevlar No. 50 type thread	192	16.3968*	29184*
Type 9	Improved stitching with Culimeta MN30 type glass thread	192	20.5056*	24576*
Type 10	Simple stitching** with 1K IVW CF thread (Tenax HTA 5641)	96	7.2192*	27456*
* = calculated values ** = improved stitching with reduced stitch number				

In comparison with the measured results (Table 3.4) the theoretical values verify the observations that the threats are very strong degrade during the stitching process.

3.3.1 Experiments and results

In order to compare the different assembly technologies, static tensile tests were carried out on high performance threads stitched specimens. During the experiment the force needed for specimen fracture was measured and the characteristic failure modes were observed. All parameters of the tests were identical with the parameters used in case of the polyester threads (see in chapter 3.1 and chapter 3.2).

Tensile tests on stitched inserts (Type A) with improved stitching (Type 3 and Type 4) revealed that the characteristic failure mode of the system is not the breakage of single stitching threads but the breakage of the metallic insert. Alone this event occurred when double PET stitches were applied as reinforcements (Type 4) (Figure 3.13).

If Kevlar® fiber were applied as stitching thread, the characteristic failure mode was also the breakage of inserts (Figure 3.19). Hence, the real load capacity of these

yarns could not be examined due to the insert weakness. On the other hand, it was found that the load capacity of the metallic insert (Type A) can be achieved if single stitches are used. The poor stitching properties of Kevlar fibers have to be taken into consideration since they influence the applicability in a negative way. The results of fixing inserts (Type A) with glass threads (Culimeta MN30) and carbon threads did not show great improvements concerning load capacity (Figure 3.18). The reason for this phenomenon is that the characteristic failure was again the breakage of metallic inserts (Figure 3.19b) as well.

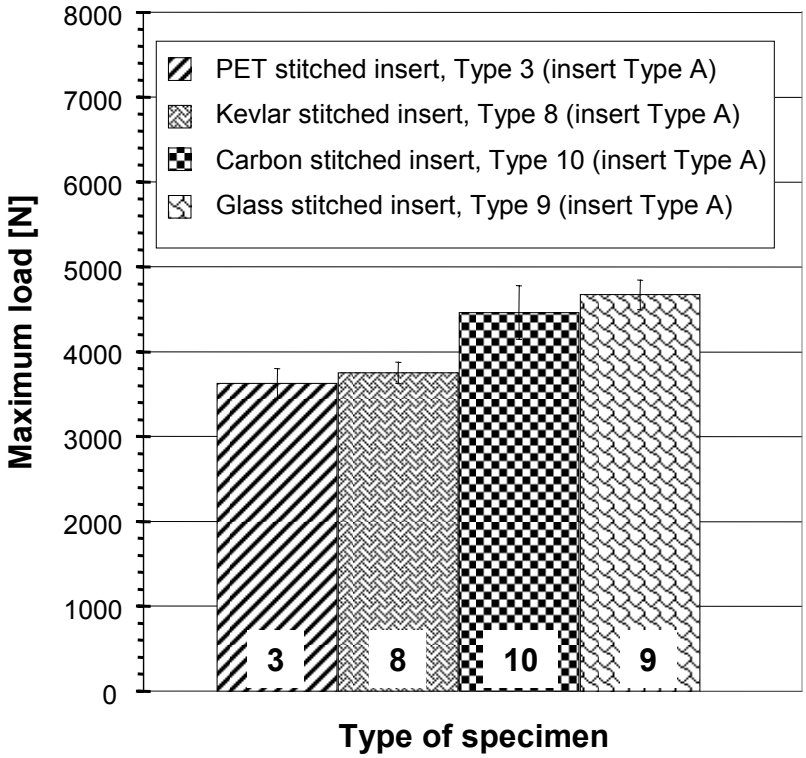

Figure 3.18: Results of the tensile tests with high performance threads, in case of inserts Type A

Nevertheless the low improvement of the load capacity arises from the higher theoretical maximum thread force (Table 3.7) and the thicker resin film above the metallic insert which is caused through the higher thread thickness in case of carbon and glass threads. The high stiffness and rigidity of glass and carbon fibers cause serious problems during stitching. Hence, these fibers can only be applied in a difficult way: only very low stitching speed and low thread tension can be set in this case. Since several fiber breakages occur during stitching, the process of stitching becomes slow and unreliable.

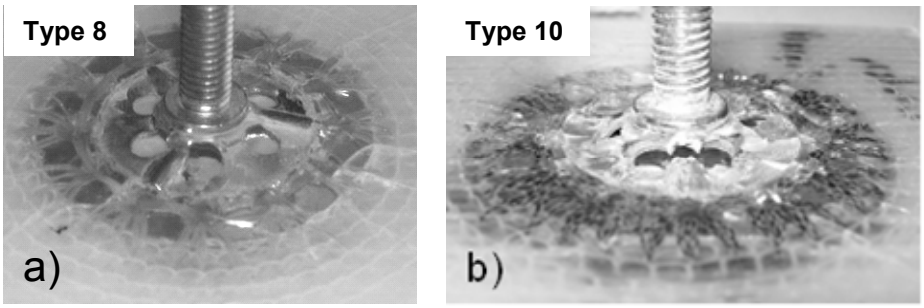

Figure 3.19: Failure mode by reinforcing with a) Kevlar® thread and b) carbon thread

In case of insert Type A the mechanical properties of the PET Saba C50 thread improved stitched reach the mechanical properties of the metallic inserts. Since stitching with PET threads is easy and involves no problems, a higher stitching speed can also be applied. The price of PET is lower than that of all the other investigated fibers, hence, its application can be recommended when considering economical aspects.

3.4 Specimen development

The real load capacity of fibers could not be measured due to the poor mechanical characteristics of inserts Type A, though a need for an improved insert emerged. For these investigations Big-Head® (Type A) inserts and inserts with improved base plate geometry (Type B) were applied as load carrying elements. In order to be able to compare the results exactly, only one geometrical parameter of the insert was changed. The existing results show that the failure of metallic inserts occurred at the base plate, and the weak point was the lamella between the inner pitch-circle holes. A new, improved insert (Type B) with a thicker base plate was applied in the next experiments (Figure 3.20). The improved steel insert (material: St 50-2 / S355J2G3, R_m= 470-610 MPa, R_{eH} = 295 MPa, A_5= 20%) consists also of a screwed bolt (M6) and a base metal plate perforated with two circular rows with 6 and 12 holes. The diameter of the holes at the inner and the outer pitch-circle is 4 mm and 5 mm, respectively and the thickness of the base plate in case of improved inserts (Type B) is 3 mm (Figure 3.20).

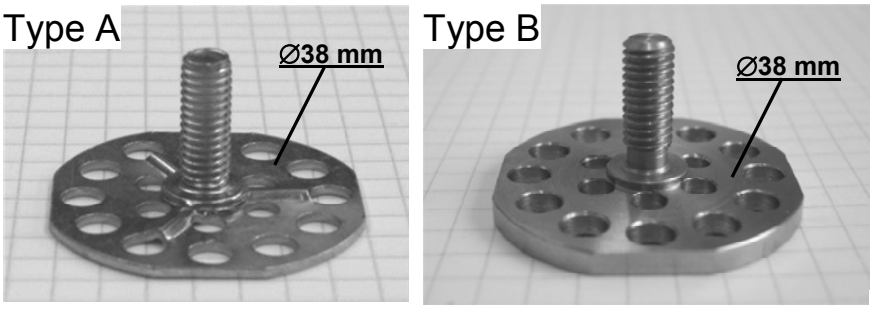

Figure 3.20: Metallic insert (Type A) and improved metallic insert (Type B)

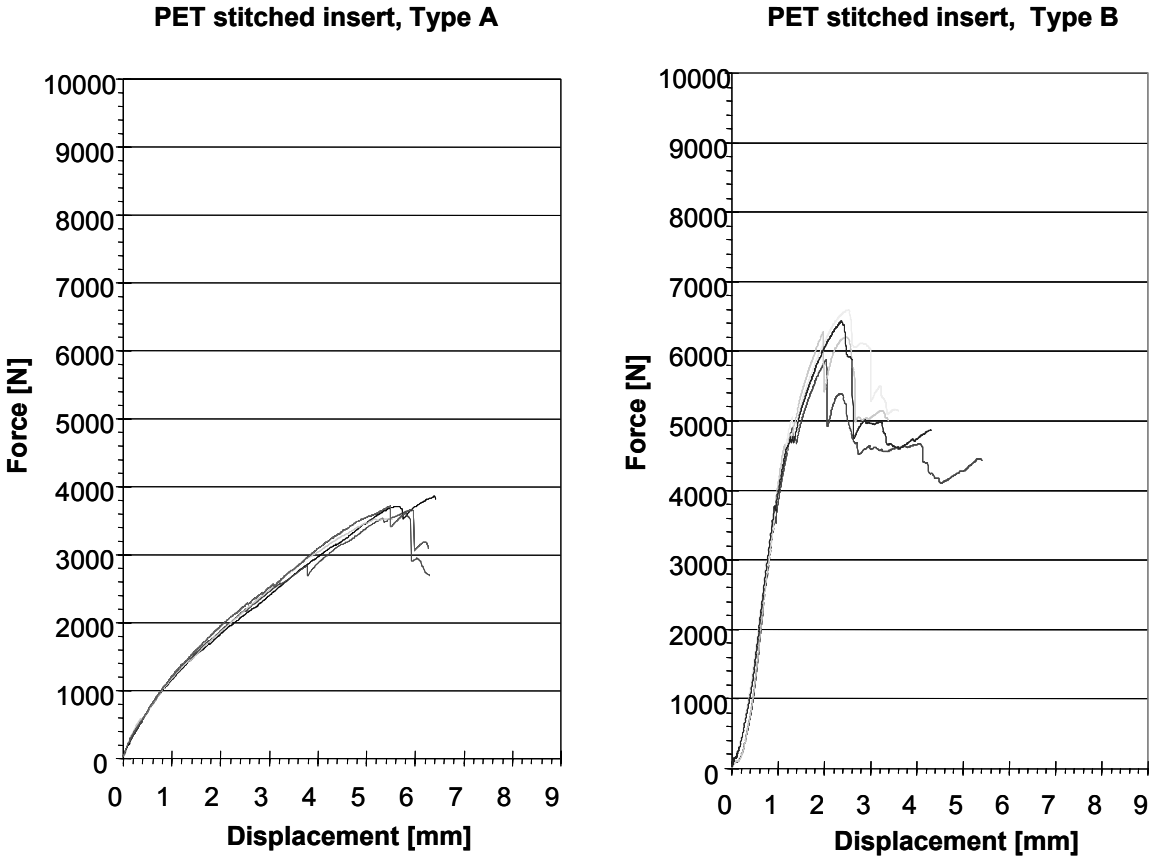

Figure 3.21: Result of the tensile tests on the PET stitched (Type of specimen: Type 3) inserts (Type A and B)

This way the breakage of the base plate could be eliminated, hence, the real load capacity of fibers could be studied and the results could be compared with the results obtained from the experiments of inserts Type A.

Investigation on insert Type B proved that specimens produced with improved polyester stitches show higher values than Type A inserts reinforced with the same stitching. The reasons for these values are the larger adhesion surface from the

higher insert base plate thickness and higher stiffness and strength of insert Type B. The base plate of the improved inserts did not bend, it transferred the loading to the fibers evenly, and hence they could express their impact commonly. As a result, it could be observed that all specimens with insert Type B were loaded safely up to 4500 N (Figure 3.21). The first delamination always took place at higher values than in case of inserts Type A (Figure 3.21).

In order to carry out comparative measurements, specimens of the same assembly but without stitching and with two further fabric layers with insert Type B (Figure 3.4b) were also manufactured.

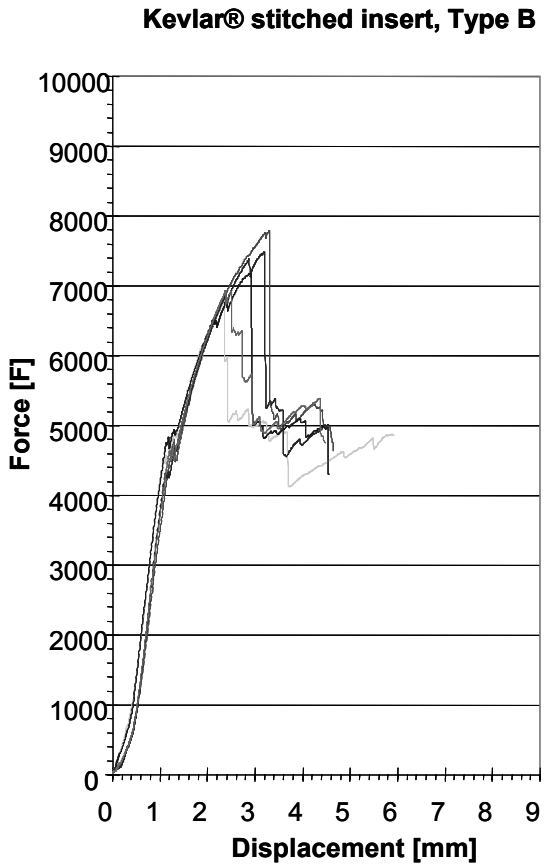

Figure 3.22: Result of the tensile tests on Kevlar® stitched (Type of specimen: Type 8) inserts (Type B)

The specimens produced with Kevlar® stitching threads show higher maximum values than inserts stitched with polyester fibers. However the first breakage however occurres at approx. 4500 N, then the specimens could be loaded reliably up to 6500

N (Figure 3.22). This fact reveals that the first delamination under the screwed bolt evolves at approx. 4500 N. The measured values show that the quality of thread does not have an impact on this phenomenon; primarily the stiffness of the insert influences this value.

Examinations of inserts produced with double stitches of polyester threads revealed that the higher quantity of fibers result in higher load capacity, but this increase is not linear. In average it provides 8000 N tensile force, while the single stitch results in a load capacity of approx. 6200 N (Figure 3.23). The reason for this phenomenon is that the thread already stitched in is damaged by the needle penetrating it in the next step. Hence the thread can only fulfill its function partially. This damage is more significant in case of multiple stitched inserts.

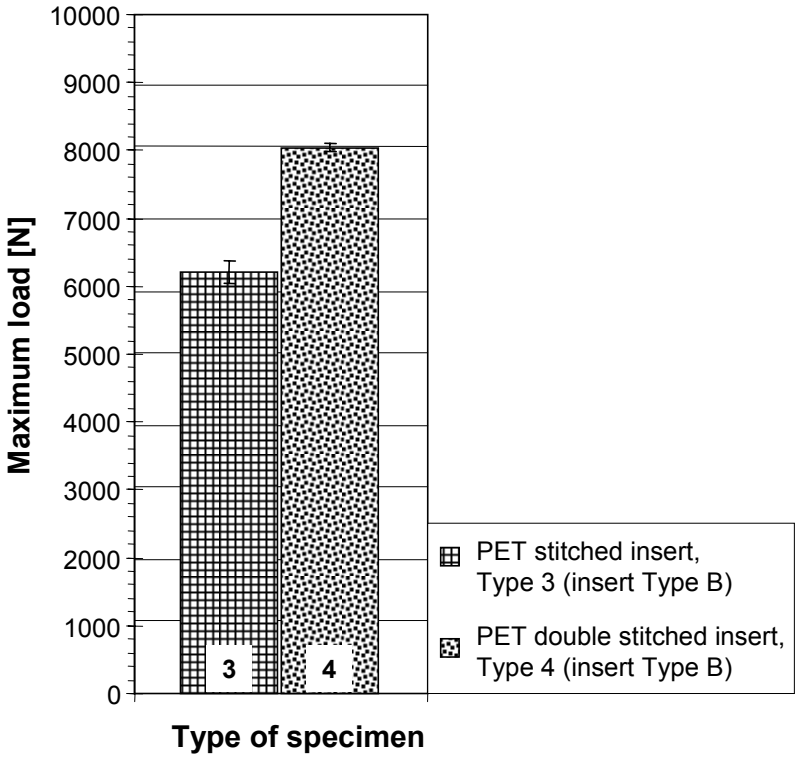

Figure 3.23: Results of the tensile tests with PET threads (Type of specimen: Type 3 and Type 4), in case of insert Type B

3.5 Cyclic tensile test of insert Type B

In case of double stitched (Type 4) Type B inserts, the first delamination breakage occurred only in the range above ca. 6000 N and the reason for it is the high stiffness of the insert base plate. However, a smaller crack could be observed before the first

breakage. The unevenness caused by this crack can be seen in the tensile test diagrams (Figure 3.24) around the 4000 N load. Despite this phenomenon, the specimens could be loaded until app. 6000 N without a significant change in the steepness of the tensile curve. Based on this phenomenon it can be concluded that the first cracks do not influence the further loadability of the insert, and the formed cracks, which are not visible, are not likely to serve as a base point of further cracks. A cyclic loadability test has been carried in order to prove this assumption. The upper limit of cyclic tensile tests was 5200 N, while the lower one was set to 2000 N. The specimen was loaded until total failure after five cycles. With the help of this examination it can be observed whether further crack propagation occurs after the appearance of the first cracks.

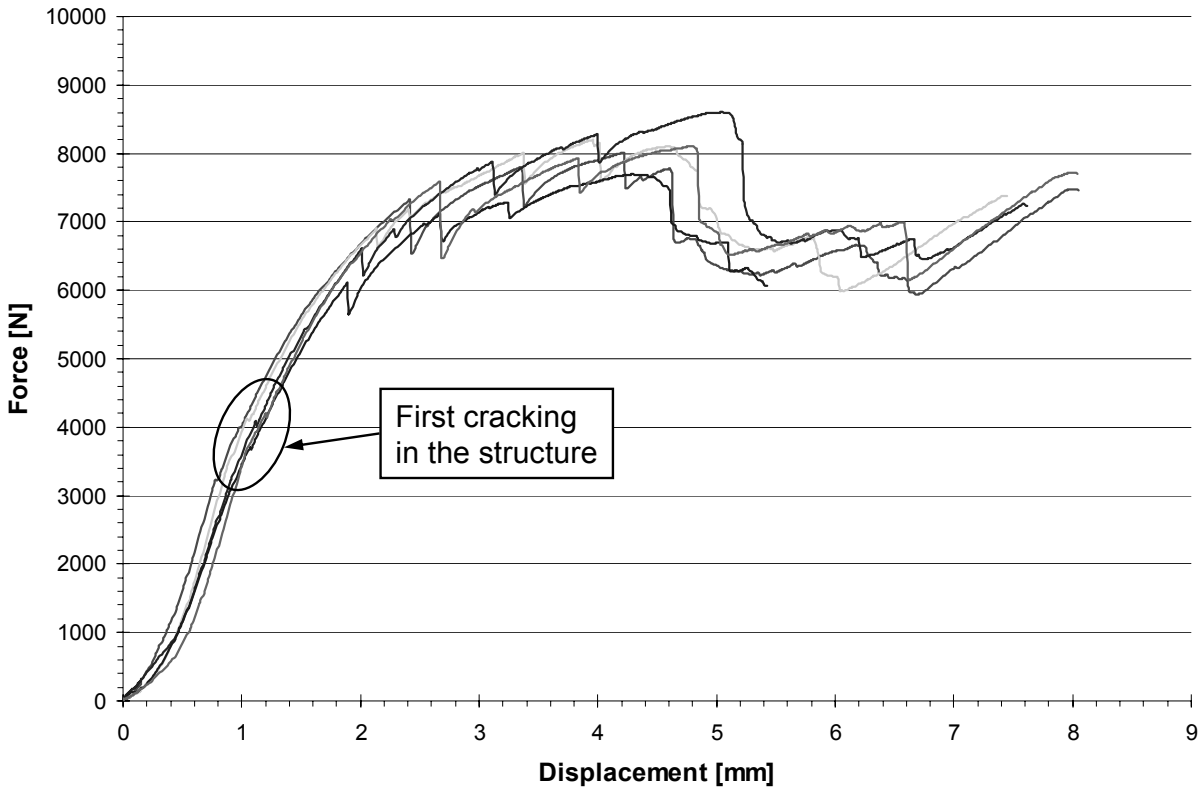

Figure 3.24: Force – displacement diagram of the tensile tests on insert Type B (Type of specimen: Type 4)

Figure 3.25 illustrates the characteristic force – time diagram in case of a tensile test carried out on a Type 4 specimen (insert type: Type B). The diagram reveals well that the small crack that occurred during the first cycle disappears in the next cycles in

the range between 2000 and 5200 N. Furthermore, the part of the curve after the maximal load shows that the multiple loads in that range do not influence the mechanical properties. The maximal force measured in the cyclic test is almost the same as the value experienced in simple tensile tests (app. 8000 N). The first delamination breakage occurred at the value of 6000 N in both cases.

The measurements revealed that the first hair-line cracks during the tensile test are probably caused by the stress formed during the production of the matrix. However, the occurrence of these hair-line cracks has in this case no significant influence on the mechanical characteristics of the insert – composite contact.

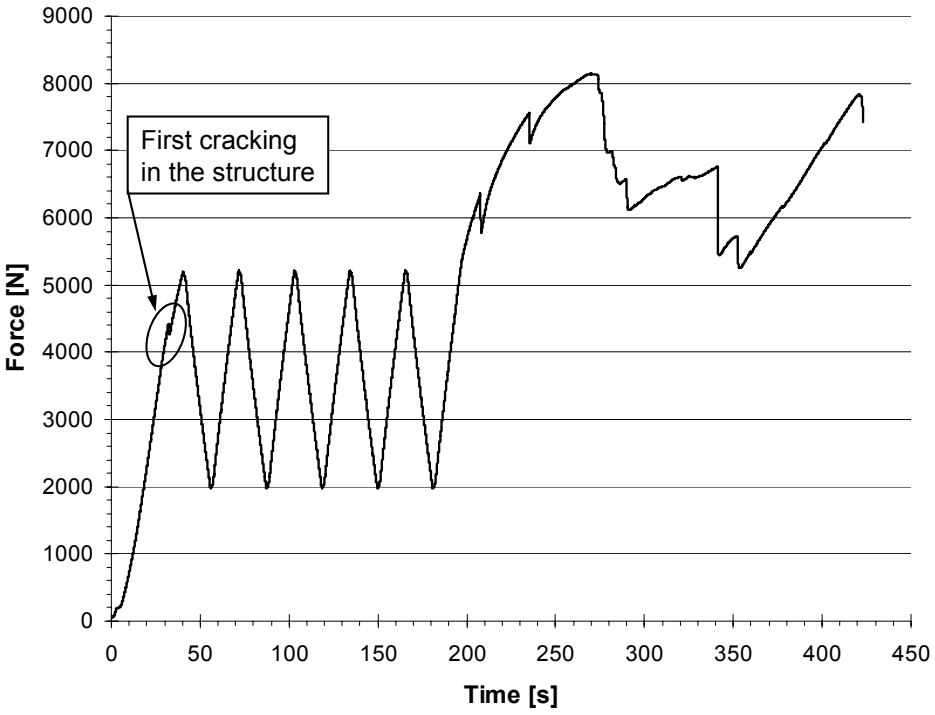

Figure 3.25: Cyclic tensile diagram of the stitched insert Type B (Type of specimen: Type 4)

3.6 Tensile tests of inserts fixed on the inner pitch circle

Since the first delamination breakage always occurs under the screwed bolt, the examinations were extended to an insert variation where the inner pitch-circle was also fixed (Figure 3.26, embedding type: Type 11). In this case the stitching threads next to the screwed bolt eliminate or delay the first delamination. Since the fibers are placed much closer to the place of the first delamination, their reinforcing impact is more effective.

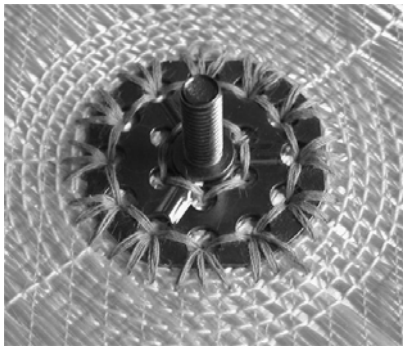

Figure 3.26: Insert (Type A) stitched on the inner pitch circle (Type of specimen: Type 11)

Examinations on PET stitched inserts Type A (Figure 3.1) showed that due to the small stiffness of inserts the first breakages start in the range of approx. 2000 N. Although the system can be loaded up to 4000 N, the tensile test diagrams show more, successive breakages (Figure 3.27).

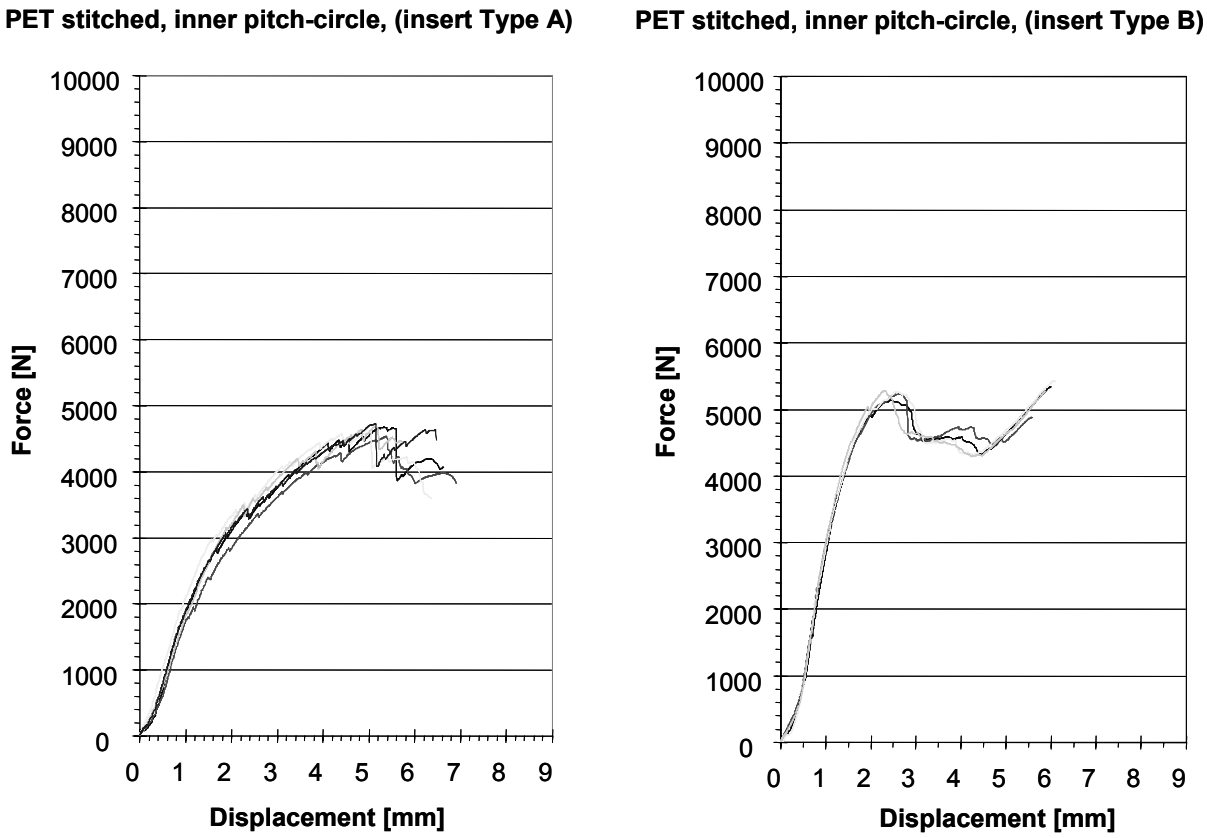

Figure 3.27: Result of the tensile tests on the inserts (Type A and B) stitched on their inner pitch circle (Type of specimen: Type 11)

It can be concluded that reinforcing inserts Type A on the inner pitch circle does obviously cause positive changes on the load capacity of the construction (Figure 3.21 and Figure 3.27). In case of insert Type B, it can be seen, that the stitching on the inner pitch circle causes no positive changes on the load capacity of the construction.

When examining inserts Type B, it was found that stitching the inner pitch circle prevented the occurrence of the first delamination that is expected at load values of 4500 N. The tensile test diagrams (Figure 3.27) showed that there is no breakage at these values, but at 5200 N a significant drop is revealed referring to the breakage of the stitches at the outer edge of the inserts.

The inserts do not delaminate from the base plate under the screwed bolts. Since the insert is very stiff and cannot bend with the base plate, high stress evolves at the edges of the insert plates. As a consequence, the ultimate breakage occurs within a relatively small range after the first fiber breakage. The results reveal that in case of insert Type B the first delamination can be hindered by reinforcing the inner pitch circle with stitches, but this reinforcing mode did not increase the load capacity of the system (Figure 3.21, type of specimen: Type 3, insert type: Type B).

3.7 Finite element modeling of tensile tests

Nowadays the numerical methods widespread in engineering shorten the design process significantly. With their help, the strength and other parameters of the parts can already be examined and hence optimized according to the requirements in the design phase. In case of mechanical calculations, the most widespread numerical method is finite element modeling (FEM), a node oriented process. This can also be considered as the classical Ritz method with a special property that the base functions for discretization use the principle of local approach [101]. This principle provides the solution in nodes (discretized points) among which the displacement field can be interpolated with the help of the form functions. The simple, linearly elastic FEM calculations can be described by the known equation of $\underline{\underline{K}}\,\underline{U} = \underline{f}$ (where $\underline{\underline{K}}$ is the sum of the stiffness matrix of the elements, $\underline{U}$ is the generalized node displacement, $\underline{f}$ is the typical right side vector and the external loading is presented in

nodes) in the range of small displacements [102]. If this matrix is known, the displacement of nodes is obtained.

Since in our case the calculations also involve nonlinear parts in the second step, the nonlinear method was used for the modeling of stitched inserts. Due to the large displacements, ($\underline{\varepsilon}^{L}$), the Lagrange type deformation tensor, can be applied. Matrix $\underline{\underline{B}}$ that describes the node displacement connection of deformation is of simple shape in linear FEM, however in the nonlinear case it can be written as follows:

$$\underline{\underline{K}}_{G} = \left[\underline{\underline{B}}_{L0} + \frac{1}{2} \cdot \underline{\underline{B}}_{L1}(\underline{U}) \right] \cdot \underline{U} \tag{3.3}$$

where $\underline{\underline{B}}_{L0}$ is the linear term that - in case of small displacements - converges to the one known in linear FEM. $\underline{\underline{B}}_{L1}(\underline{U})$ is the nonlinear term that depends on the displacement. The nonlinear FEM basic equation is $\underline{p}(\underline{U})$-$\underline{f}$ = 0. This equation is usually solved with the Newton-Raphson process, hence the tangential stiffness matrix ($\underline{\underline{K}}$= $\underline{\underline{K}}_{M}$ + $\underline{\underline{K}}_{G}$) can be produced with the Taylor series expansion.

In the first step the testing configuration (Figure 3.7) of the metallic insert with composite layer component has been modeled. The glass fiber orientation inside the composite laminate is presented in Figure 3.29 (embedding type: Type 1). To be able to model this composite structure, the calculations of the material properties along with the different layers have been performed and can be transformed to a global coordinate system.

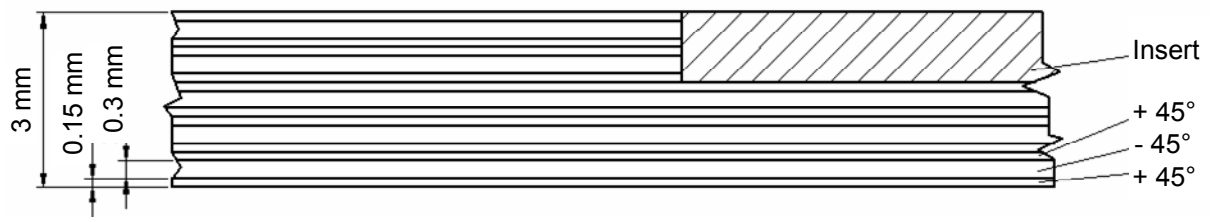

Figure 3.28: The structure of the composite layers

In this case, the lay-up is reinforced by using unidirectional glass fibers (NCF). It means that the composite layers can be modeled transversely quasi isotropic. A transversely isotropic material has three planes of symmetry and thus, it is orthotropic in nature. When the material is reinforced with unidirectional fibers, all the

fibers are aligned in direction *p*. In this case the in plane material properties perpendicular to the fibers (*q*-*r* plane) are modeled isotropic, due to a homogeneous fiber distribution in this cross section (Figure 3.29) [103].

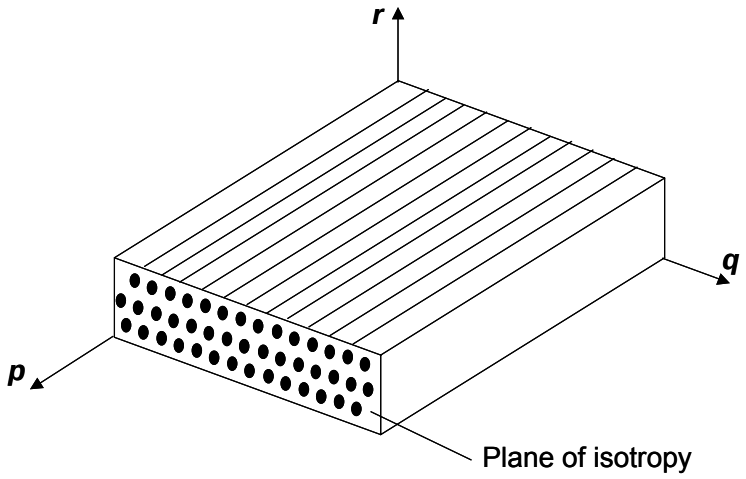

Figure 3.29: The fiber orientation of the composite layers (transversely isotropic composite material)

The stress strain relationship in the primed coordinate system written by the transformation matrices is shown in equation (3.4) and (3.5).

$$\underbrace{\left[\underline{\underline{T}}_{\sigma}\right]\underline{\sigma}}_{\underline{\sigma}'} = \underbrace{\left[T_{\sigma}\right]\left[\underline{\underline{C}}\right]\left[\underline{\underline{T}}_{\varepsilon}\right]^{-1}}_{\left[\underline{\underline{C}}'\right]}\underbrace{\left[\underline{\underline{T}}_{\varepsilon}\right]\underline{\varepsilon}}_{\underline{\varepsilon}'} \tag{3.4}$$

$$\underline{\sigma}' = \left[\underline{\underline{C}}'\right]\underline{\varepsilon}' \tag{3.5}$$

Where:

σ is the stress matrix in the coordinate system of the fibers

$\left[\underline{\underline{T}}_{\sigma}\right]$ is the three dimensional stress transformation matrix

$\underline{\sigma}'$ is the stress matrix transformed into the primed coordinate system

ε is the strain matrix in the coordinate system of the fibers

$\left[\underline{\underline{T}}_{\varepsilon}\right]$ is the three dimensional strain transformation matrix

$\underline{\varepsilon}'$ is the strain matrix transformed into the primed coordinate system

$\left[\underline{\underline{C}}\right]$ is the stiffness matrix in the coordinate system of the fibers

$\left[\underline{\underline{C}}'\right]$ is the stiffness matrix transformed into the primed coordinate system

The transformed stiffness matrix is written by the three dimensional stress and strain transformation matrices (equation 3.6) [103].

$$\left[\underline{\underline{C}}'\right] = \left[\underline{\underline{T}}_{\sigma}\right]\left[\underline{\underline{C}}\right]\left[\underline{\underline{T}}_{\varepsilon}\right]^{-1} \tag{3.6}$$

With the actual material data (E_p= 40 GPa, E_q= 6 GPa, G_{pq}= 3.75 GPa, ν_{pq}= 0.27, ν_{qr}= 0.4) and using the equations (3.4), (3.6) the stiffness matrices for both layers with +45° and -45° fiber orientation can be calculated. The calculation results show the (3.7) and (3.8) matrices.

$$\left[C'_{+45°}\right] = \begin{bmatrix} 17.362 & 9.862 & 2.924 & 0 & 0 & -8.545 \\ 9.862 & 17.362 & 2.924 & 0 & 0 & -8.545 \\ 2.924 & 2.924 & 7.332 & 0 & 0 & 0.122 \\ 0 & 0 & 0 & 2.946 & -0.803 & 0 \\ 0 & 0 & 0 & -0.803 & 2.946 & 0 \\ -8.545 & -8.545 & 0.122 & 0 & 0 & 10.81 \end{bmatrix} [GPa] \tag{3.7}$$

$$\left[C'_{-45°}\right] = \begin{bmatrix} 17.362 & 9.862 & 2.924 & 0 & 0 & 8.545 \\ 9.862 & 17.362 & 2.924 & 0 & 0 & 8.545 \\ 2.924 & 2.924 & 7.332 & 0 & 0 & -0.122 \\ 0 & 0 & 0 & 2.946 & 0.803 & 0 \\ 0 & 0 & 0 & 0.803 & 2.946 & 0 \\ 8.545 & 8.545 & -0.122 & 0 & 0 & 10.81 \end{bmatrix} [GPa] \tag{3.8}$$

3.7.1 Finite element analysis

The target of the FE investigations in the first stage is to study the modeling methods of a layered composite structure with embedded metallic insert. The first section of the inserts loading before of the failure of the structure was modeled by FE. The characteristic failure mode after this section is delamination between the metallic insert and the composite structure. The delamination was observed as a characteristic failure mode in case of embedding type Type 1. A 3D FE model has

been developed to simulate the construction of the composite layers and the metallic insert. The various fiber orientations were modeled layer by layer in the composite structure. The material law given for composites is linear anisotropic and the elements of the matrix stiffness applied for both layer types can be found in matrices (3.7) and (3.8). The material law of the metallic insert is linear isotropic. The material constants of the steel insert taken for the calculations are: E=210 GPa, v=0.3.

The hypothesis that the composite layers and the steel insert has been made are well embedded. The ideal insert – composite base plate contact is modeled with common nodes. The bonding by stitching is not modeled in this first case. In the model, the steel clamping part (Frame) of the testing machine is connected to the test specimen by contact elements. Figure 3.30 shows a FE mesh and the loading of the model. The frame parts were fixed and a force pulled up the bolt of the metallic insert. The measurement configuration allows free displacement between the frame and the base plate, so contact elements were used between the frame parts and the composite base plate (Figure 3.30). These FE investigations were carried out with FE Software Cosmos Design Star. The model contains 50907 nodes, 59357 TETRA elements and 1579 contact elements. The calculations were linearly generated and the time required for the simulation was app. 22 hours on a P4 machine.

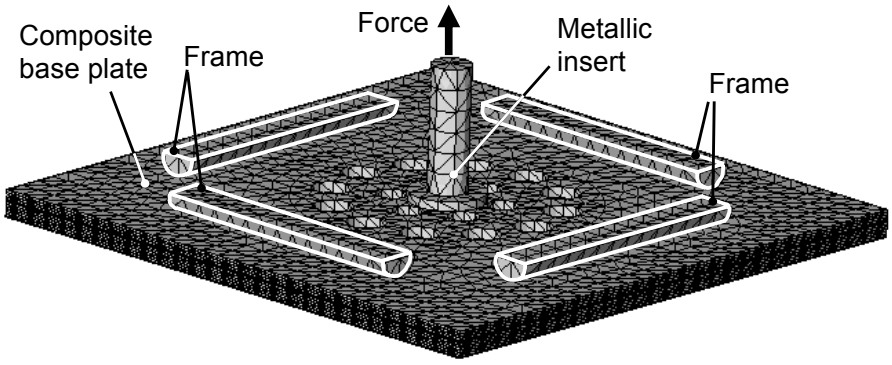

Figure 3.30: The FE mesh, the boundary conditions and the load of the FE model

The correspondence between the FE calculated and the experimentally observed load displacement results of the specimen are shown in Figure 3.31. Here, it can be concluded that the used constraints as well as the load values, the material data are very realistically calculated in the case of unstitched inserts until the first delamination.

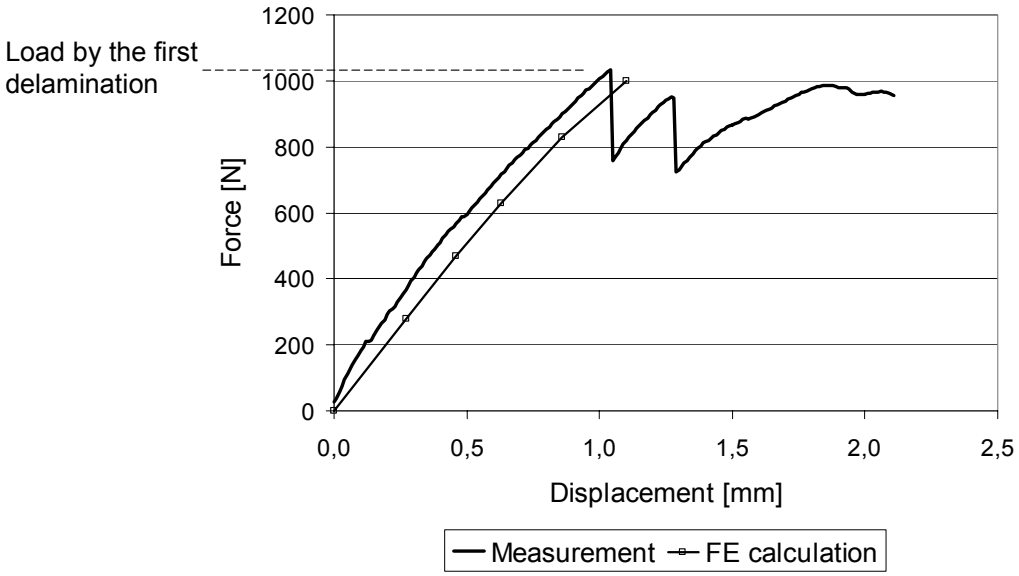

Figure 3.31: The FE calculated and the measured load displacement curve

The calculated resultant deformation of the specimen (Figure 3.32) is similar to the deformation observed in the experiments. The displacement results of the FE calculation (Figure 3.32) show the largest displacement at the edges of the specimen, which supports the spherical deformation of the specimen during the testing.

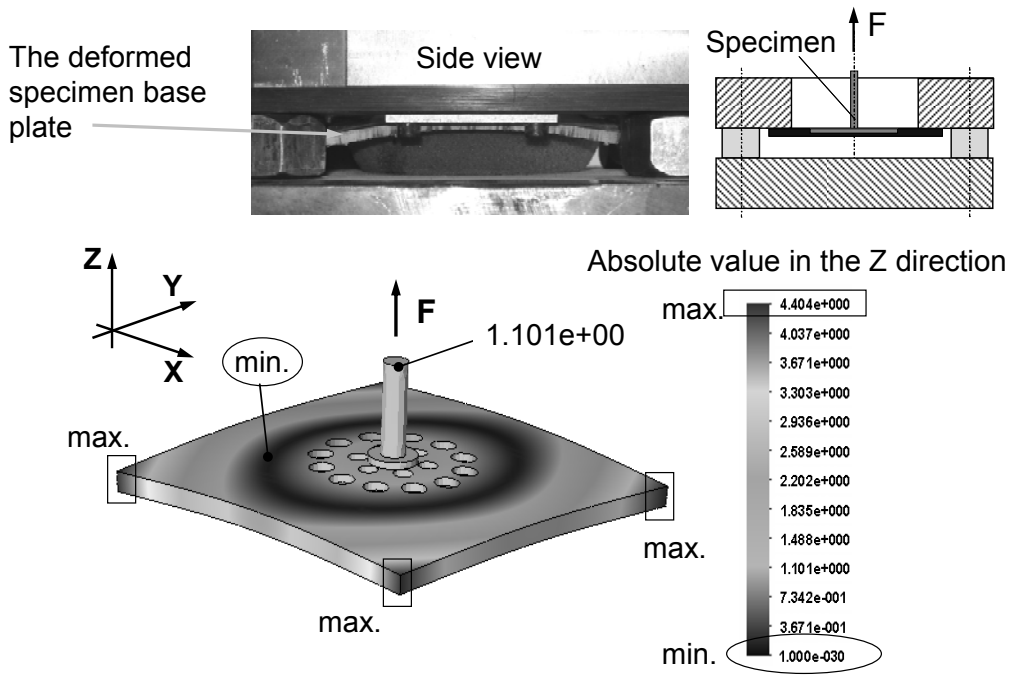

Figure 3.32: The deformed specimen base plate during tensile testing, and the deformed shape of the FE model

The resultant displacement values are the absolute values of displacements effected by the loading.

In Figure 3.33, the Von Mises stress result shows that the maximal stress will be evaluated at weakest points of the steel insert. The experimental results shows, the failure of the insert base plate is observed exactly at the calculated highest Von Mises stress. In the composite laminates the evaluated Von Mises stress results are lower than the stress in the steel insert, because of the lower values of the laminate material properties. At this stress level no failure are observed in the composite material.

Figure 3.34 shows the calculated equivalent strain results where the failure initiation location at the maximum equivalent strain can be observed. In the composite laminates the evaluated equivalent strain results are in the same range as in the steel insert (Figure 3.15, Type 7).

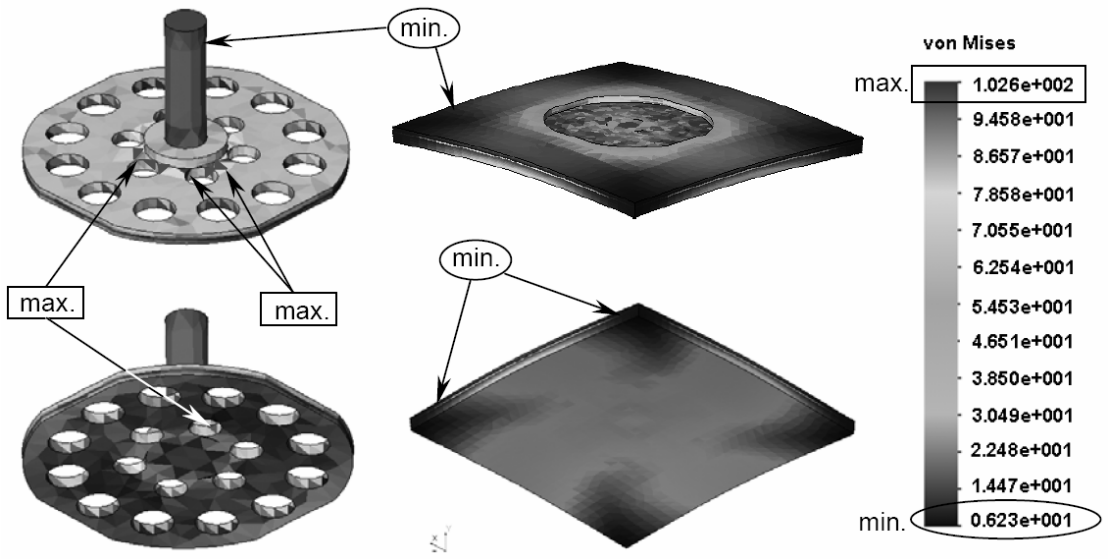

Figure 3.33: The Von Mises stress FE calculation results by 1000 N load on the insert and for the layers

The steel insert cannot be deformed as an ideal sphere segment because of the thick neck of the thread on the base plate. So the delamination process between the steel insert and the laminates will be evaluated under the thread at the backside of the insert. The holes around the neck are stress expanding places.

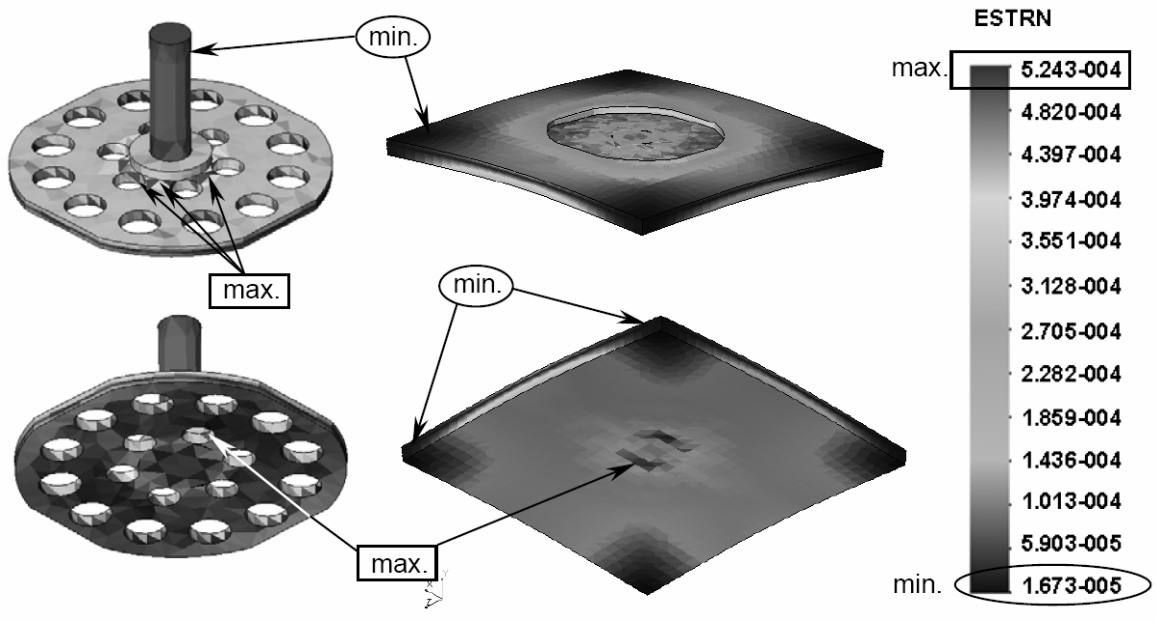

Figure 3.34: The equivalent strain FE calculation results by 1000 N load for the insert and for the laminate

The next step is to improve the model and to simulate the inserts fixed by stitching. Table 3.8 shows the mechanical properties of the dry stitching thread (without resin) applied for the modeled specimen.

Table 3.8: Data sheet of the applied thread

Thread type	**Maximum Force F_{max} (N)**	**Specific weight tex (g/1000m)**	**Density ρ (g/cm^3)**	**Theoretical cross-section A (mm^2)**	**Elongation ε (%)**	**Theoretical maximal stress σ (MPa)**
PET, Amann Saba c50	31	67.2	1.34	0.0501*	19	620*
* = calculated values						

The calculated theoretical total cross section and the maximum load force of the stitching thread applied for the modeled embedding are represented in the Table 3.9.

Table 3.9: Theoretical total cross section and maximum force of the stitching thread applied for the modelled embedding type

Type of specimen		**Stitches**	**Theoretical total thread cross-section A (mm^2)**	**Theoretical maximum thread Force F_{max} (N)**
Type 3	Improved stitching with Amann Saba c50 type PET thread	192	19.2384*	11904*
* = calculated values				

The simulations were carried out with the ANSYS 10.0 software (supplier: ANSYS, Inc.). The material constants used in the calculations are included in Table 3.10. The embedding type of the simulated specimen is Type 3 (insert Type B).

Table 3.10: Applied material constatnts

Components	Materials	E [GPa]	G [GPa]	ν [-]	R_m [MPa]	ε_{max} [%]
Insert	Steel	210		0.3	300 (R_{eH})	3.2
Stitching yarn	PET	7.5			620	19
Matrix	Epoxy	3.4	1.2	0.35	64	1.9
Reinforcing material	E-glass	80	37	0.18	3200	4.0

Where:

E Young's modulus
G Shear modulus
ν Poisson's ratio
R_m Ultimate tensile strength
R_{eH} Yielding strength
ε_{max} Ultimate elongation

Since the task is to model a complex system, the different elements were defined with different material laws. In case of stitched inserts, the primary load bearing element is the stitching thread. The connection between the insert and the matrix material formed during the injection can also be defined as a load bearing element. The modeling task can be divided into three parts accordingly:

- Modelling the composite plate and the metallic insert
- Modelling the insert bonding (reinforcing) stitching
- As well as modelling the bonding effect of the matrix material on the insert

The applied material laws for the participating elements:

- Insert — linear elastic – ideal plastic, isotropic
- Stitching yarn — linear elastic, isotropic
- Matrix — linear elastic, isotropic
- S-glass — linear elastic, isotropic
- Insert-matrix bonding — special sigma-epsylon characteristic defined

Three different element types were used to model the different parts of the stitched insert-composite base plate structure (Table 3.11). For the calculations in the model, the orthotropic material properties of the composite base plate were defined with the help of the correspondent *real constants* of the FE software.

Table 3.11: Element types for the FE modeling using the definitions of ANSYS 10.0

Components	Element type	Element description	Node	Number of elements
Stitching yarn	LINK10	LINK10 is a 3-D spar element having the unique feature of a bilinear stiffness matrix resulting in a uniaxial tension-only (or compression-only) element.	2	180
Metallic insert	SOLID95	SOLID95 is used for the 3-D modeling of solid structures. The element is defined by 20 nodes having three degrees of freedom per node	20	5760
Insert-matrix bonding	SOLID95		20	1520
Composite plate (orthotropic)	SOLID95		20	350

In order to be able to model the insert – matrix adhesion (Figure 3.36 b), an intermediate layer between the composite base plate and the insert has to be defined (insert-matrix bonding). The material law of this layer is defined with a given sigma-epsilon curve that provided the good approximation of the effect of real adhesion in the model. The maximum value of the tensile stress in the insert-matrix bonding is set to 17.5 MPa and the maximum elongation is set to 2.9% [75]. According to the material law, this intermediate layer can only reach a definite stress value, after which the stress arising in the material will remain constant, i.e. the sigma-epsilon curve will continue in a horizontal line (Figure 3.35). This way after reaching the yielding stress in the insert-matrix bonding, the whole load of the insert will be transferred through the stitching threads to the composite base plate. This behavior corresponds to the already examined characteristic failure modes approximately. The inserts delaminated from the composite plate under the threaded pin after a given load value, and then the load was only taken by the stitching threads.

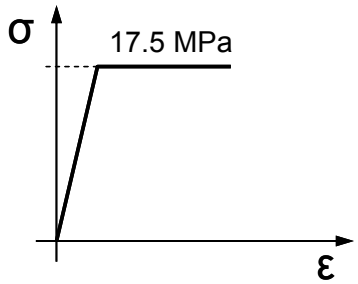

Figure 3.35: The defined material law of the insert-matrix bonding

The four different parts of the whole model are illustrated in Figure 3.36. Figure 3.37 shows the exact position of the modeled stitching threads in the structure. The

threads are modeled with eight linear elastic, isotropic, *LINK10* elements coupled to the single insert holes. There through 64 elements hold the insert to the modeled composite plate. Because the calculated total cross section of the stitching threads are 19.2384 mm^2 per insert (Table 3.9) to a first approximation the single thread element cross sections were set to 0.3006 mm^2 in the model.

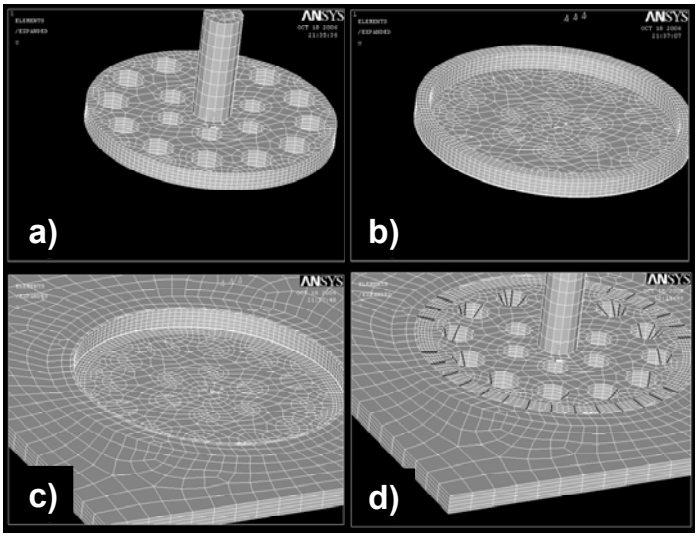

Figure 3.36: Parts for the whole model: a) insert, b) insert-matrix bonding, c) composite base plate, d) the whole model with the stitching yarns

The parametric structure of the model makes it possible to choose the strength properties of single parts, and this way the model can be adapted to the real values. Due to the nonlinear element of the model, the simulation can approach the curves that belong to real behavior of the structure well, even in case of stitched inserts.

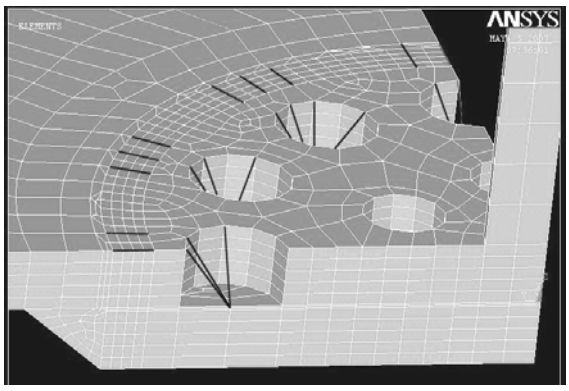

Figure 3.37: Stitching threads in the FE model

After the set of the mechanical properties of the single modeled parts to the real values (Table 3.10), the stitching thread cross section was changed to approach the

measured curve characteristic of the static tensile test carried out on the specimen Type 3 (insert Type B). The model was in this manner optimized.

The force-displacement curve shows that the simulation corresponds well to the measurement results of an improved PET stitched, Type B insert (Figure 3.38).

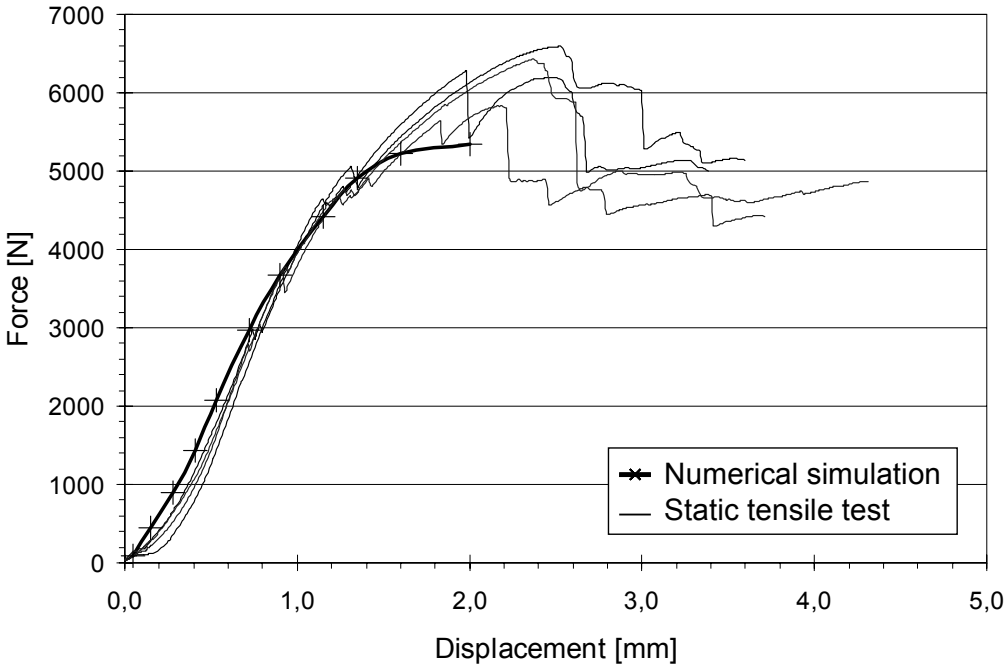

Figure 3.38: Result of the numerical simulation in case of stitched insert Type B (Type of specimen: Type 3) compared with the measured values

Arrived the adequate curve characteristic the resultant cross section of the modeled single stitching threads was 0,2147 mm^2, thus the total resultant cross section of the threads is 13.74 mm^2. In comparison to the calculated theoretical total cross section (19.2384 mm^2) the values indicate the above-mentioned stitching thread degradation during the stitching process.

Furthermore, the result of load simulation reveals the reasons for the characteristic failure modes experienced in the measurements. In case of Type A inserts the first breakage was always the delamination below the screwed bolt of the insert (Figure 3.11). The reason for this phenomenon is the different stiffness of the insert base plate and the composite sheet. If the stiffness of the composite plate is higher than that of the insert base plate, then large stresses may evolve in the zone below the threaded pin during the bell-shaped deformation of the insert base plate, and as a result the metal separates from the composite plate. This phenomenon is described

by the large stress and strain values generated in the model in the intermediate layer (Figure 3.39). This can also be observed in the tensile test of specimens manufactured with base plates of different thicknesses. It is well visible in Figure 3.12 that in case of thicker, hence stiffer composite plates (6 NCF layers in the composite base plate) the breakage caused by the first delamination can be seen in the curve more definitely than in case of a system of small stiffness (2 NCF layers in the composite base plate). Nevertheless, in the further stages of loading the stitching threads take the load, hence the diagrams reveal that the value of final failure is not so significantly influenced by the change in the thickness of layers.

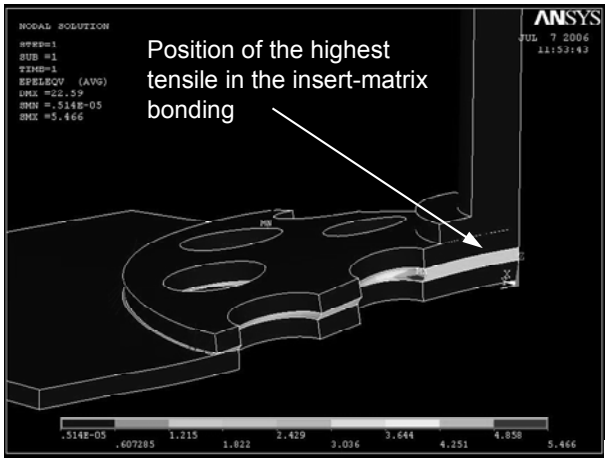

Figure 3.39: Bell-shape deformed, stitched metallic insert with low stiffness

If the stiffness of the composite base plate is significantly smaller than that of the insert base plate, then the insert base plate cannot follow the deformation of the composite base plate, hence large stresses evolve at the edges of the insert base plate. This phenomenon is illustrated in the image created of the model Figure 3.40. This effect is the reason for the values measured on the Type B inserts fixed by stitching on the inner pitch circle. In this case the assumption was that the insert (Type B) with thick base plate, stitched on the inner pitch circle shows higher values than a B type insert stitched only on the outer pitch circle. However, the measurements did not reveal significant improvement (Figure 3.27). The reason is the large stiffness of the Type B insert and the effect of the seam prepared on the inner pitch hole. The seam fixed the composite base plate in the zone below the threaded pin of the insert, hence it moved together with the insert in the tensile tests. The distortion of the composite plate resulted in the formation of large stress at the

edges of the insert base plate. Hence the seam there broke due to the large load, and then the loading could only be taken by the seam at the inner pitch circle but this seam could not bear this large loading.

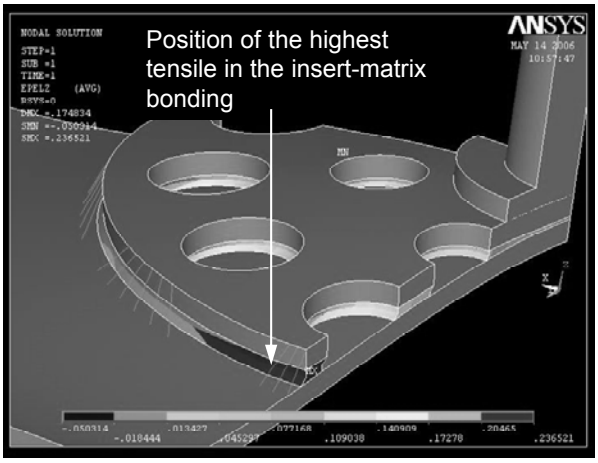

Figure 3.40: Strain of the insert-matrix bonding in case of high insert stiffness

Fundamentally, it can be stated that the insert-composite connection can take up the maximal load if the stiffness of the two connecting elements (stitched insert base plate and composite base plate) is almost the same.

Further examinations can be eliminated with the help of the synchronization of the model with the real, measured values. Hence, instead of the expensive production of specimens and mechanical tests, the different assembly methods can be studied. Since the diameter of the LINK10 used for modeling the seams can be modified, inserts stitched to different extents can be studied. This way not only the system but even the production technology can be optimized. The necessary and sufficient maximum number of seams, and hence the time and energy required for preform production can be determined this way.

The examination of simple and double stitched inserts revealed that the reinforcing effect is not in direct proportion with the amount of fibers used. The reason for this phenomenon is that the thread already stitched in is damaged by the needle penetrating it in the next step. Hence the thread can only fulfill its function partially. The extent of this damage is of course more significant in case of multiple stitched inserts. Furthermore this mechanical degradation depends on different parameters, e.g. stitch frequency, stitching yarn thickness, and properties, needle geometry, applied yarn force etc.

The simulations make the thorough investigation of inserts fixed by stitching possible. This way the characteristics of the connection between the insert and the composite base plate can be revealed at a given load level. The stresses that evolve in the insert and the base plate can be studied, the places of stress peaks can be found, and hence an optimized geometry can be created. The aim of optimization is to produce an insert that fulfills the geometrical expectations of stitched reinforcing. Hence the requirements of optimized inserts (Type C) are the following:

- The insert has to reduce the weight compared to Type B. The weight of type A inserts is 11 g, while that of Type B inserts is 22 g.
- Besides the reduction of the insert weight, another expectation is to reach the same mechanical properties as in case of Type B inserts.
- In order to fulfill these requirements, optimization has to be carried out with the following boundary conditions:
- Based on the characteristic failure modes observed during the simulations and measurements, the inner pitch circle of the insert has to be eliminated.
- There is a need for a large rounding-off between the insert base plate and the threaded pin of the insert. The role of rounding-off is to increase the stiffness of the insert base plate directly next to the threaded pin, and to eliminate a stress collection zone between the pin and the insert.
- In order to reduce the weight, the thickness of the insert base plate has to be decreased compared to Type B. The maximum thickness of the base plate is set to 2 mm.
- In order to reach a further reduction in the weight, the diameter of the insert base plate has to be reduced compared to the original size (38 mm).
- Since the first delamination breakages always occurred in the zone below the threaded pin, the diameter of the insert pitch circle has to be reduced. This way the seams can prevent the occurrence of the first delamination more efficiently.
- In order to reduce the time of stitching preforming, the number of holes on the insert base plate has to be decreased. The maximum number of holes is set to 10. A further improvement in the mechanical properties of seams can be reached if a thicker thread is used.

- The diameter of holes on the insert base plate has to be reduced, and hence the cross section of the parts among the holes has to be increased. According to the simulations, a stress peak can be formed at these ribs due to loading. If the accuracy of the stitching machine used for preforming is considered, the minimum diameter of the holes can be 3 mm.
- Since a stress collection zone can be formed at the edges of the insert base plate and at the connection of the composite base plate and the covering layer, the edges of the insert base plate have to be chamfered.

Figure 3.41 illustrates the insert geometry modified according to the above mentioned conditions and requirements. The insert material is the same which is used for the insert Type B.

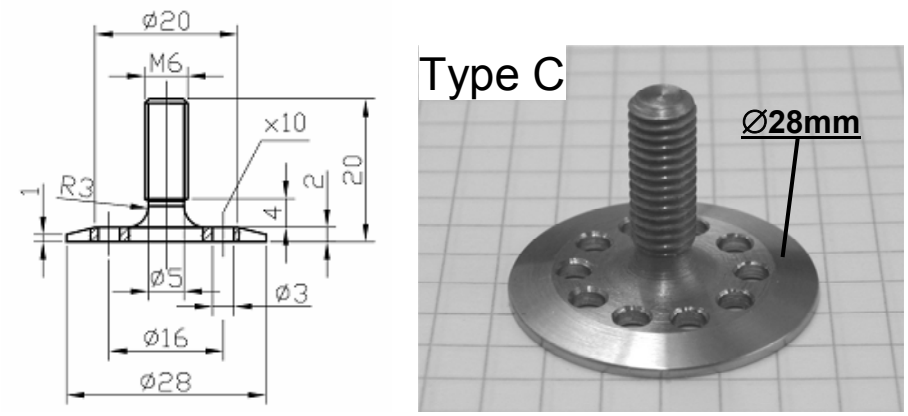

Figure 3.41: Optimised metallic insert for stitching supported reinforcing

The FEM simulations carried out on the models of the three insert types without embedding clearly revealed that the equivalent stress in critical zone of insert Type C is greatly lower than the maximal equivalent stress in the inserts Type A and B. The critical zone in case of insert Type C observed during the tensile load is the lamella between the holes on the insert base plate as well as the screwed bolt. The position of the clamping of the three inserts and their loading was the same in the load simulations. Figure 3.42 shows that the weight of Type C inserts is 11.4 gram, hence it is almost the same as that of type A inserts. On the other hand, the equivalent stresses that evolve in Type C inserts are lower than in case of Type A and Type B inserts. However, the reduction in the mass of Type C inserts is around 50%

compared to Type B inserts. Hence the simulations forecast that the optimization of the inserts was successful.

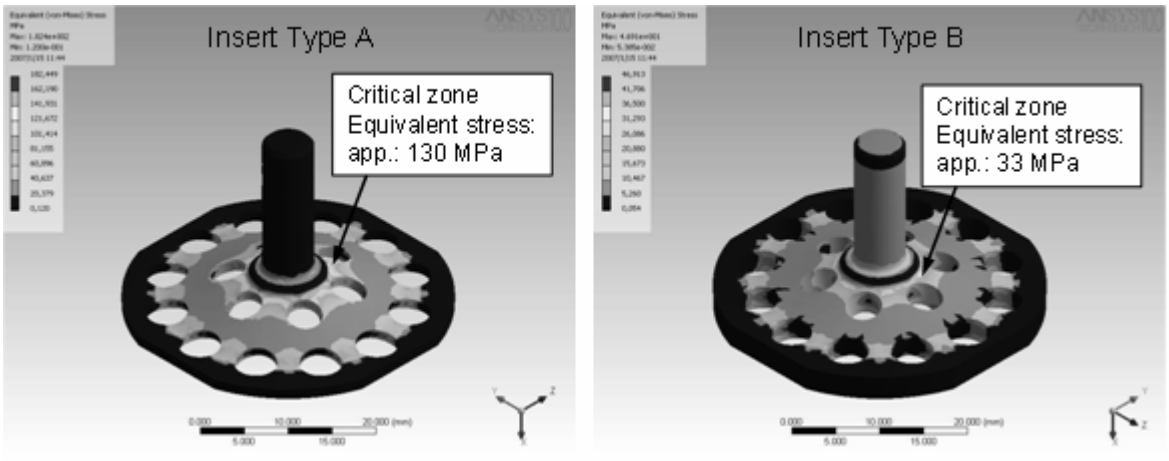

Figure 3.42: Load simulation on the inserts Type A and Type B

In order to verify the simulations, different tensile tests were carried out on Type C inserts. A stitching pattern similar to that of inserts Type A and B was applied to fix the insert, but the stitch number was reduced correspondent to the fewer holes. Hence the Type C insert was fixed to the composite base plate with 160 elementary stitching threads. The type of the applied stitching threads (Improved stitching with Amman Saba c50 type PET thread, Type 3 with reduced stitch number) and the parameters of stitching and injection, as well as tensile tests were the same as in case of Type A and B (Table 3.3, Figure 3.7, Figure 3.8).

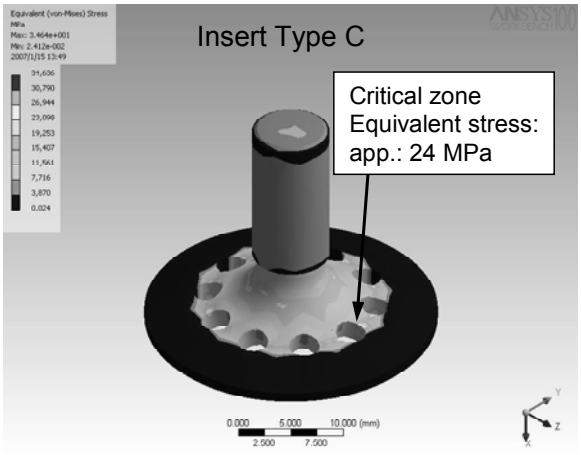

Figure 3.43: Load simulation on insert Type C

Figure 3.44 illustrates the results of tensile tests carried out on Type C inserts compared to the improved stitched (Type 3) Type A and B inserts.

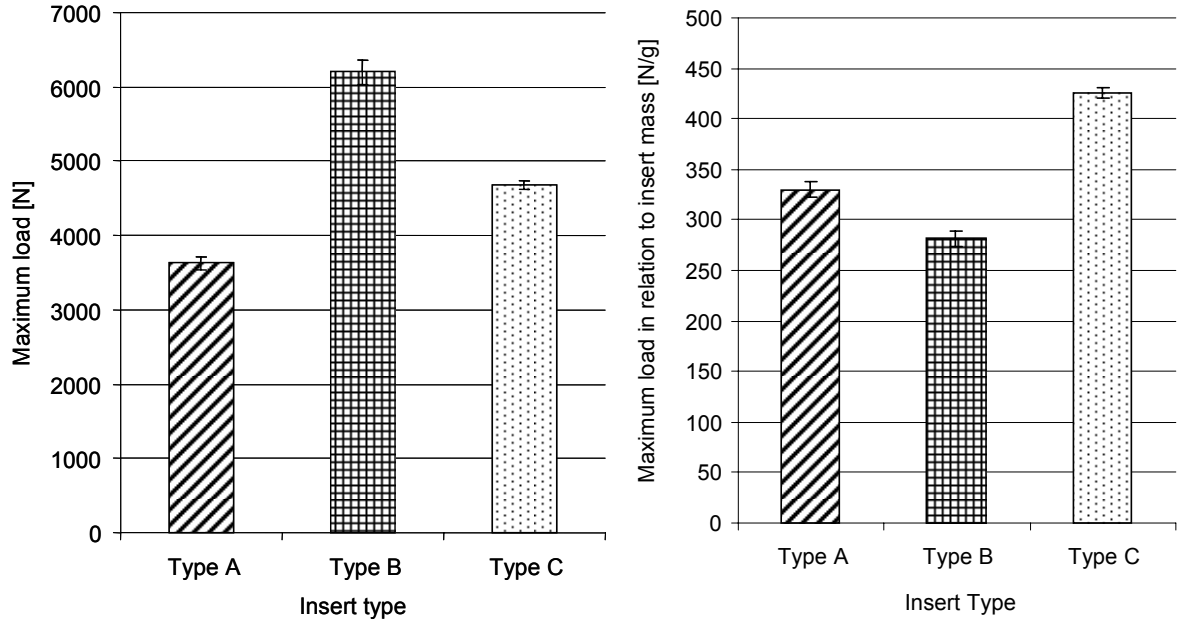

Figure 3.44: Results of the tensile test on different stitched inserts and the maximum load in relation to the insert mass (Type of specimen: Type 3)

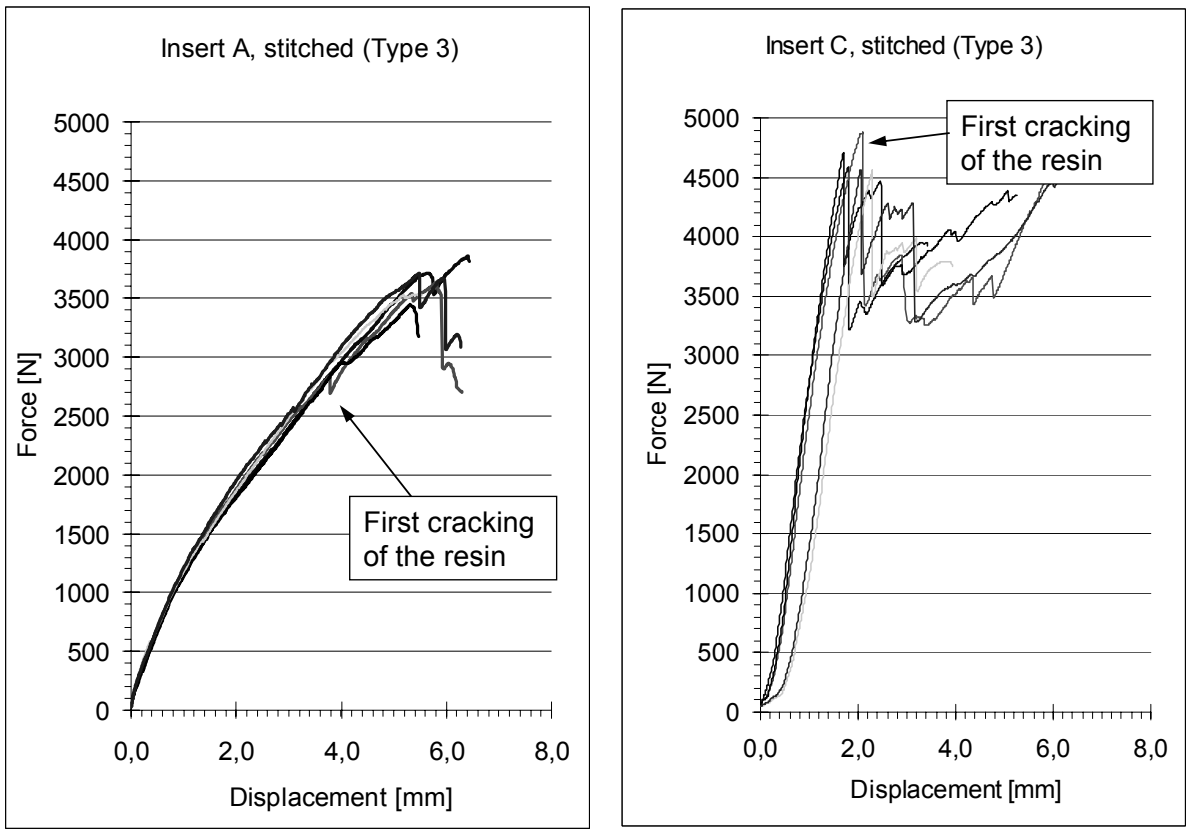

Figure 3.45: Cumulated force-displacement diagrams of inserts Type A and C (Type of specimen: Type 3)

The results reveal clearly that the loadability of Type C inserts is lower than the loadability of the insert Type B (weight: ca. 22 g) (Figure 3.46) but approximately 35% higher than the maximum loadability value of Type A inserts as apposed to the reduced mass (ca. 11 g) of Type C inserts. Besides the maximum force values measured on the specimens, the force – displacement curve (Figure 3.45) of the tests also involves essential information. The figure reveals that in case of Type A inserts the first cracks appeared in the structure at 2500 N, while Type C inserts could be loaded until 4500 N without any crack occurrence. This phenomenon is due to the optimization of the stiffness of the specimen. In this case the stiffness of the insert was not significantly lower than that of the composite base plate, hence the two phases could deform together until a high degree of loading.

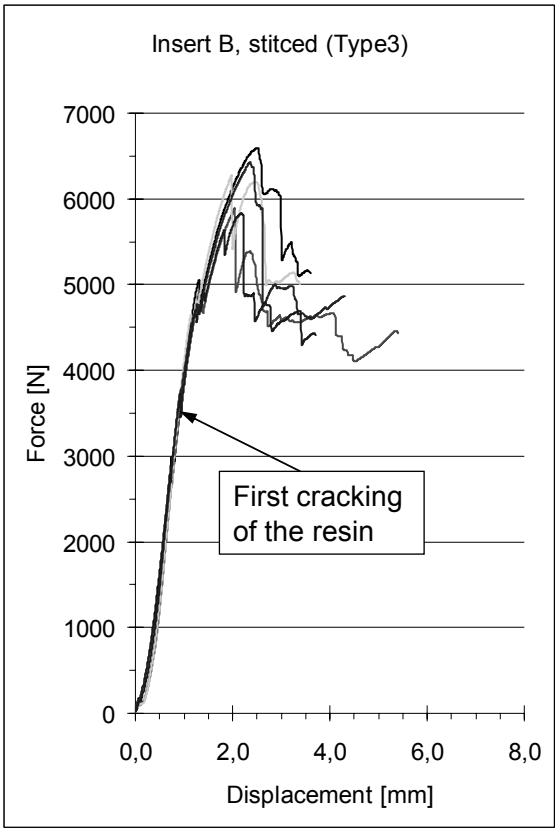

Figure 3.46: Cumulated force-displacement diagrams of insert Type B (Type of specimen: Type 3)

Furthermore, it could be observed during the measurements that in case of Type C inserts the first cracks did not appear in the zone below the screwed bolt as in case of Type A inserts but at the edges of the insert base plate. Hence the seams could

take up the load immediately. This phenomenon reveals that the mechanical properties can be improved further with high strength threads that can block the cracks that appear at the edge, and force the insert to deform together with the composite base plate to a greater extent. A further consequence of insert optimization is that Type C inserts have ten holes, hence the number of stitches is also lower. This way the time required for preform production is also reduced, since the preparation of reinforcing seams decreases by approximately 20%.

Further examinations revealed that a more significant improvement could be achieved with the application of type C inserts in case of inserts fixed by stitching and supplied with a cover layer (Embedding type: Type 6). Figure 3.47 illustrates the results of tensile tests compared to the values measured on Type A and B inserts. While the maximal force in case of specimens prepared with Type A inserts is app. 6000 N, that of specimens with Type C inserts is 12200 N. In case of Type A inserts the characteristic failure mode is the breakage of the lamella between the inner holes on the insert base plate. In case of Type C inserts, the characteristic failure mode is the breakage of the screwed bolt in the bottom part of the thread in the vicinity of clamping. Furthermore, Figure 3.48 shows clearly that in case of Type A inserts, the first breakages occur in the range of 3000 – 4000 N due to the small stiffness and large extent deformation of the insert. This failure mode occurs although the cover layer inhibits the deformation of the insert greatly. Obviously, this deformation enhances the propagation of delamination cracks among layers, and this phenomenon is prevented by the seams efficiently in case of embedding Type 6.

In case of Type C inserts, the first crack occurred between 5500 and 6000 N, and this is revealed by the tensile test diagrams well. After this crack the system could be loaded until approximately 9500 N, where further breakages occurred.
Figure 3.49 illustrates the force-displacement curve of tensile tests carried out on Type B inserts fixed by stitching and supplied with a cover layer (embedding Type 6). Figure 3.47 and Figure 3.49 reveals well that the measured values have great deviations. Type B inserts can be loaded well until 9000 N in case of Type 6 embedding, and afterwards the first cracks occur in the system. In this case the characteristic failure mode is the breakage of screwed bolts and the breakthrough of the lamella among the inner hole circle in the inserts.

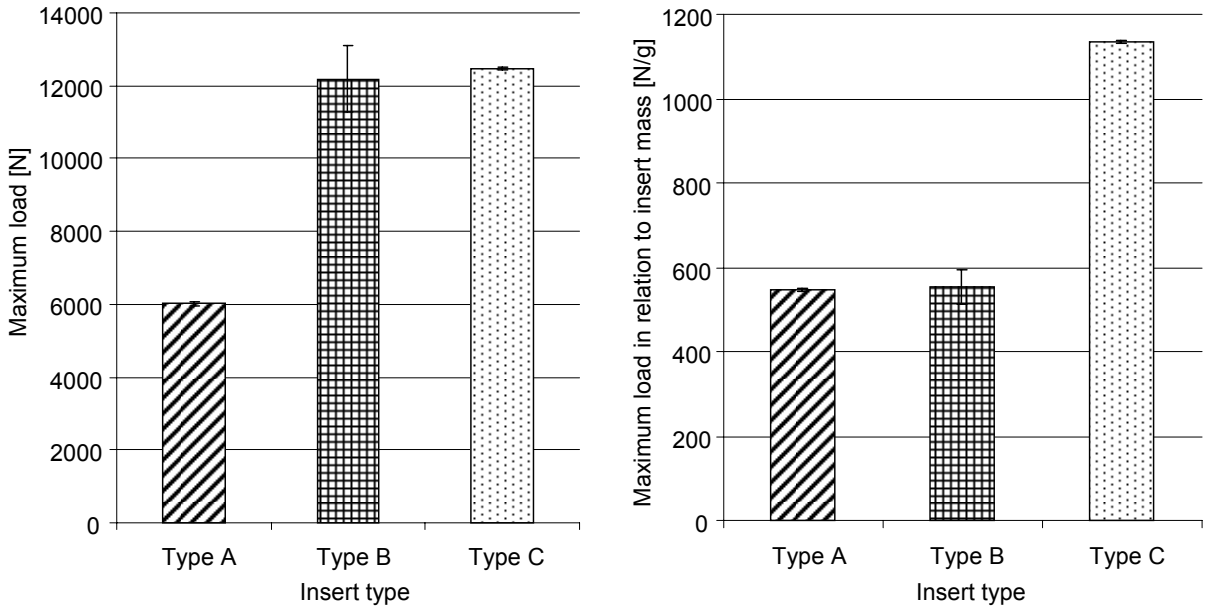

Figure 3.47: Result of the tensile tests on different stitched inserts and the maximum load in relation to the insert mass (Type of specimen: Type 6)

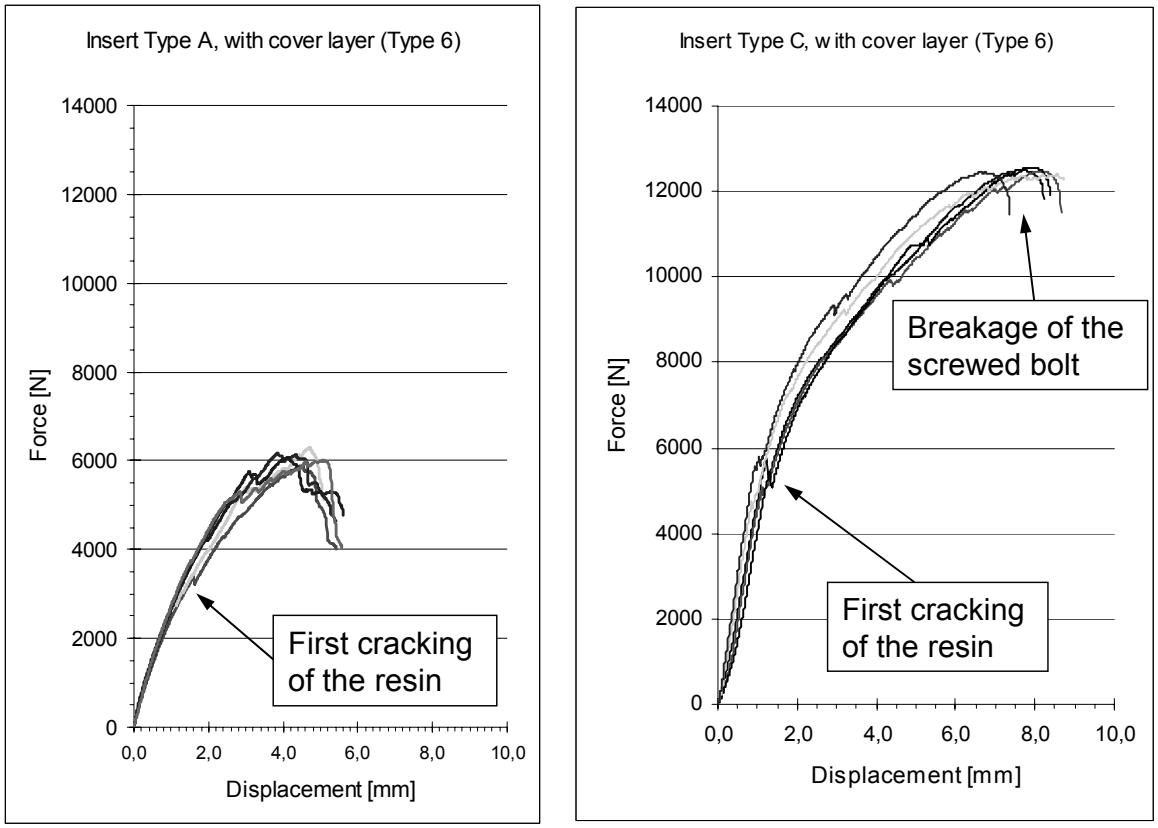

Figure 3.48: Cumulated force – displacement diagram of inserts Type A and C (Type of specimen: Type 6)

The contraction and breakage of the screwed bolts took place at around 10000 N, while the shearing of the lamellae among the holes happened only at ca. 13000 N loading. The position of flaw locations in the metal insert can be the explanation for these two different kinds of failure modes. The significantly lower force value can be caused by the stress collection zone in the bottom of the threads in the screwed bolt. Nevertheless, the FE modelling carried out prior to the tests also revealed that stress peaks can be found at these two places in Type B inserts, hence these are the expected positions of breakage.

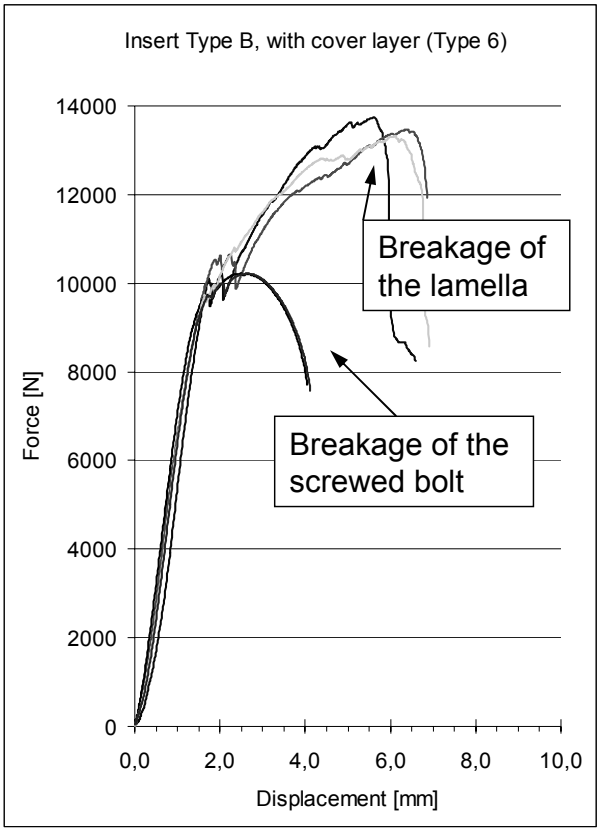

Figure 3.49: Cumulated force – displacement diagram of insert Type B (Type of specimen: Type 6)

However, considering that the material of the inserts is ST 50-2 (S355J2G3), the highest guaranteed tensile strength (R_m) is 470 – 610 MPa, while its yield point is (R_{eH}) 295 MPa. The core diameter of the M6 screwed bolts of the inserts is (d_3) 4.77 mm. The critical cross section calculated using this data is (A_s) 17.87 mm^2. Considering a static tensile loading, the maximum allowed force, F_{max}, can be calculated with the following formula:

$$F_{max} = \sigma_{(ReH)} A_s \tag{3.9}$$

where $\sigma_{(ReH)}$ is the stress that belongs to the yield point. The maximum allowed force for this material, obtained this way is app. 5272 N. Hence loading above this value is not allowed owing to the yield point of the metal insert.

It can be seen that in case of Type C inserts (stitched and supplied with a cover layer, Type 6 with reduced stitch number), the breakages occurred at app. 5500 N. This reveals that the allowed maximum loading for the metal insert can be achieved with the insert – composite connection prepared this way. Hence the insert can be utilized to a maximum extent, and all the possibilities can be exploited as well.

The modeling of the static tensile test supported the knowing of the actions in the structure during the tensile load. The simulation of the load on the inserts Type A and B indicated the disadvantages of the insert architecture. The exploration of these helps to develop a new type of insert for stitching supported embedding.

3.8 Results of shear tests

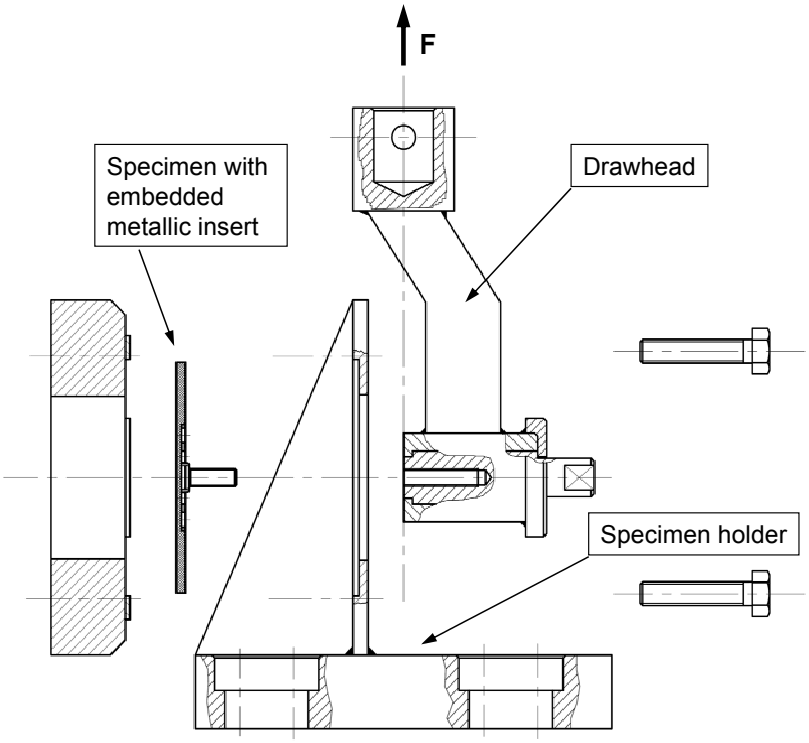

Figure 3.50: Set-up of the shear tests equipment for embedded inserts

The set-up of the test rig shown in Figure 3.50 was used for shear tests carried out on inserts Type A. The construction allowed setting the distance of the load introduction point to the insert (Figure 3.51) and hence the failure modes of specimens could be studied in each case.

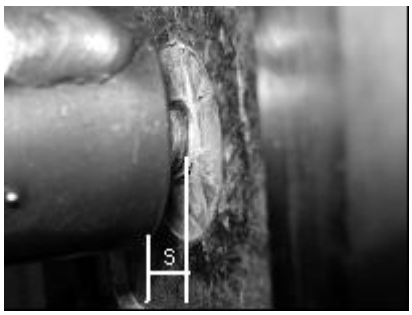

Figure 3.51: Clamping distance (s) between the insert base plate and testing tool

Three measurement series were completed with different clamping distances (s). Keeping three, six, and nine millimeter distance from the base plate of the insert, it can be observed that the characteristic failure mode, depending on the type, is pure shearing (in case of a distance of 3 mm) and shearing as well as bending (in case of distances of 6 and 9 mm) (Figure 3.52).

Further experiments were carried out at 6 mm work point distance, since this set up approximates the stress of real loading the best way.

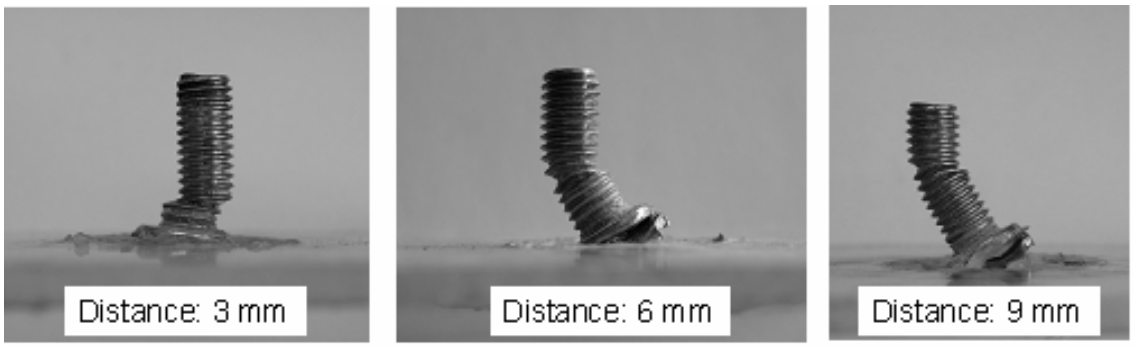

Figure 3.52: Damage modes at different clamping distances (s)

Based on the investigations carried out on unstitched inserts it can be seen that the characteristic failure mode is the tilting of the insert base plates out of the composite and the breakage of the base plate (Figure 3.53). It can also be observed that the inserts cannot slide in the plane of the base plate due to the embedding. The failure modes reveal the insufficient mechanical properties of the insert base plate.

Figure 3.53: The characteristic failure mode of the unstitched inserts Type A (Type of specimen: Type 1)

The characteristic failure modes of inserts stitched with polyester threads were the breakage of the insert base plate and the shearing of the screwed bolt (Figure 3.52). It can also be observed that the base plate of the insert did not move from its place, hence, reinforcing with stitching prevented the tilting of the base plate out of the composite effectively.

No higher shear strength values were found during the application of high performance fibers. The breakage of the metallic inserts occurred in the shear tests showed that the insert base plate stays at its place and the screwed bolt broke at its neck in the weakest point of the base plate (Figure 3.54). Hence, it was not possible to measure the difference among the real strength values of Kevlar, carbon, and glass fiber reinforcements (Figure 3.56).

Figure 3.54: Characteristic failure mode of the carbon thread stitched inserts Type A (clamping distance: s = 6 mm) (Type of specimen: Type 10)

The embedded inserts, both in stitched and unstitched states, had such high in-plane strength that only the shearing of the screwed bolt was the observed failure mode (Figure 3.55). This reveals that embedding without stitching is sufficient for the fixation of the insert in case of major shear loading without a significant tension ratio.

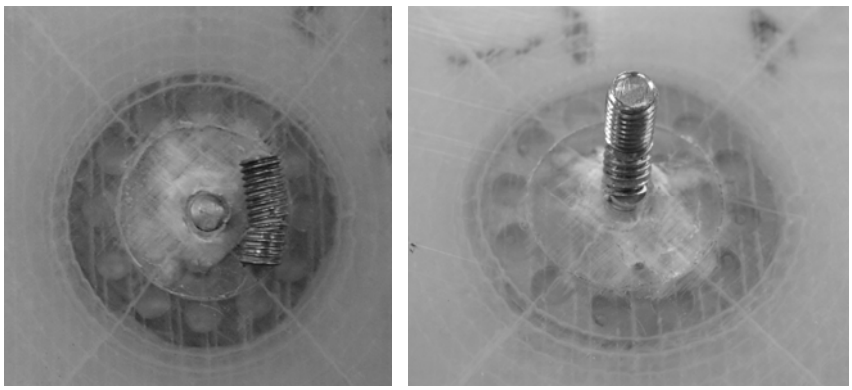

Figure 3.55: Characteristic failure mode of embedded inserts (Type A) without stitching (Type of specimen: Type 5)

As a general result of shear testing it can be concluded that the mechanical shear performance of an embedded unstitched insert is as good as stitched inserts.

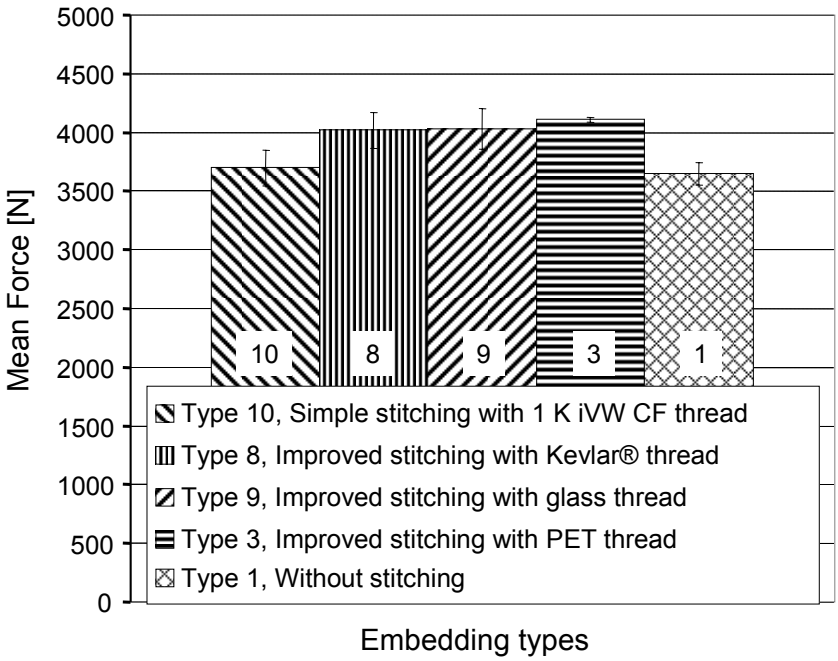

Figure 3.56: Results of the shear tests on specimens with different embedding types, in case of inserts Type A

3.9 Summary of the experiments

The results of the mechanical tests showed that reinforcing with local stitches can be used to improve the mechanical properties of embedded metallic inserts in composite structures.

The manufacturing of stitched insert-preform indicates that high performance fibers, like carbon, glass and Kevlar® cause different problems during the stitching process. The high rigidity (carbon, glass), friction and cut resistance (aramid) prevent the fast and effective manufacturing process. Therefore, it can be suggested to use PET threads with good matrix bonding to stitch metallic inserts.

The comparison of the different embedding and stitching types gave a view on the characteristic failure modes, the forces and the direction of further development for each case.

The testing of the specimens revealed that the optimisation of insert geometry is necessary to exploit the real mechanical efficiency of the stitched reinforcing structure. With the improved insert geometry it is possible to realize approximately 400% improvement in the tensile force (see Figure 3.9 and Figure 3.44). It can also be seen that no relevant benefit can be obtained from the stitching when shearing is the major load characteristic.
The evaluation of results and finite element analysis verified the hypothesis, which proposes fixing of metallic inserts by stitching leads to a significant increase in the tensile strength. The results reveal that if the proper preforming technology and materials are used, the metallic inserts can perform as an integrated part of the complete FRPC. This is of great importance for the design and analysis of lightweight composite structures for new applications.

4 Structural health monitoring of FRPC parts

The aim of sensor integration in composite structures is that they can control the manufacturing process, the load, the part and the system operation. Load monitoring can support the optimization of the maintain once intervals and life time, furthermore the recognition of misuse. Monitoring of aging fiber reinforced polymer composite (FRPC) structures is a crucial issue in the engineering area [104, 105]. The use of condition based maintenance coupled with continuous online structural health monitoring could significantly reduce the costs of inspection programs [106]. “Exclusion-for-cause” instead of “exclusion-as-planned” could reduce the costs while maintaining a safe operation life. The replacement of the present manual inspection with automatic health monitoring would substantially reduce the associated lifecycle costs. Hence there is a need for reliable structural health monitoring (SHM) systems that can process the data automatically, assess structural conditions and signal the need for corrective action. Thus, the development of a real-time, in-service structural health monitoring and damage detection technique has recently attracted a large number of academic and industrial researchers [107, 108, 109, 110]. The goal of this researches is to allow systems and structures to monitor their own integrity while in operation and throughout their life in order to prevent catastrophic failures and to reduce the costs by minimizing explicit maintenance and inspection tasks.

Figure 4.1 shows the most distributed instruments of the structural health monitoring. These are the optical sensors [111 ,112 ,113], piezo sensors and actuators [114, 115], the conductive measurement cells [116], and the acoustic sensors [117]. Figure 4.2 presents the function principles of the structural health monitoring methods of the different SHM instruments. The most popular approach of structural health monitoring is to use modal parameters, such as natural frequencies, damping ratios and mode shapes to determine the existence of structure damage. Adams *et al.* [118] found that a state of damage could be detected by a reduction in stiffness and an increase in damping [119]. A method to locate damages from measurements of natural frequencies was also demonstrated [120].

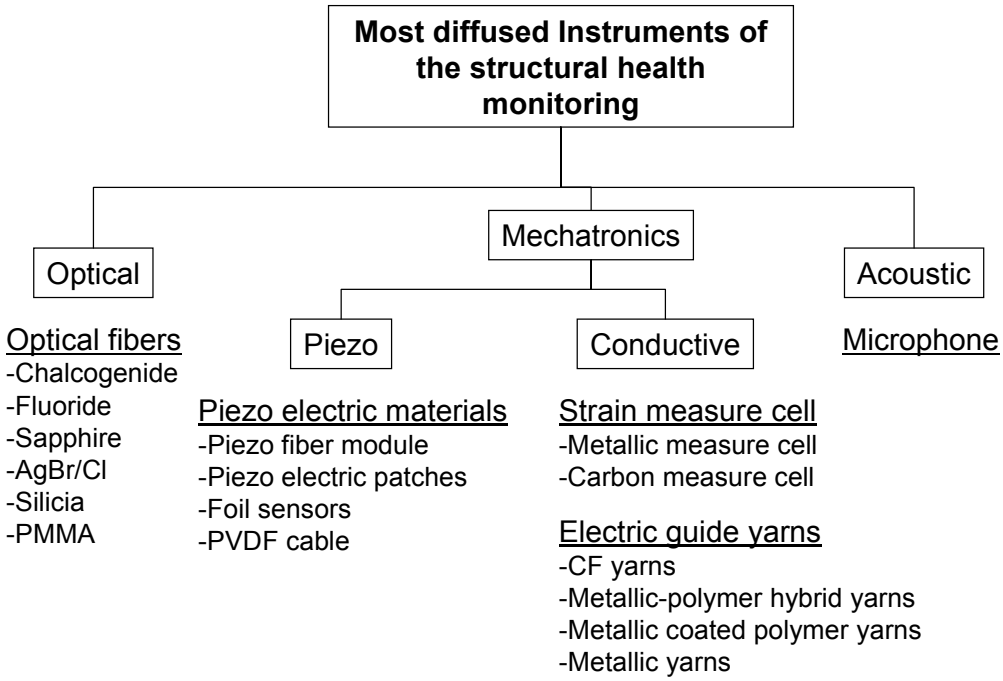

Figure 4.1: Instruments of structural health monitoring

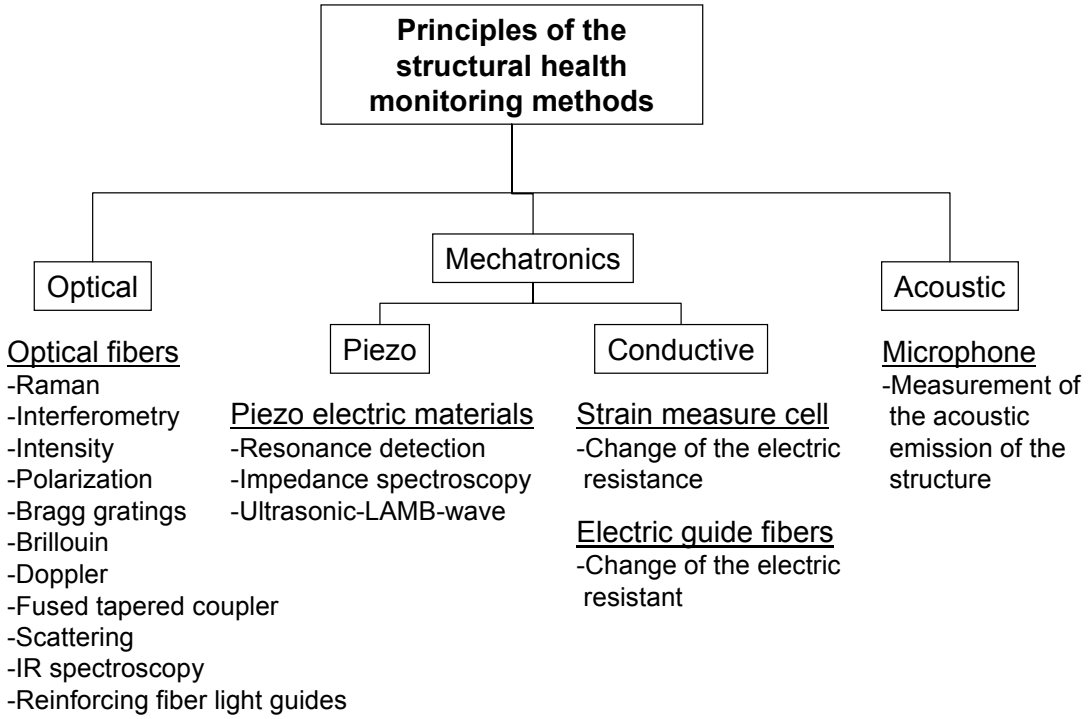

Figure 4.2: Measuring principles of the different instruments for SHM

Other modal properties, such as sensitivity [121], eigenvector and eigenvalue matrix [122], curvature mode shapes [123], modal assurance criterion [124] and energy transfer ratio [125] have been examined for damage detection. Aktan et al. [126] presented extensive work on civil infrastructures monitoring. Even piezoelectric

patches can be used not only for monitoring of the resin flow during the resin transfer molding (RTM) process, but also for lifetime monitoring of FRPC parts [127,128, 129, 130]. Piezoelectric sensors have a number of advantages but disadvantages too, hence their usability in composite SHM is difficult. The disadvantages are: brittle due to crystalline structure, cannot withstand high shear and tension, material ages, uses active control (can lead to instability) and can become depolarized (high voltages, high temperatures, large stresses). Apart from this, PZT (lead-zirconate-titanate piezoelectric ceramic material) is a non-reinforcing material, thus, use of matrix compatible CF thread can be introduced for SHM [131].

In recent years the studies on neural networking [132], wireless active sensing [133], and wireless monitoring [134] are growing. In composite engineering wireless monitoring is a very effective method but the costs involved in the implementation of health monitoring is too high. Thus, development of a cost-effective method is obligatory. Within this part of the study, carbon fiber threads (IVW-CF thread [135]) have been used as a health monitoring element.

4.1 Carbon fiber patches

In the past, some researches concentrated on the carbon fiber itself as a monitoring element but mostly the use of carbon UD-fiber patches was preferred.
Smart patches made up of uni-directional (UD) carbon fiber sheets can be used for damage detection [136]. The change in the electrical resistance of carbon fibers as a response of impact will be detected by this method.

Figure 4.3 shows the arrangement of carbon fibers and corresponding electrical conductive elements with varied electrical resistance. The theoretical background is explained by N. Takeda [137]. The deformation of conductive carbon fibers can be written as:

$$\frac{\Delta R_{cf}}{R_{cf}} = \alpha \frac{\sigma}{E} \tag{4.1}$$

where, $R_{c.f}$ = resistance of carbon fiber; $\Delta R_{c.f}$ = change in the resistance of carbon fiber; α = constant; σ = stress; E = Young's modulus.

Fiber breakage after the impact will be considered as a loss of conducting path. The amount of fiber volume content affects the effective electrical length, in other words δ_{ec} varies for different fiber volume fractions.

$$\delta_{ec} = \frac{L}{(N_{cp} - 1)} \tag{4.2}$$

Where, δ_{ec} = electrical ineffective length; L = fiber length; N_{cp} = number of fiber contact points (Figure 4.3).

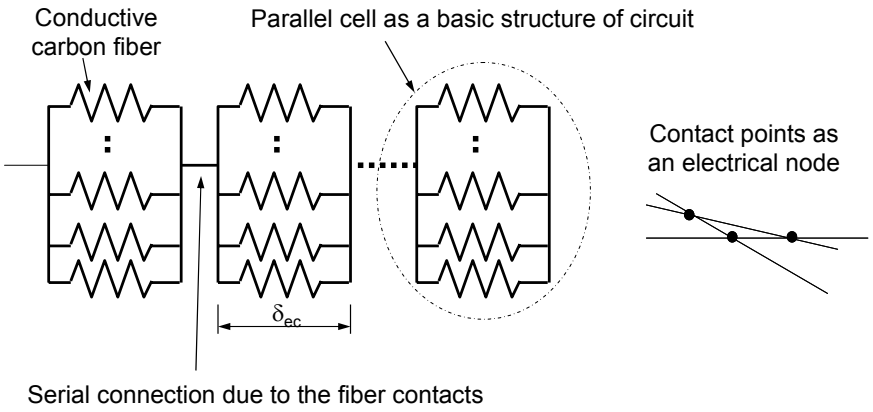

Figure 4.3: Schematics of CF patch and sensing behavior of fiber

The aim of this study is to develop structural health monitoring based on the electrical properties of carbon fibers. Manufacturing of separate carbon patches requires an extra process, furthermore, an exact positioning of the patches is necessary. Thus, within the implemented investigations the benefits of carbon fiber stitching threads (IVW-CF) have been utilized to validate its usability as a health monitoring element. The reason behind the selection of IVW-CF threads for the experimentation was based on laminate performance and consistency in material utilization (only reinforcing fibers in the structure of the laminate). IVW-CF thread is very thin and flexible, therefore, it is suitable for stitching composite panels. The special construction of threads enables them to stitch metallic inserts by forming several loops without damaging individual carbon filaments. Use of foreign materials as a sensor system which will be a part of the laminate may affect the laminate properties adversely. The reason behind that the sensors integrated into the laminate may disturb the reinforcing fiber orientation. Furthermore, the integrated IVW-CF thread sensor shows real intensity of damage as these threads represent sections of the

actual load carrying laminate. Apart from this, distribution of carbon threads over the complete area of the component is easily executable.

Selection of the experimental sensor is based on the goals to be achieved and allowed time frame for successful development of a sensor system. In this case the following criteria should be considered:

- Cost of the sensor system and accessories: For the initial trials the costliest sensor system may not be worthwhile, and furthermore for vast applications of the sensors, the basic system should be of marginal cost.
- User friendliness: The complete system needs to be easy in monitoring which helps to detect damages quickly.
- Observation area (effective sensitive area): Observation area depends on the number of sensors involved in the part, furthermore, IVW-CF threads are relatively cheap, thus, more can be put into the structure. In this case damage detection will be easier.
- Robustness: The used sensors should not be damaged during the integration process. Unlike optical fibers and piezoelectric sensors, CF patches are more robust and easier to handle during the integration process (for instance during preforming, stitching, and resin transfer molding).
- Sensitivity: Sensitivity of highly sophisticated sensors is not a question but when it comes to the robust, user friendly IVW-CF thread sensors; its sensitivity is not like piezoelectric patches but enough to distinguish generated signals.

The test plan is based on the carbon fiber reinforced polymer uni-directional-grid, which will be placed on the glass fiber preforms and the change of the electrical resistance of carbon fibers will be measured. SEN-T test, metallic insert failure test and impact test of glass fiber reinforced laminates were performed to prove the utility of electrical resistance of carbon thread, to analyze debonding of individual stitches at the insert and its influence on the change in resistance, and rupture of carbon thread to locate approximate failure location, respectively. All the three tests can show different aspects of carbon thread utility for structural health monitoring.

4.2 Selection of material and specimen manufacturing

Carbon fiber thread (IVW-CF) was used as an intelligent monitoring material (Figure 4.4). Plain woven (200 g/m^2) and bi-axial non-crimp fabric (NCF 250 g/m^2) made of glass fiber was used as textile reinforcement. Composites were manufactured by using a low viscosity (120 ±20 mPas) epoxy matrix system Rutepox VE 4908 (producer: Bakelite AG) and vacuum assisted resin transfer molding technique.

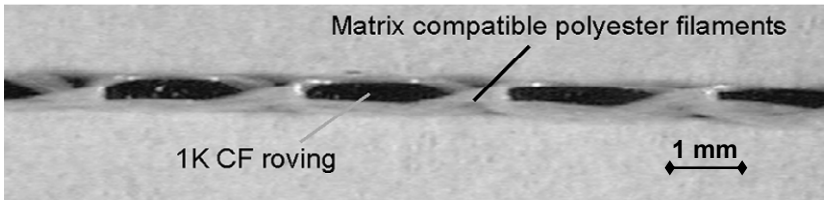

Figure 4.4: IVW patented carbon fiber hybrid stitching thread [135]

4.3 Preliminary tests

The preliminary test plan is based on the carbon fiber reinforced polymer uni-directional-grid, which will be placed on the glass fiber preforms and the change of the electrical resistance of carbon fibers will be measured.

4.3.1 Specimen development for tensile tests

For tensile tests (Single Edge Notched Tensile, SEN-T) a glass fiber woven fabric has been used as the base material. Preforms were stitched in such way that the carbon fiber thread position was in a straight line without deviation. Modified lock stitch gives the advantages of positioning the roving at the bottom of the preform. Here, a polyester multifilament thread was used as an needle thread and a IVW-CF thread as a bobbin thread (Figure 4.5).

Stitching parameters used for preform manufacturing are stated in Table 4.1. The manufactured panels were then injected by means of a liquid matrix based on an epoxy system. The standard vacuum assisted resin infusion (VARI) method was used for manufacturing the laminates.

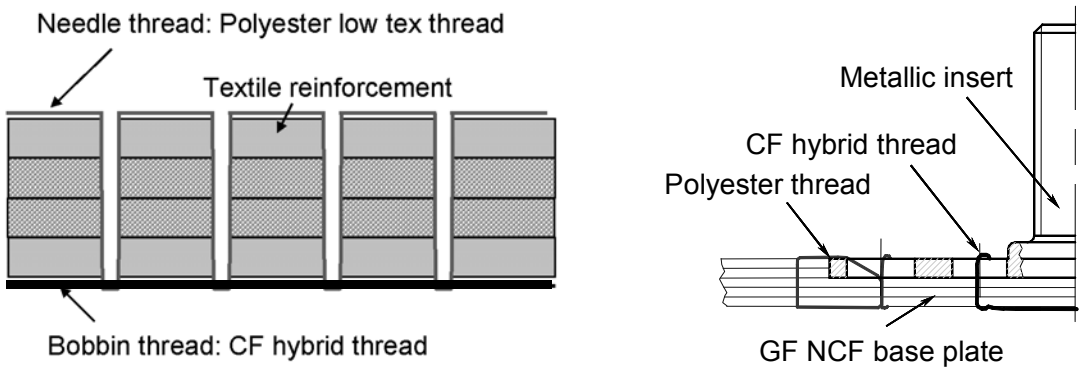

Figure 4.5: Modified lock stitch for monolithic laminate and insert monitoring

Lay-up building on the heating plate for the VARI process is the following: a) coating of release agent; b) stitched preform panel (IVW-CF threads facing top); c) glass fiber woven fabric; d) perforated foil; e) distribution media (glass fiber mat); f) vacuum foil. The glass fiber woven fabric (position c) helps avoid direct contact of the IVW-CF thread and the test instrument in the later stage (Figure 4.6).

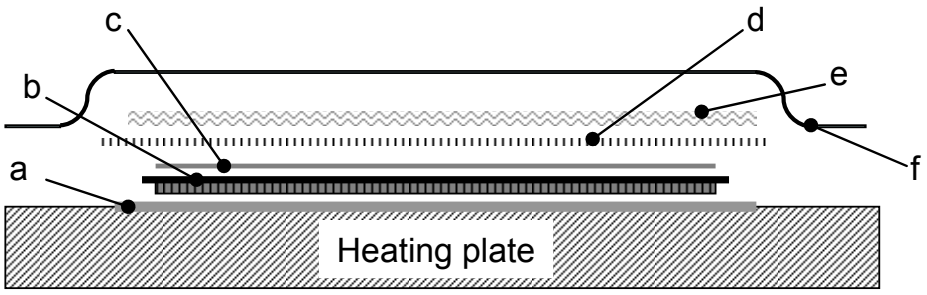

Figure 4.6: Lay-up bilding fort he VARI process

Tacky tape was used as a vacuum foil sealing medium.

Table 4.2 shows the parameters set for the VARI process. Manufactured panels were then cut to the exact size for SEN-T testing.

Table 4.1: Parameters of preform manufacturing

Fabric used	Glass fiber woven fabric/ noncrimp fabric
Stitching machine used	Pfaff 3574
Stitch type	Modified lock stitch (bobbin thread at the bottom)
Stitching speed	1000 1 / min
Needle thread force	320 cN
Bobbin thread force	140 cN
Stitch length	3 mm
Smart element	IVW-CF thread (used as bobbin thread)

Table 4.2: VARI process parameters

Release agent	Freekote
Preform material evacuation	10^{-2} mbar, 1 h
Matrix used	VE 4908 A + B
Degassing of liquid matrix	10^{-1} mbar, 10 min
Vacuum during infusion	1-10 mbar
Injection time	15 min
Curing	80°C, 6 h

4.4 Manufacturing of preforms with inserts

Another use of CF patch / thread considered was monitoring the delamination of metallic inserts. For these tests, inserts and glass fiber non-crimp fabrics (NCF) were stitched together using polyester multifilament twisted threads. Here, the NCF was used as a preforming material (see Chapter 3). The IVW-CF thread was used to form seams at the critical positions which are supposed to be the delamination initiation zones (Figure 4.5). These seams were connected with a conducting wire, which is not a part of the whole laminate.

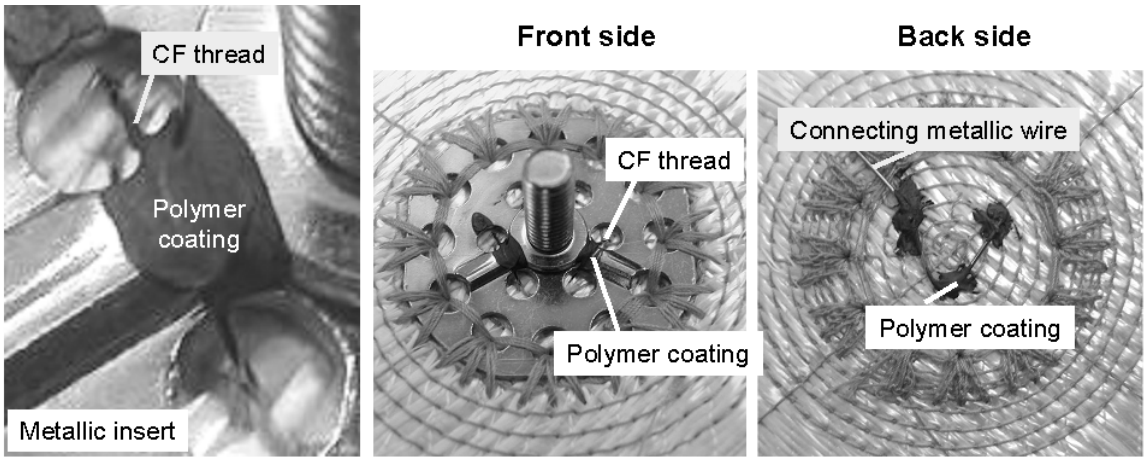

Figure 4.7: Insert (Type A) preform with stitched IVW-CF thread

Figure 4.7 shows a preform stitched with the polyester thread and then with the IVW-CF thread including electrical connection. Six of such preforms were injected simultaneously using a special designed tool. The tool helps to inject only the base of the insert and the reinforcing glass fabric.

Preforms with inserts for delamination sensing were manufactured according to the measurement reliability. All the stitched preforms were then injected and tested for the reliability and exactness of measurement.

4.5 Experiments and results

Two different experiments were carried out to observe the application possibilities as monitoring sensor inherent in the carbon fiber threads. The investigations were the SEN-T test and the static insert pull out test.

4.5.1 SEN-T test

The schematic view of the specimen and the experimental setup used in this study are shown in Figure 4.8. A Zwick 1474 tensile testing machine was used for testing. The machine appears on the principle of constant rate of traverse 0.5 mm/min. The specimen dimensions are stated in Table 4.3. A specimen is mounted on the machine and CF threads are internally connected by using electrical wires. Both ends of a specimen were connected to the signal converter which is connected to the plotter. As the test progresses, due to applied force, the individual CF thread starts breaking until the complete specimen fails. A failed specimen is also shown in Figure 4.8.

Table 4.3: Specimen specifications for SEN-T test

Width (W)	Length (C)	Thickness (B)	Notch length (a)	Notch width (H)	Clamping length (F)
30 mm	110 mm	1 mm	10 +1 mm	1 mm	15 mm

During the failure mechanism, due to the gradual breakage of individual CF threads, the voltage value increases which can be later calculated in terms of change in electrical resistance. As shown in Figure 4.9 the force – displacement diagram correlated with the voltage – time diagram.

The voltage-time diagram is helpful to analyze phenomenon of changes in the electrical resistance. As shown in the same figure, there is very low electrical resistance at the initial stage and as the CF threads start breaking the electrical resistance starts increasing and at the end it converges to infinity.

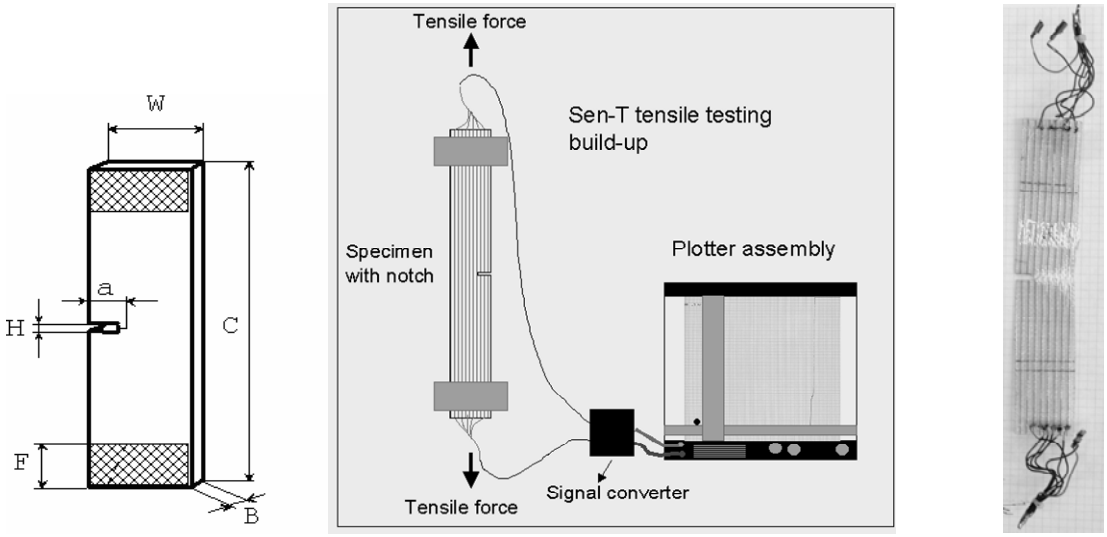

Figure 4.8: Specimen for SEN-T test and testing instrument: schematic diagram and the tested specimen

The gradual increase in the electrical resistance from 14 Ω to ∞ and the corresponding peaks on the plot diagram is shown in Figure 4.9 (equation for calculating R [Ω] from value of U [V] where is U = IR).

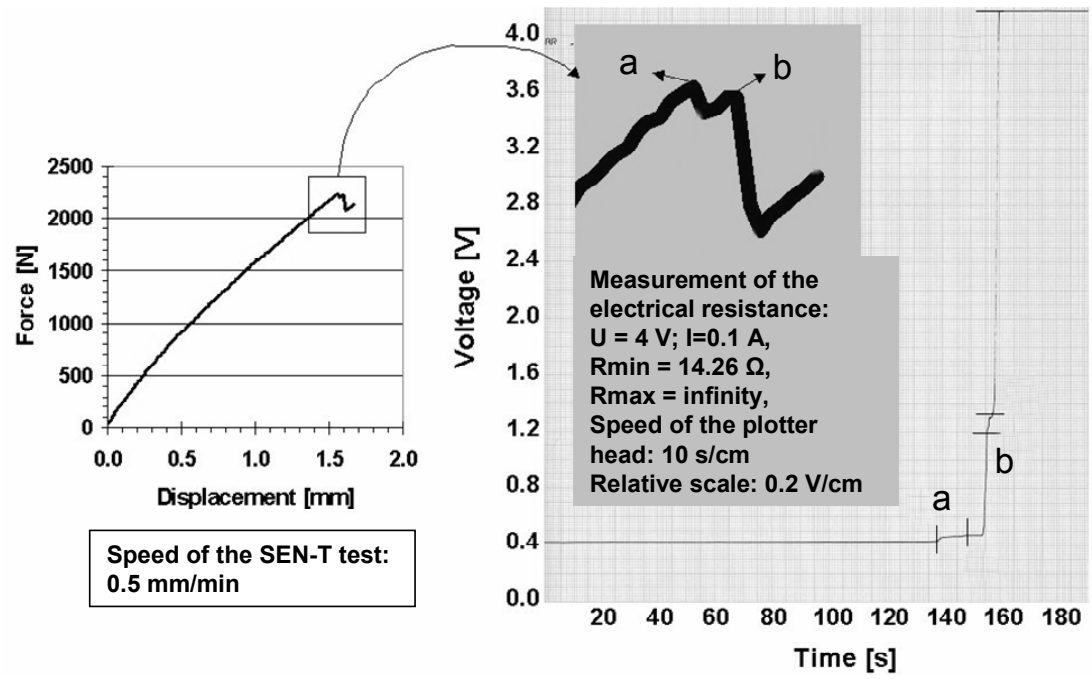

Figure 4.9: Force-displacement diagram, failure and corresponding voltage peaks and plot diagram of change in voltage on time scale during the SEN-T test

Due to the operation principle of the testing instrument (constant rate of traverse) the time required for initial breakage is too much compared to the final thread breakage.

Thus, on the time scale the occurrence of the peak is very quick at the end of the test, but the change in electrical resistance is still visible. The changes in resistance of the carbon fibers calculated from the plot diagram are very small but not invisible. Magnification of signals will be helpful while implementing this technology in the final product assembly.

This test helps monitor changes in resistance of carbon threads before and after fracture and thus helps validate the usability of threads as a sensor in the components subjected to tensile strength or even extreme bending where tensile force is involved. Broken or elongated carbon threads show higher resistance and help to conclude intensity of damage corresponding to electrical resistance.

4.5.2 Insert pull out test

IVW-CF thread integrated (stitched) metallic fasteners (Insert Type A) were tested to monitor delaminations of metallic parts from the glass fiber reinforced polymer composite. Monitoring the first delamination and the corresponding change in resistance shown by the CF thread was the basic concept behind this experimentation. The testing instrument (b) and the close up picture of the test equipment (c) is shown in Figure 4.10.

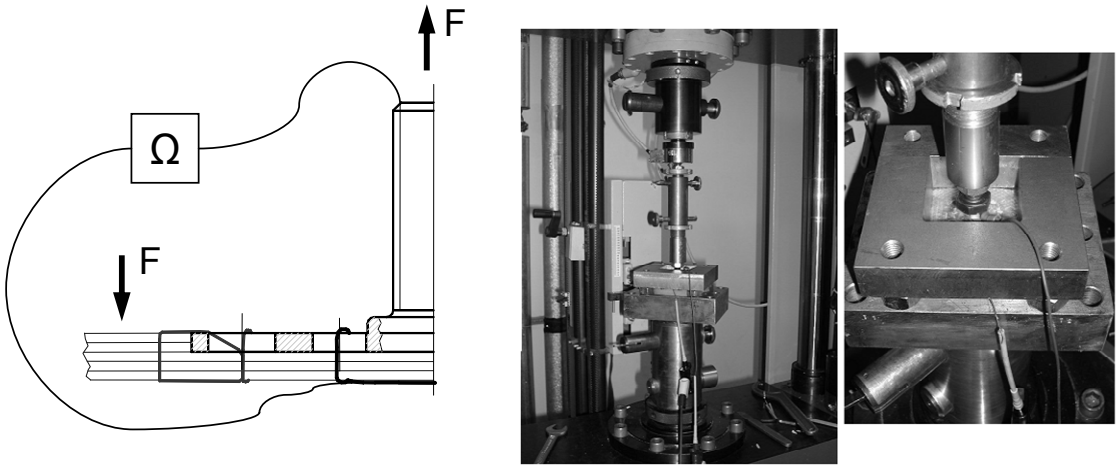

a) b) c)

Figure 4.10: Insert testing set up: (a) schematics; (b) complete instrument; (c) close up of the test zone

A Zwick 1474 tensile testing machine was used for the testing, the test velocity was 1 mm/min. Figure 4.5 shows stitched inserts and the position of CF threads at the critical delaminating zone under the screwed bolt and connecting metallic wires. CF seams connected to metallic wire and section of metallic insert were connected to the signal converting unit and then to the plotter.

As the experimentation progresses, the tensile force applied on the metallic insert pulls the CF thread (stitch) in the vertical direction [100]. The corresponding change in voltage shows no change till the first delamination and the CF thread breaks at the critical area, under the threaded bolt of the insert.

Figure 4.11 shows the plot of change in voltage vs. time. After the first CF seam breakage a peak of change in voltage forms and follows the same trend after the breakage of the subsequent seams.

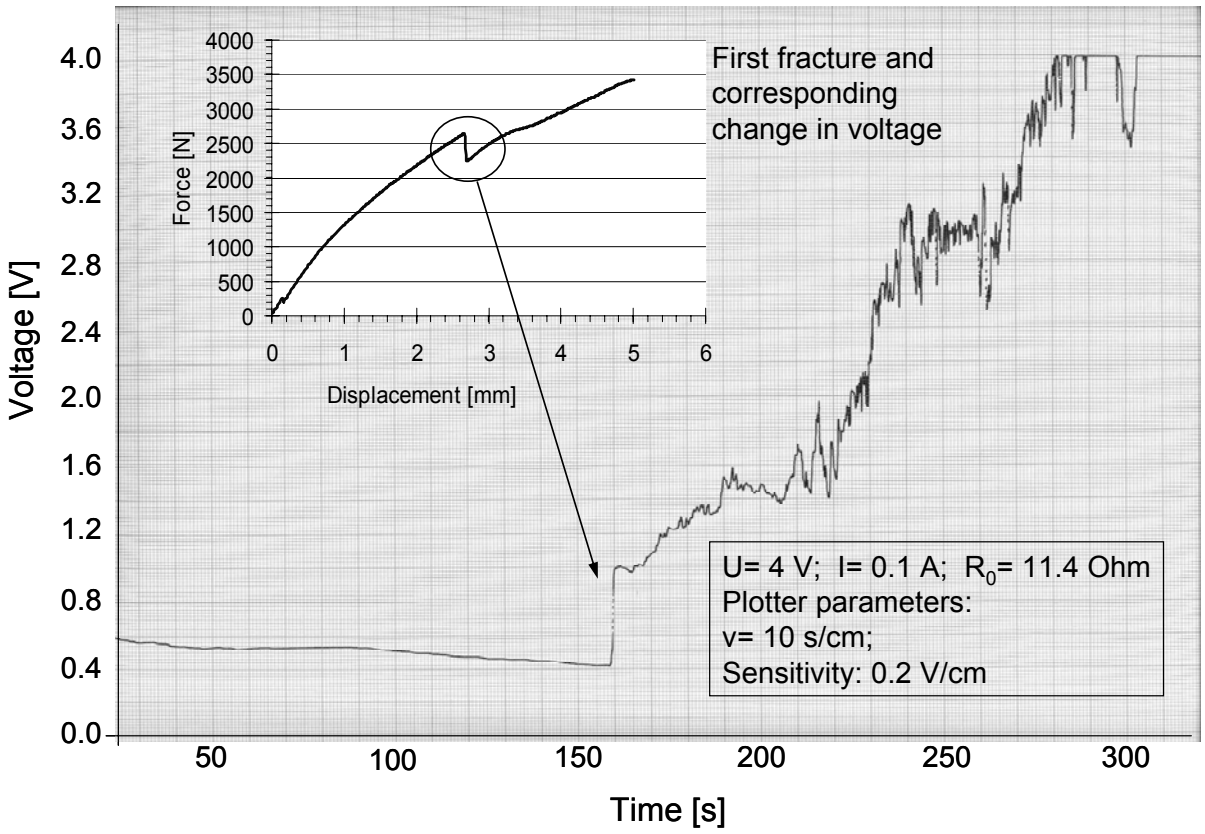

Figure 4.11: Influence of CF thread breakage on change in voltage and comparison between force displacement diagram and change in voltage

Theoretically, the plot should show the sudden deflection on the voltage scale, but practically the phenomenon of CF thread breakage and possible contact between broken filaments reveals the progressive deflection of the curve. Figure 4.11 shows that the first delamination of the insert where the CF thread breaks and the first voltage rise occurs takes place at the same time.

Incorporation of very little amount of CF thread at the exact damage zone will help validate the thread usability for integration of metallic inserts in the FRPC laminates. Strain caused in the CF thread during initial load can also be detected in terms of minute change in resistance. However, major damage in insert bonding with the main laminate can be easily detected.

The use of IVW-CF stitching thread as a sensor system for life cycle monitoring and life expectancy of fiber reinforced composite seams is advantageous. The results of different tests based on various forms of CF-thread placement shows the effectiveness of the system. IVW-CF thread works as an integrated part of the laminate, thus, the influence of the CF thread damage on the change in resistance helps monitor real fracture impact of the FRPC. The robust nature of sensors and cost-effectiveness of incorporation processes (process of stitching is relatively cost effective for sensor mounting and the costs of IVW-CF thread compared to modern sensing systems is very low) increases the possibility to use these sensors e.g. in automotive parts. The current monitoring system with CF thread can be made more accurate by improved connectivity between sensor and monitoring instrument. The measurement system can be made more user-friendly and accurate. Implementation of CF sensors only at the critical zones reduces the efforts of monitoring the complete part area / volume and still provides the required damage information.

5 Conclusion

The aim of the present dissertation is the exploration of the possibilities inherent in the stitching supported preform technology. It details the different types of stitching applied in the preform technology, such as *joining (preforming)*, *assembly* or *structural* stitching with the help of examples, according to the basic sorting. As a manufacturing study, a net shape technology was developed to create a load bearing stiffening structure. The manufacturing study analyzes the applicability of the stitching technology and demonstrates a multistage preform manufacturing process, which facilitates the production of complex, three-dimensional composite parts. Furthermore, the study revealed that a high-grade automated preform manufacturing system could be developed, and that allows not only a net-shape manufacturing process but it can help to achieve a quality controlled manufacturing as well.

As a next step, a three-dimensional preform manufacturing process was worked out with different low melting temperature thermoplastic stitching threads. With the application of this technology the advantages of the binder technology and the stitching supported preforming can be alloyed. Thus a shape-retaining ready-to-impregnate three-dimensional preform, the application of which simplifies the handling and the positioning of the preform into the injection tool, can be formed. Quantitative measurement methods were worked out to reveal the mechanical properties of the fusible thread stitched three-dimensional preforms. These measurement methods indicate the effect of the orientation and density of the stitching in the reinforcing structure after thermal treatment. Three basic properties of the thermoformed preforms were tested: the *specific bending stiffness*, the *spring back angle* after thermoforming, and the *restoring force* in case of different material architectures and stitching types. The most important material property of the joining stitching threads besides the low melting point is the solubility essentially in unsaturated polyester and epoxy resins. With the matrix solubility, it is possible to ensure the dissolution of the threads after they accomplished the binding function. Stitch holes from the preforming can be removed with this effect, and the reduction of the mechanical properties degradation of the composite parts can be ensured. With the help of the investigations two polymeric threads were selected, the melting temperature of these polymers is less than 100 °C, they show good solubility properties, and have the mechanical properties required for stitching.

The stitches can be applied in the structure for not only joining or assembly function but also can be the essential elements of the reinforcement structure. These are called as structural stitching, the essentially function of which is the interlaminar reinforcement in monolithic or sandwich structures. These also have great possibilities to use for fixation of metallic load transmission elements in composite structures. The static tensile tests carried out on stitched transmission elements (inserts) showed that app. 200% improvement of maximal load force could be achieved against the unstitched BigHead® inserts. The investigations revealed that the highest reinforcing effect could be achieved through the simultaneous interlaminar embedding and stitching of the inserts. In this case, the reinforcing stitching can prevent the delamination of the composite layers that is the characteristic failure mode in case of interlaminar embedded inserts. The static shear tests carried out on the embedded metallic inserts gave a possibility to observe the characteristic failure modes and the evaluation of the stitching technique supported reinforcing. Since the characteristic failure mode of the stitched inserts was not the damage of the stitching thread but the insert breakage, the next step of the investigations was the development of a new insert with modified base plate geometry. The application of this insert type enables the testing of the real loadability of the stitching threads. The results revealed that the high performance stitching threads as glass carbon or aramid can only be applied with restrictions to fixed inserts, while polyester (PET) threads show adequate reinforcing properties. As the next step the finite element modeling of the insert-composite contact and the optimization of the metallic insert geometry were accomplished.

Through the electric conductivity of the fibers, the carbon stitching threads can be used as sensors for structural health monitoring. The investigations carried out on carbon thread stitched composite parts indicated that the damage in the composite structure could be detected through the change in electric resistance of carbon threads. The results of the investigations revealed that carbon threads are adaptable not only as reinforcement but also as sensors of the damage in metallic inserts.

The research carried out in frame of the present work indicates the large potential inherent in the stitching supported preform technology. The results verify that the adorning the stitching threads with additional functions ensure further extensive possibilities in the applications of preform technology.

6 References

1 Stauber, R.: Vorwort in “Kunststoffe im Automobilbau”, VDI-Geselschaft Kunststofftechnik. Düsseldorf: VDI-Verlag, pp. 1-2, 1999

2 N.N., BMW: Composites to be mass-produced soon. Composites International, 46, July-August pp. 48-50, 2001

3 Lorenz, T.: Kosteneffektive CFK Fertigungsverfahren der nächsten Generation. 7. Nationales SAMPE Symposium 2001, Erlangen, pp. III.2.1-III.2.10, 2001

4 Beardmore, P., Johnson, C. F.: The potential for composites in structural automotive applications, Composite Science and Technology 26, pp. 251-288, 1986

5 Mallic, V.: Thermoplastic composite based processing technologies for high performance turbomachinery components. Composite part A, 32 pp. 1167-1173, 2001

6 Michaeli, W.: Innovationspotential Kunststoff im Automobilbau, In: Kunststoff im Automobilbau- Zukunft durch neue Anwendungen, VDI-Verlag Düsseldorf 1998, 11

7 Neitzel, M., Breuer, U. P.: Die Verarbeitungstechnik der Faser-Kunsstoff-Verbunde. München, Wien, Karl Hanser Verlag, 1996

8 Ehrenstein, G. W.: Faserverbund-Kunststoffe, Carl Hanser Verlag, München, Wien, 1992

9 Michaeli, W., Wegner, M.: Einführung in die Technologie der Faserverbundwerkstoffe, Carl Hanser Verlag München, Wien, 1989

10 Carter, J., Lo, F. C.: Beyond mechanical performance:Product design for low cost manufacturing of composites for aerospace applications, in Stephan A. (Hg.): Proceedings of the 1st Stade Composite Colloquium, Stade, 7.-8. Sept. 2000

11 Hayse, S.: RTM as the low cost alternative, in Earth, M. A. (Hg.): Proceedings of the 21st International SAMPE Europe Conference of the Society for the advancement of Material and Process Engineering, Paris, France, 18.-20. April 2000, p 35-36

12 Beckwith, S. W., Hyland, C. R.: Resin Transfer Moulding: A Decade of Technology Advances, SAMPE Journal. 34, 6, pp. 7-19, 1998

13 Rückers, B.: Faserverbundwerkstoffe, Entwicklungstrends am Beispiel des Airbus, Proceedings DGM-Tagung, Klaus Fridrich (Ed.) Kaiserslautern. October 1997.

14 N.N.: RTM Moves Ahead, Reinforced Plastics, pp. 26-33, 1997

15 N. N.: HTMA Market Forecast, High Tech Materials Alert, 7, pp. 5-6, 1997

16 N. N.: Process Refinement Key to RTM Succes, Reinforced Plastics, 2, pp. 26-30, 1999

17 Fabio, R., Rao, N.: Experiences with Exterior Composites on the DaimlerChrysler viper andProwler Programs, Proceedings „Praxis-Forum-Tagung: The 2010 Plastic car Body Vision“, Ebert F., Woydt M. (Ed.) Bad Nauheim. Germany, pp. 355-366, 1999

18 Wallentowittz, H., Adam, H., Bröckling, J.: Potential of fiber reinforced plastics space frame structures. VDI-Tagung Entwicklung im Karosserienbau, Hamburg, 14.,15. Mai 1996, p. 477-495

19 Beckwith, S. W.: RTM, VARTM, and SCRIMP processing infusion technologies. SAMPE 44th ISSE / SAMPE 99´, Long Beach, CA, 05. 1999, Beckwith Technology Group, Murray, Utah, 1999

20 Fleming, M., Ziegmann, G., Roth, S.: Faserverbundbauweisen, Fasern und Matrices, Springer Verlag, Berlin, Heidelberg, 1995

21 Fleming, M., Ziegmann, G., Roth, S.: Faserverbundbauweisen, Halbzeuge und Bauweisen, Springer Verlag, Berlin, Heidelberg, 1996

22 Fleming, M., Ziegmann, G., Roth, S.: Faserverbundbauweisen, Fertigungsverfahren mit duroplastischer Matrix, Springer Verlag, Berlin, Heidelberg, 1999

23 Chavka, N. G, Dahl, J.-S.: P4: Glass Fiber Preforming Technology for Automotive Application. Resin Transfer Molding SAMPE Monograph No. 3, SAMPE Publications, Corvina, 1999

24 Büsgen, W.-A.: Neue Verfahren zur Herstellung von dreidimensionalen Textilien für den Einsatz in Faserverbundwerkstoffen, Dissertation RWTH, Aachen, 1993

25 Feltin, D.: Neue textile Preformtechniken zur kostengünstigen FV-Bauteilherstellung. 2. Internationale AVK-Tagung für verstärkte Kunststoffe und Formmassen, Baden-Baden, pp. B 10, 12.-13- Okt. 1999

26 Bogdanovich, A., Singletary, J.: 3-D Woven Preforms and Composites: Experimental Characterization and Predictive Analysis, Proceedings of the 5th International Conference on Textile Composites, Leuven, 18.-20. September 2000, p4

27 Kobayashi, H., Nakama, N.: Fabrication of mechanical properties of Braided Composite Truss Joints. Proc. Of the 36th International SAMPE Symposium, pp. 1089-1103, 1992

28 Kendal, M.: Keynote on Textile Composites for Automotive Applications. ACP 2000. Automotive Composites and Plastics. Essex, 5.-6. December 2000

29 Wiedmer, S.: Zur Pultrusion von thermoplastischen Halbzeugen: Prozessanalyse und Modellierung, Dissertation, IVW, Kaiserslautern, 2006

30 Bibo, G. A., Hogg, P. J., Backhouse, R, Mills A.: Carbon fiber non crimp fabric laminates for cost effective damage-tolerant structures. Composites Science and Technology, 58, pp. 129-143, 1998

31 Warrior, N. A., Rudd, C. D., Gardner, S. P.: Experimental studies of embroidery for the local reinforcement of composites structures 1. Stress concentrations. Composite Science and Technology , Vol 59, pp. 2125-2137, 1999

32 Matheij, P., Gliesche, K., Feltin, D.: Tailored fiber placement – Mechanical properties and applications. Reinforced Plastics and Composites, Vol. 17, 9, pp. 774-787, 1998

33 Hörsting, K., Huster, M,.: Maßgeschneiderte Verstärkungstextilien für Verbundwerkstoffe, in DWI Reports (Hg.): Aachener Textiltagung. Aachen, pp. 190-201, 25.-26. November 1998

34 Bischof, T. H., Wulfhorst, B.: Rundwirke mit multiaxialen Stehfäden für neue Anwendungsgebiete. Technische Textilien, Vol. 42, pp.151-153, 1999

35 Laourine, E., Schneider, M., Wulfhorst, B.: Production and Analysis of 3D Braided Textiles Preform for Composite. Proceedings of the 5th International Conference on Textile Composites, Louvain, 18.-20. September 2000, p. 4

36 Witting, J.. Roboted 3-dimensional Stitching Technology, Stephan A. (Hg.): Proceedings of the 1st Stade Composite Colloquium, Stade, 7.-8. September 2000

37 Keilmann, R., Jäger, M.: Präsentation Blindstitchtechnologie, in Stephan A. (Hg.): Proceedings of the 1st Stade Composite Colloquium, Stade 7.-8 september 2000

38 Palmer, R. J., Dow, M. B., Smith, D. L.: Development of Stitching Reinforcement for Transport Wing Panels, 1 st NASA Advanced Composite Technology Conference, Seattle, WA, 29.10.-1.11.1990, NASA CP-3104, Part 2, pp. 621-646, 1990

39 Mouritz, A. P., Leong, H. K., Herszberg, I.: A review of the effect of stitching on the in-plane Mechanical Properties of Fibre-Reinforced Polymer Composites. Composite Part A, 28 A, pp. 979-991, 1997

40 Mouritz, A. P., Cox, B. N.: A Mechanistic Approach to the Properties of Stitched Laminates. Composite Part A, Vol. 31 1, pp. 1-27, 2000

41 Mignery, L. A., Tan, T. M., Sun, C. T.: Use of Stitching to Suppress Delamination in Laminated Composites, In Johnson, W.S.: Delamination and Debonding, AST STP 876. Philadelphia: American Society for Testing and Materials, 1985, p. 371-385

42 Cahuzac, G., His, S.: AEROTISS 4.5D – A New Technology for Thick Multiply Composite Panels, in Earth, M. A. (Hg.): Proceedings of the 21st International SAMPE Europe Conference of the Society for the Advancement of material and Proces Engineering, Paris, France, 18.-20. April 2000, p. 233-241

43 Chung, W. C., Jang, B. Z., Chang, T. C., Hwang, L. R., Wilcox, R. C.: Fracture Behavior in Stitched Multidirectional Composites. Materials Science and Engineering (1998), A 112, p. 157 173

44 Mouritz, A. P., Jain, L. K.: Further Validation of the Jain and Mai Models for Interlaminar Fracture of Stitched Composites. Composites Science and Technology, Vol. 59, p. 1653-1662, 1999

45 Parnas, R. S.: Liquid Composite Molding. München, Hanser Gardner, 2000

46 Dexter, H. B.: Development of Textile Reinforced Composites for Aircraft Structures. Proceeding of the 4th international Symposium for textile composites, Kyoto, Japan 12-14 October 1998, pp.0-32-1 – 0-32-8.

47 Williams, C., Summerscales, J., Grove, S.: Resin Infusion under Flexible Tooling (RIFT), A review. Composites Part A, Vol. 27 A (1996), p. 517-524

48 Single, C.: Neue kostengünstige Fertigungsferfahren für CFK-Strukturen. 4. Nationales SAMPE Symposium, Braunschweig 12.-13. März 1998, p. 1-15

49 Single, C.: Ein Beitrag zur kostenoptimierten Herstellung von großflächigen Hochleistungsverbundbauteilen. Dissertation TU Braunschweig 1998

50 Neitzel, M., Mitschang, P.: Handbuch Verbundwerkstoffe, Carl Hanser Verlag, 2004.

51 Mitschang, P., Ogale, A., Schlimbach, J., Weyrauch, F., Weimer, C.: Preform Technology: a Necessary Requirement for Quality Controlled LCM-Processes. Polymers & Polymer Composites, No. 8, Vol. 11, pp. 605 – 622, 2003

52 Klopp, K.; Moll, K.-U.: Stitching process with one-sided approach of the textile for the production of reinforcing textiles for composites and other technical textiles. Proceedings 5th International Conference on Textile Composites, 18-20 September, 2000, Leuven, Belgium, p. 4.

53 Ogale, A., Weimer, C., Ladstätter, E., Billinger, W.: A presentation on: Compaction behavior of stitched fabric preforms. European Congress on Advanced Materials and Processes (EUROMAT), Lausanne, Switzerland, 1-5 September 2003.

54 Adanur, S., Tsao, Y. P.: Stitch bonded textile structural composites 26th International SAMPE Technical Conference October 17-20, 1994

55 Mitschang, P. (Hrsg.): Prozessentwicklung und ganzheitliches Leichtbaukonzept zur durchgängigen, abfallfreien Preform-RTM Fertigung (Pro-Preform RTM – Abschlussbericht, IVW – Schriftenreihe, Band 46) 2004

56 FORD GLOBAL TECHNOLOGIES, INC.: Robotic systems for automated preform processing, United States Patent US 6497 566, 2002

57 http://www.aplicator.se/prod/p4.htm

58 Brandt, M. R., Reeve, S. R.: Direct Fiber Preform Case Studies, Composites 2001 Convention and Trade Show, Composites Fabrications Association, Tampa, FL USA, October 3-6, 2001

59 DIN 53362: Prüfung von Kunststoff-Folien und von textilen Flächengebilden (außer Vliesstoffe), mit oder ohne Deckschicht aus Kunststoff-Bestimmung der Biegefestigkeit- Verfahren nach Cantilever, 2003-10

60 Pascault, J.-P., Sautereau, H., Verdu, J., Williams, R. J. J.: Thermosetting Polymers, 2002 Marcel Dekker, Chapter 10, pp. 282-322

61 Carraher, C. E., Seymour, R., B.: Polymer Chemistry, 2003 Marcel Dekker, Chapter 3, pp. 61-73

62 Wolf, B. A.: Solubility of Polymers, Pure and Applied Chemistry, 57, 2, pp. 323-336, IUPAC, 1985

63 Gossens, S., Goderis, B., Groeninckx, G.: Reaction-Induced Phase Separation in Crystallizable Micro- and Nanostructured High Melting Thermoplastic/Epoxy Resin Blends, Macromolecules 2006, 39, pp. 2953-2963

64 Peng, M., Li, H., Wu, L., Chen, Y., Zheng, Q., Gu.: Organically Modified Layered-Silicates facilitate the Formation of Interconnected Structure in the Reaction-Induced Phase Separation of Epoxy/Thermoplastic Hybrid Nanocomposite, Polymer 46, 7612-7623, Elsevier 2005

65 Fernandez, B., Arbelaiz, A., Diaz, E., Mondragon, I.: Influence of Polyethersulfone Modification of a Tetrafunctional Epoxy Matrix on the Fracture Behavior of Composite Laminates Based on Woven Carbon Fibers, Polymer Composites 25, 480-488, 2004

66 Giannotti, M. I., Mondragon, I., Galante, M. J., Oyanguren, P. A.: Morphology profiles obtained by reaction-induced phase separation in epoxy/polysulfone/poly(ether imide) systems, Polymer International 54 pp. 897-903, 2005

67 Gianotti, M. i., Bernal, C. R., Oyanguren, P. A., Galante, M. J.: Morphology and Fracture Properties Reationship of Epoxy-Diamin Systems Simultaneously Modified With Polysulfone and Poly(ether imide), Polymer Engineering and Science 45, pp. 1312-1318, 2005

68 Terjack, A., Remiro, P. M., Mondragon, I.: Phase Separation and Rheological Bahavior During Curing of an Epoxy Resin Modified With Syndiotactic Polystyrene, Polymer Engineering and Science, 45, pp. 303-313, 2005

69 Vanden, Poel R., Goossens, S., Goderis, B., Groeninckx, G.: Reaction Induced Separation in Semicrystalline Thermoplastic/Epoxy Resin Blends, Polymer 46 pp. 10758-10771, 2005

70 Chen, C.-C., Chen, Y.-C., Shen, K.-S., Yu, T. L.: Phase Separation of Poly(ether sulfone imide) Modified Epoxy Resins, Journal of Polymer Research 10, pp. 39-46, 2003

71 Munz, M., Sturm, H., Stark, W.: Mechanical Gradient Interphase by Interdiffusion and Antiplasticisation Effect-Study of an Epoxy/Thermoplastic System, Polymer 46, pp. 9097-9112, 2005

72 Wylen G. J., Sonntag R. E., Borgnakke C., Borgnakke C.: Fundamentals of Classical Thermodynamics, John Wiley and Sons (WIE), 1994

73 Van Krevelen, D. W.: Properties of Polymers, Elsevier 1997, Chapter 7, pp. 189-225

74 Schievenbusch, F.: Beitrag zu Hochbelasteten Krafteinleitungselementen für Faserverbundbauteile, Dissertation TU Chemnitz, FMV, 2003

75 Habenicht, G.: Kleben: Grundlagen, Technologie, Anwendungen, Springer-Verlag 1990. Kap. 8 Festigkeiten von Metallklebungen, pp. 270-350

76 Sasdelli, M., Karbhari, V. M., Gillespie, J. W.: On the use of metal inserts for attachment of composite components to structural assemblies-a review, International Journal of Vehicle Design, 14,4, pp. 353-369 1993

77 Matthews, F. L.: Joining Fibre Reinforced Plastics, Elsevier, London, New York, 1987

78 Hart-Smith, L. J.: Mechanically fastened joints for Advanced Composites-Phenomenological Considerations and Simple Analysis, Fibrous Composites in Structural Desingn, Plenum Press, New York, 1980

79 Hart-Smith, L. J.: Bonded-Bolted Composite Joints, Journal of Aircraft, 22, 11, pp. 993-1000, 1985

80 Müller, W.: Krafteinleitung in Faserverbundwerkstoffe-Hinweise für Zukunft- und Fertigungsgerechten Gestaltung, Dissertation, RWTH Aachen, 1991

81 Grüninger, G.: Möglichkeiten der Krafteinleitung in Faserverstärkte Bauteile, Kunststoff- und Aramidfaserverstärkte Kunststoffe, VDI-Verlag, Düsseldorf 1997

82 Hütter, U.: Probleme der Krafteinleitung in Glasfaser-Kunststoff-Bauteile, Kunststoffe. 56, 12, pp. 843-846, 1966

83 Hart-Smith, L.J.: Further Developments in the Design and Analylsis of Adhesive-Bonded Structural Joints, ASTM Conference on Joining of Composite Materials (STP 749), Minneapolis Minnesota, 1980

84 Sasdelli, M., Karbhari, V. M.: The Design and Use of Molded-in Inserts and Attachments in Resin Transfer Molding, Proc 8th Annual ASM/ESD Conference, pp. 407-413, 1992

85 Ferret, B., Anduze, M., Nardari, C.: Metal Inserts in Structural Composite Materials Manufactured by RTM, Composite Part A 29, A, pp. 693-700, 1998

86 Freitag, P.: Metallische Gewindeeinsätze für Thermo- und Duroplaste, Plastverarbeiter 42, 9, pp. 60-66, 1991

87 Hoa, S.V., Lulham, I., Sankar, T. S.: Aluminium Inserts for Fastening Sheet Moulding Compounds, Proceedings 3rd Int. Conf. Composite Structures, Paisley, Scotland, pp. 575-583, 1985

88 Hoa, S. V., Di Maria, A.: Metal Inserts for Efficient Joining of Sheet Molding Compoud Structures, Proc. Of the 4th Annual Conference on Advanced Composites, Dearborn, Michigan, 1988

89 Schwarz, M.; Magin, M.; Peil, C.; Schürmann, H.: Thin-walled FRP-laminates and local bending moments incompatible or solvable by a skillful design? Proceedings 7. Internationale AVK-TV Tagung, Baden-Baden, September 2004.

90 Trinter, F., Ehrenstein, G. W.: Mechanisches Verbinden von Bauteilen aus SMC mit umpressten Gewindeeinsötzen, AVK-Tagung, pp. 19.1-7, 1987

91 Trintner, F., Ehrenstein, G. W.: Schraubenverbindungen mit Gewindeeinsätzen und gewindeerzeugenden Schrauben an Bauteilen aus faserverstärkten Fließpresswerkstoffen, VDI-Bericht 852, VDI-Verlag, Düsseldorf, pp. 493-510, 1991

92 Evans, R. L.; Heller, M.: Effect of Bonded insert Shape and Adhesive Thickness on Critical Stresses in a Loaded Plate, DSTO Aeronautical and Maritime research Laboratory, Melbourne Victoria 3001, August 1996, p. 1.

93 Mignery, L. A., Tan, T. M., Sun, C. T.: The use of stitching to suppress delamination in laminated composites. Delamination and debonding, ASTM STP 876, ed. W. S. Johnson, American Society of Testing and Materials, Philadelphia, PA, pp. 371-81, 1985.

94 Skelton, T. J.: Localized Stitching to Reinforce Inserts in Composite Sandwich Panels, M.S. Thesis, Department of Mechanical Engineering, University of Utah, Salt Lake City, UT, December 2004.

95 Roth, M. A.: Strukturelles Nähen: Ein Verfahren zur Armierung von Krafteinleitungen für Sandwich-Strukturen aus Faser-Kunststoff- Verbund, Dissertation IVW GmbH Kaiserslautern 2006

96 Ogale, A., Weimer, C., Mitschang, P.: Selection of sewing threads for preform manufacturing, Advanced composite letters No. 4 (2004), Vol. 13, pp. 145-153.

97 Mitschang, P.: Faser-Kunststoff-Verbund-Bauteil mit Inserts, OS DE 198 34 772 A1, 1. August 1998.

98 Ogale, A., and Mitschang, P.: Tailoring of textile preforms for fibre-reinforced polymer composites, Journal of industrial textiles No. 2 (2004), Vol. 34, pp 77-96.

99 Brandau, E.: Duroplastwerkstoffe: Technologie, Prüfung, Anwendung, VCH Verlag 1993.

100 Molnar, P., Ogale, A., Mitschang, P.: Incorporation of Functional Elements into the Fibre Reinforced Polymer Structure by Means of Tailoring Technology. Proceedings Reinforced Plastics International Balaton Conference, Balatonvilágos 2004.

101 Zienkiewicz, O. C., Taylor, R. L.: The Finite Element Method for Solid and Structural Mechanics, Butterworth-Heinemann; 6 edition (September 20, 2005)

102 Zienkiewicz, O. C.: Methode der finiten Elemente, Carl Hanser Verlag München, Wien 1975, pp. 17-29

103 Kollár, P. L., Springer S. G.: Mechanics of Composite Structures, Cambridge University Press 2003, pp.18-20. and 50-61.

104 Van der Auweraer H., Peeters B.: International Research Projects on Structural Health Monitoring: An Overview. SHM - Structural Health Monitoring. Vol. 2. pp. 341-358. 2003

105 Kalamkarov, Saha, Georgiades, Challagulla, Newhook: Smart FRP Reinforcements for Long-term Health Monitoring in Infrastructure. Journal of Thermoplastic Composite Materials. Vol. 17. S. 359-381. 2004

106 Kessler, S. S.; Sperling, S. M.: Structural Health Monitoring of Composite Materials Using Piezoelectric Sensors, internet web page: http://web.mit.edu/sskess/www/papers/materials_evaluation.pdf. (accessed on August 14. 2004

107 Wang, Q., Quek, S. T.: A Model of the Analysis of Beams with Embedded Piezoelectric Layers. Journal of Intelligent Material Systems and Structures. Vol. 13. S. 61-70. 2002

108 Ping, T., Liyong, T.: A delamination detection model for composite beams using PFRC sensor/actuator. Composites Part A: Applied Science and Manufacturing. pp. 231-247. 2004

109 Qing, Beard, Kumar, Chan, Ikegami: Advances in the development of built-in diagnostic system for filament wound composite structures. Composites Science and Technology. Vol. 66. pp. 1694-1702. 2006

110 Giurgiutiu, Zagrai, Bao: Piezoelectric Wafer Embedded Active Sensors for Aging Aircraft Structural Health Monitoring. SHM - Structural Health Monitoring Vol. 1. pp. 41-61. 2002

111 Gerard, F. F.: Fibre optic sensor systems for monitoring composite structures. Reinforced Plastics. S. 41-49; 2005

112 Skontorp, A.: Composites with Embedded Optical Fibers at Structural Details with Inherent Stress Concentrations. Journal of Composite Materials 22. S. 2501-2515, 2002

113 Betz, Staudigel, Trutzel, Kehlenbach: Structural Monitoring Using Fiber-optic Bragg Grating Sensors. SHM - Structural Health Monitoring. Vol. 2. S. 145-152. 2003

114 Brei, D., Cannon, B. J..: Piezoceramic hollow fiber active composites. Composites Science and Technology. S. 245-261. 2004

115 Pohl, J.: Zerstörungsfreie Charakterisierung adaptiver CFK-Piezokeramik-Verbunde. ZfP-Zeitung 87. pp. 37-42. 2003

116 Horoschenkoff, A.: Strukturintegrierte DMS für Faserverbundwerkstoffe. FH München, Kunststofftechnik Online Seminar, http://www.lrz-muenchen.de/~p3001gu/webserver/webdata/3_semina/v3_piezo/38_piezo.htm, 2004

117 Travis, L. T.: Structural acoustic response of a shape memory alloy hybrid composite panel (lessions learned). SPIE's Annual International Symposium on Smart Structures and Materials. San Diego, 17.-21. März 2002. NASA Langley Research Center

118 Adams, R. D.; Cawley, P.; Pye, C. J.; Stone, B. J.: A Vibration Technique for Non-Destructively Assessing the Integrity of Structures. Journal of Mechanical Engineering Science, Vol. 20, No. 2, pp. 93-100, 1978

119 Gachagan, A., Hayward, G., Banks, R.: A Flexible Piezoelectric Transducer Design for Efficient Generation of Reception of Ultrasonic Lamb Waves. IEEE

Transactions on Ultrasonics, Ferroelectrics, and Frequency Control. Vol. 52. pp. 1175-1182. 2005

120 Cawley, P.; Adams, R. D.: The Location of Defects in Structures from Measurements of Natural Frequencies, Journal of Strain Analysis, Vol. 14, No. 2, pp. 49-57, 1979

121 Adelman, H. M.; Haftka, R. T.: Sensitivity Analysis of Discrete Structural systems", AIAA Journal, Vol. 24, No. 5, pp. 823-832, 1986

122 Zimmerman, D. C.; Kaouk, M.: Structural damage detection using a minimum rank update theory. ASME Journal of Vibration and Acoustics, Vol. 116, No. 2, pp. 222-231, (1994).

123 Pandey, A., Biswas, K. M.; Samman, M.: Damage detection from changes in curvature mode shapes. Journal of Sound and Vibration, Vol. 145, No. 2, pp. 321-332, (1991).

124 Samman, M. M.: Structural damage detection using the modal correlation coefficient (MCC). Proceedings of the 15th International Modal Analysis Conference, Orlando, FL, pp. 627-630, (1997).

125 Liang, Z., Lee, G. C.; Kong, F.: On Detection of Damage Location of Bridges. Proceedings of the 15th International Modal Analysis Conference, Orlando, FL, pp. 308-312, (1997).

126 Aktan, A. E., Brown, D. L., Farrar, C. R., Helmicki, A., Hunt, V., Yao, J.: Objective global condition assessment. Proceedings of the 15th International Modal Analysis Conference, Orlando, FL, pp. 364-373, 1997

127 Stöven, T., Wang, X., Neitzel, M., Mitschang, P.: Monitoring the Resin Transfer Molding Process by Piezoelectric Elements, Processing Online Sensing and Control for Liquid Molding of Composite Structures, Steiner, K.V., Advani S.G. (Eds.), Annapolis, MD / Apr. 14-15, CCM

128 Hillger, W.: Lamb-Wellen zur Schadensanzeige in faserverstärkten Kunststoffen. DGZfP Jahrestagung 2005. Rostock, 2.-4. Mai 2005

129 Park, G., Sohn, H., Farrar, C. R., Inman, D. J.: Overview of Piezoelectric Impendance-Based Health Monitoring and Path Forward. The Shock and Vibration Digest No. 6. pp. 451-463. Vol. 35. 2003

130 Park, Kabeya, Cudney, Inman: Impendance-Based Structural Health Monitoring for Temperature Varying Applications. JSME International Journal No. 2. 42/1999. pp. 249-258

131 Haase, Pusch, Laourine, Cherif, Illing-Günther, Zschenderlein, Möhring, Fritzsche, Haiduk, Nowottne: Energie und Informationsübertragung in Smart Textiles. Technische Textilien. pp. 256-259. 2006

132 Yan, L., Fraser, M., Elgamal, A., Conte, J. P., Fountain, T.: Applications of Neural Network in Structural Health Monitoring, Internet web page: http://healthmonitoring.ucsd.edu/documentation/public/CJUHMCS2004-NNApplications.pdf. Accessed on 10.08. 2004

133 Lynch, J. P., Sundararajan, A., Law, K. H., Sohn, H., Farrar, C. R.: New Opportunities for Structural Monitoring: Wireless Active Sensing, Proceedings of the int. workshop on advances sensors, structural health monitoring and mart structures, keio University, Tokyo, Japan, 2003

134 Fu, C. C.: Wireless Structural Monitoring of a Newly Replaced Fiber Reinforced Plastics (FRP) Bridge Deck, internet web page http://best.umd.edu/projects/frp.html, Accessed on 12.08. 2004

135 Weimer, C.: Kohlenstofffasernähgarn für Faser-Kunststoff-Verbund-Bauteile German patent DE19932842 A1. 1999

136 Tajima, N., Sakurai, T., Sasajima, M., Takeda, N., Kishi, T.: Overview of Japanese Smart Materials Demonstrator Program and Structures System Project. Adv. Composite Mater., Vol. 13, No. 1, pp. 3-15. 2004

137 Takeda, N.: Electromechanical Modeling of Damage Growth Prediction of Unidirectional CFRP Composite Patch. Internet web page: http://zeisei5.dpri.kyoto-u.ac.jp/us_j/3_2/takeda_hp.pdf., August 10, 2004

Liste der betreuten Studien- und Diplomarbeiten

1. Attila Hodács, 2005
   Integration of Structurally Stiffened Metallic Fasteners with the Textile Reinforcing Structures by Means of Sewing Technology, Diplomarbeit

2. Cecília Reizer, 2006
   Implementation of Stitching Technology to Reduce Fabric Deformation and Shear during Thermoforming, Diplomarbeit

3. Balázs Fodor, 2006
   FEM-study of Stitched Metallic Insert and Composite Structure Connection, Studienarbeit